STYRELSEN FÖR

VINTERSJÖFARTSFORSKNING

WINTER NAVIGATION RESEARCH BOARD

Research Report No 19

CREEP OF FRESH WATER ICE AT HIGH HOMOLOGOUS TEMPERATURES

BY ERKKI K M LEPPÄVUORI

Sjöfartsstyrelsen
Finland

Finnish Board of Navigation

Sjöfartsverket
Sverige

Swedish Administration
of Shipping and Navigation

CREEP OF FRESH-WATER ICE AT HIGH HOMOLOGOUS TEMPERATURES

by

Erkki KM Leppävuori

1976

ABSTRACT

This paper studies the creep of ice Ih under normal pressure and at high homologous temperatures.

The first part treats the theoretical background of deformation of ice starting from the microstructure.

The mechanical properties of ice are essentially determined by the effect of the co-called Bjerrum defects on the movements of dislocations.

There are also many other factors which contribute to the deformation of polycrystalline ice, e.g. grain boundary migration, small angle boundaries, kink bands, crack formation, recovery and recrystallization.

The results of the creep and failure experiments made during this study show wide scatter, and therefore an univocal creep model for ice is not suggested.

ACKNOWLEDGEMENTS

I wish to express my gratitude to Dr. Pauli Jumppanen for his support and encouragement during this work.

Concerning the experimental part of my study I should like to thank Mr. Ilpo Salo, Mr. Risto Grönholm and Mr. Keijo Kärkkäinen.

In the processing of the experimental data, great help has been provided by Mr. Heikki Järvinen and Mr. Hannu Sinisalo, who in spite of all misfortunes have performed their work with high spirit. For this I express them my very great gratitude.

Many thanks also to Mr. Paavo Hassinen, who has helped in the analysis of the data.

The financial support provided by Suomen Akatemia, Tekniikan Edistämissäätiö and Talvimerenkulkututkimuksen hallitus is gratefully acknowledged.

CONTENTS

LIST OF SYMBOLS

A	constant (often temperature and time dependent)
A'	constant
B	constant (often temperature and stress dependent)
D	Bjerrum defect
D	creep function defined in eq. (25)
D_i	diameter of test specimen (i = 1, 2, 3)
D_t	value of creep model in eq. (36), (37)
D_m	value of creep test curve in eq. (36), (37)
E, E_o	initial Young's modulus
Erf	error functional defined in eq. (36)
F	force affecting test piece
F_M	break load
G	weights in creep apparatus
H	height of test specimen
Ih	hexagonal ice at high homologous temperatures
L	Bjerrum defect
N	number of molecules in the ice crystal
P	weight of test specimen
Q, Q_c, Q_i	activation energy
R	gas constant
T	temperature (usually Kelvin)
T_m	melting point
V	volume of test specimen
a, a_i	constant (often temperature and stress dependent) (i = 1...4)
a_o	lattice parameter of ice crystal

b, b_i	Burgers vector, constant (often temperature and stress dependent) ($i = 1...4$)
c	c-axis of ice crystal, constant
c_o	lattice parameter of ice crystal
c_{HF}	concentration of HF in eq. (8)
f	function of stress and temperature in eq. (10)
f_i	frequence factor in eq. (1)
g	9.81 m/s^2
k	number of data points
m	constant (often temperatures and stress dependent)
n, n_i	constant (often temperature and stress dependent) ($i = 1, 2, 3$)
n_o	constant in eq. (10)
n, n'	number of test pieces
r	constant in eq. (32)
s, s'	standard deviation
s_r	relative deviation defined in eq. (37)
t	time (often hours)
v	dislocation velocity
α	constant, thermal expansion coefficient
β	constant
$\dot{\gamma}_i$	rate of deformation process i
ε	deformation
ε_1, ε_2, ε_T	errors in strain, eq. (20)...(22)
ε_o	instantaneous strain
$\dot{\varepsilon}_s$	secondary creep rate
π	constant 3.14159
ρ	density of ice, dislocation density

ϕ	angle in Table 6
σ, σ_o	stress
σ_M	strength of ice
τ	stress
τ_o	constant in eq. (6)
$\bar{x}$	mean value of x
Δx	absolute error of x
$\dot{x}$	$\partial x/\partial t$

1. STRUCTURE OF ICE

1.1 Structure of water molecule

During the formation of a water molecule the orbitals (e.g. $2p_y$ and $2p_z$) of oxygen are filled with the electrons of hydrogen according to the Pauli exclusion principle (no more than two electrons can occupy the same energy level). At equilibrium, the oxygen and hydrogen atoms are located in the structure shown in Figure 1 and form a covalentic or so called homopolar bond.

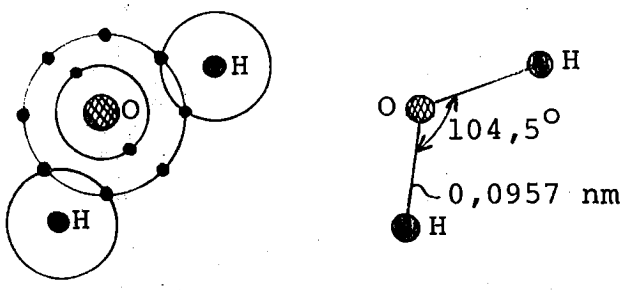

FIGURE 1 : The water molecule

At O K the enthalpy of formation of a water molecule is $15{,}236 \times 10^{-19}$J, but at higher temperatures the corresponding energy is greater (for example at 273 K $15{,}390 \times 10^{-19}$J) because of the vibrational energy of the atoms. /52, 70, 72/. It is interesting to note that the energy required to break a molecule at the first stage (H-O-H into H and O-H) is higher ($8{,}187 \times 10^{-19}$J) than the energy required to break the remaining bond ($7{,}049 \times 10^{-19}$J). The reason is that once the first bond is broken the system is no more stabile.

Deuterium as well can form a compound with oxygen called heavy water. The mass of a D_2O molecule is $3{,}326 \times 10^{-26}$ kg, and the mass of a water molecule is $2{,}992 \times 10^{-26}$ kg /52/. This study however only treats with ice formed of hydrogen and oxygen.

When a water molecule is formed the hydrogen atom becomes positively charged because the electron is drawn farther away from the nucleus during the formation of the covalentic bond. Correspondingly the oxygen atom becomes negatively charged. These electrical charges cause the formation of a permanent dipole in the water molecule and therefore the water molecule is not linear. Further, due to electrostatic forces water molecules can form a group of molecules, which is held together by secondary bonds, called hydrogen bonds. These are much weeker than primary valence bonds; the bonding energy of a hydrogen bond is only $0{,}401 \times 10^{-19}$J. (Figure 3.)

It is typical of water, as of liquids in general, that van der Waals secondary bonds occure between molecules.

When the internal energy is minimized and the water molecules are arranged locally, each molecule is surrounded by four others through hydrogen bonds. Thus a tetrahedral structure is formed (Figure 2), which is typical also of the crystal structure of ice, as shall be seen later.

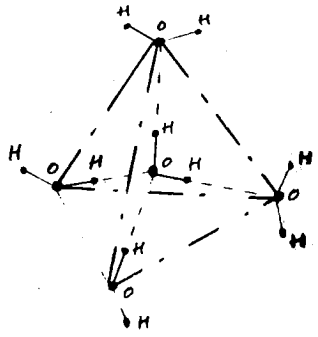

FIGURE 2 : Arrangement of water molecules

But the structure of water is not so systematic as described above, if for example the randomness of the structure caused by the vibration of atoms is considered. In their study on the internal structure of water, Sarkisov, Dashevsky and Malenkov /97/ applied the Monte Carlo method in order to take into account the randomness. Unfortunately no further developments of this method and applied into the structure of ice could be found in the litterature.

By the electrolytic analysis of the structure of water it has been discovered that the share of oxygen is 89 % by weight and that of hydrogen 11 % by weight. The same concentrations of oxygen and hydrogen have also been found in ice and water vapor. Thus the only difference between these three phases is the degree of arrangement of the molecules, which is highest in the solid phase(ice) because of, for instance, the decreasing of the vibrational energy of the molecules at low temperatures /52/.

1.2 Structure of ice crystal

This paragraph studies the structure of ice formed near the melting point and under normal pressure (ice Ih).

As early as in the year 1921 Bragg discovered that the crystal structure of ice is determined by the basic form of local arrangement of the water molecule, in which the neighbouring molecules of a given molecule are located as a tetrahedron (see Figure 2). The structure of an ice molecule remains the same as that of the water molecule; only the dimensions change (Figure 3). /70, 104, 110/.

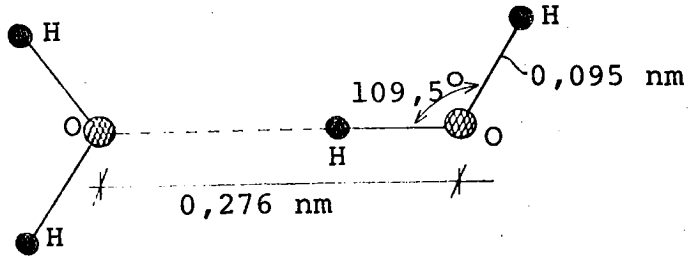

FIGURE 3 :
A hydrogen bond between two ice molecules

When studying the arrangement of ice molecules in the space, as shown in Figure 2, it can be seen (Figure 4) that there are six different possibilities to construct a tetrahedral structure containing all the hydrogen bonds required.

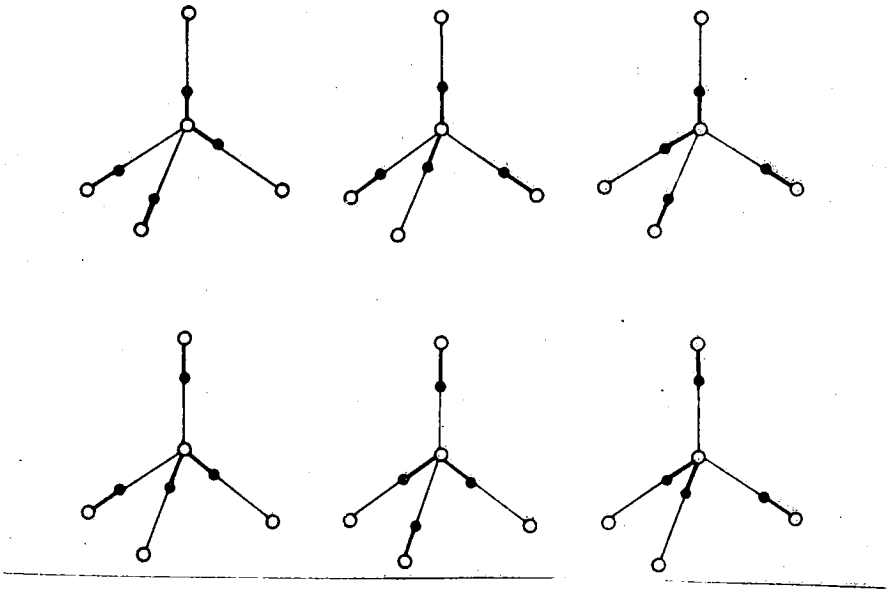

FIGURE 4 :

The six possible arrangements of the hydrogen atoms of the four bonds around each oxygen atom in ice Ih. O - oxygen. ● - hydrogen atoms. /52/

The location of the hydrogen molecules is random. Only the motive formed by the ice molecule is univocally arranged and forms a global, hexagonal crystal structure. (Figure 5.)

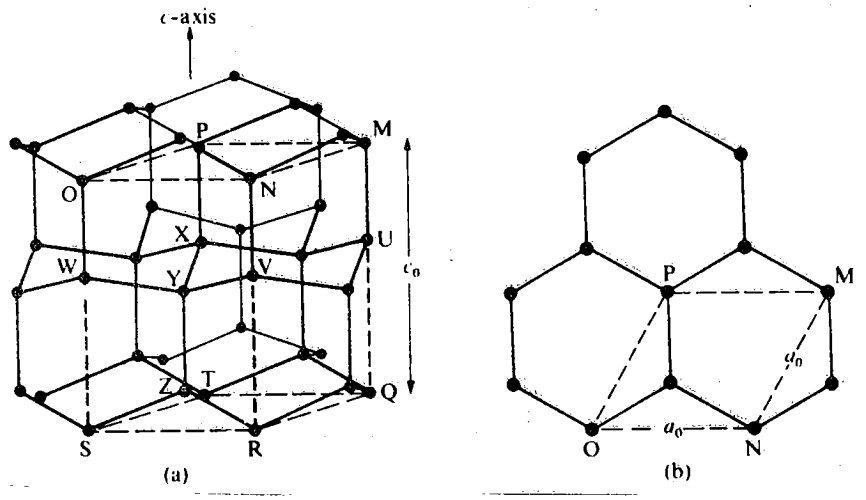

The arrangement of the oxygen atoms in ice Ih: (a) view perpendicular to the c-axis. (b) view along the c-axis /52/

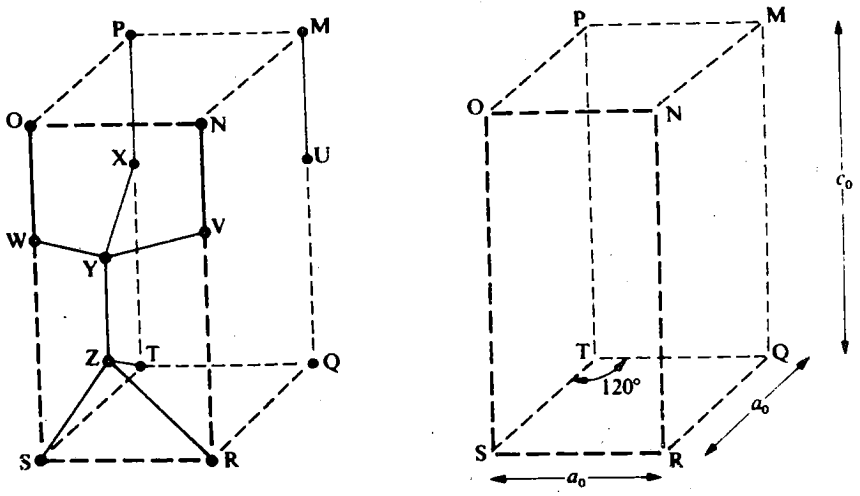

Ice Ih: (c) unit cell (d) primitive space lattice /52/

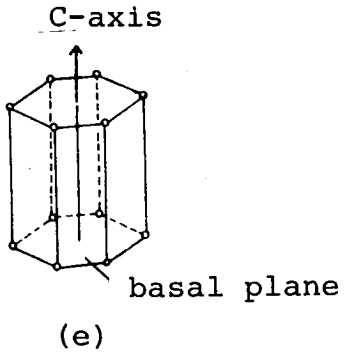

Hexagonal crystal structure. The rings present a molecule motive. /64/

FIGURE 5 : The crystal structure of ice /52, 64/

The dimensions of the unit cell a_o and c_o have been experimentally determined and found to depend on the temperature: the values differ a little from the theoretical values /20/. At 263 K La Placa and Post have obtained the following results in 1960: a_o = 0,4519 nm and c_o = 0,7362 nm /52/. Assuming that the crystal structure is ideally hexagonal and the density of ice (at 273 K) 916,7 kg/m^3, the distance between the ice molecules (Figure 3) is found to be 0,276 nm. The unit cell constant a_o is then 0,478 nm.

On the basis of the location of different hydrogen atoms of the ice crystal many different crystal models have been suggested. From todays viewpoint Pauling's model seems to be the most suitable. /28, 29, 37, 52, 72, 87/. He suggests that the ice molecules are arranged as Bragg supposed whereas the hydrogen atoms are located randomly but yet according to the Bernal-Fowler rules:

1° There are two protons near each oxygen atom
2° There is only one proton on or near the line joining two oxygen atoms

Besides this Pauling assumes that both hydrogen atoms in every ice molecule form hydrogen bonds as Bragg assumes (the tetrahedral structure is complete) (see Figure 4). According to Pauling's assumption each alternative of Figure 4 occurs with the same probability.

The water molecules at the vertices of the network may have six different orientations with respect to the crystallographic axes (see Figure 4). All 6^N configurations, where N is the number of molecules in the crystal, are not possible because of the strong correlation in the orientation of the neighbouring molecules. After Bernal - Fowler rules there are still about $(3/2)^N$ allowed configurations. It seems that the energy differences between configurations are very small. Further, at high temperatures the transitions from one configuration to another take place because of the presence of the mobile Bjerrum orientational D and L defects, as we later shall see. /41/.

When looking at Pauling's model in Figure 6 it can be seen that the bonds are mirrorsymmetric in the direction of c-axis and middlesymmetric in other directions (see also Figure 5). Because every molecule is bound with three other molecules in the same layer and only one in the next layer, 75 % of the bonds are middlesymmetric.

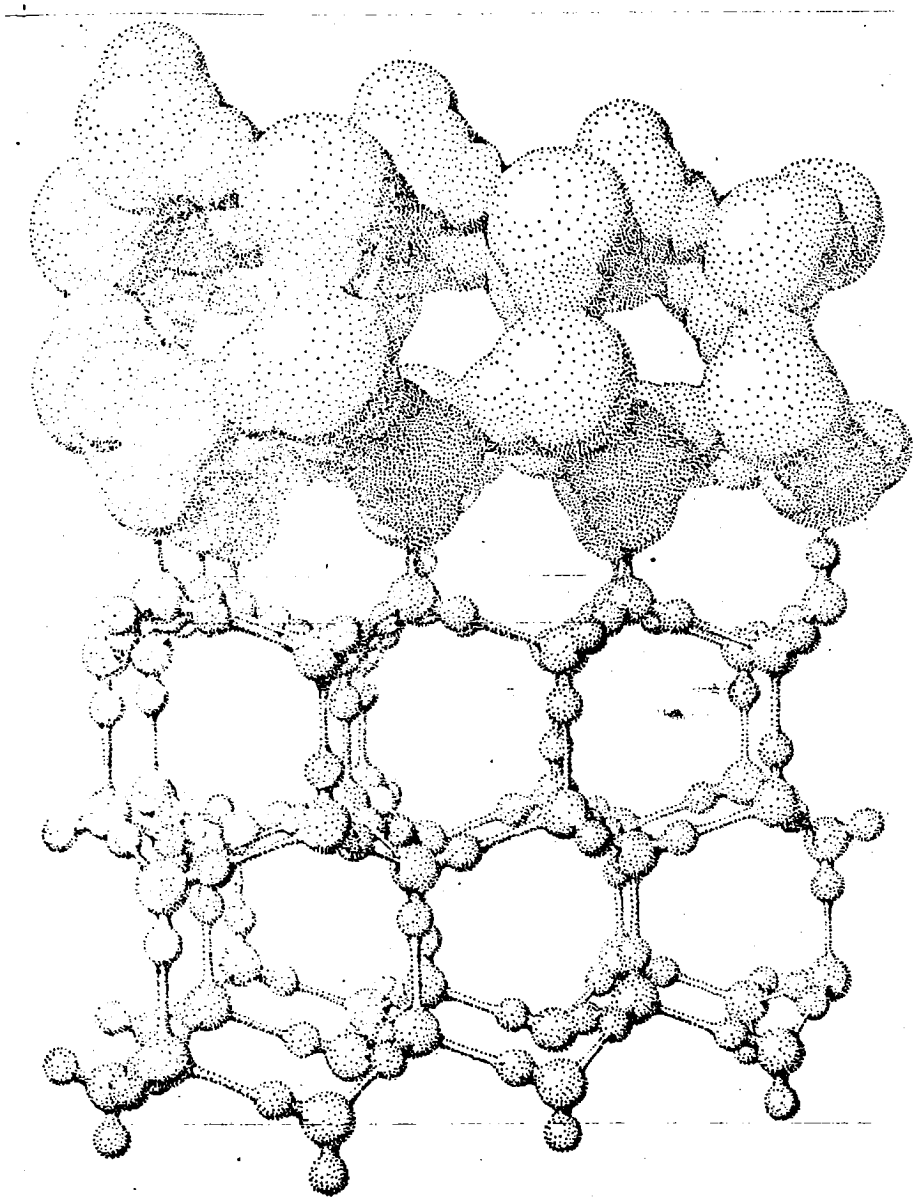

FIGURE 6 :

A small part of a crystal of ice. The molecules above are shown with approximately their correct size (relative to the interatomic distances). Note hydrogen bonds, and the open structure that gives ice its low density. The molecules below are indicated diagrammatically as small spheres for oxygen atoms and still smaller spheres for hydrogen atoms. /87/.

Besides form Ih, which was studied above, ice can occur in nine other different forms depending on the pressure and the temperature. Figure 7 shows the phase diagram for the different crystal forms of ice according to Hobbs /52/.

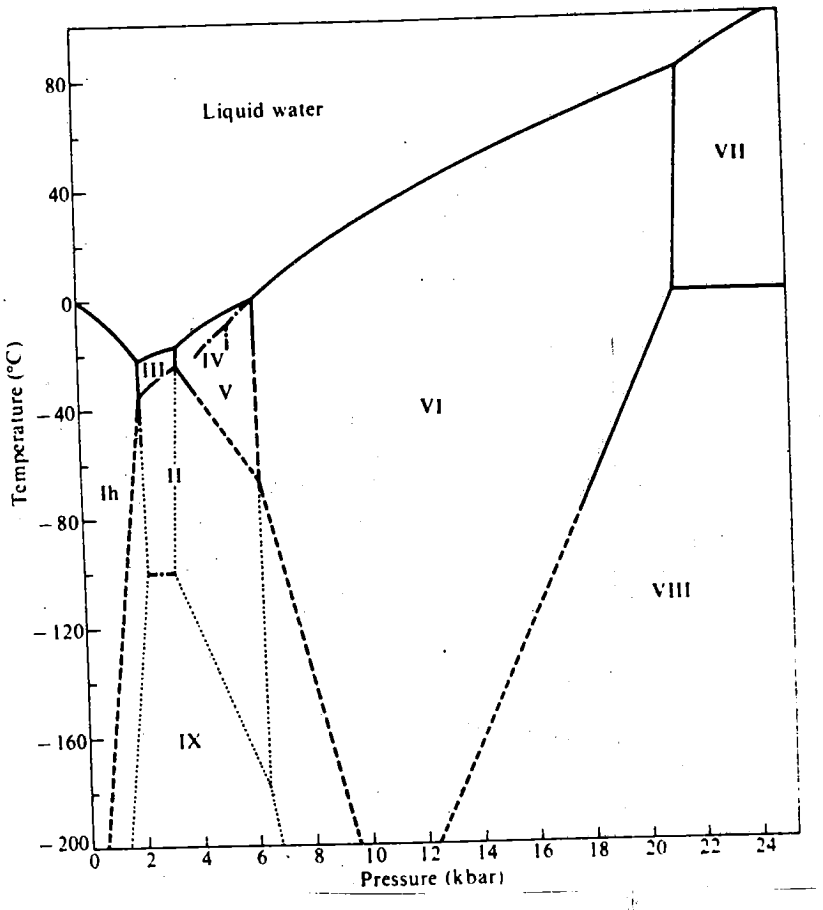

FIGURE 7 :
Phase diagram of the solid phases of water. ——— measured stable lines. -—-—-—measured metastable lines. — — — extrapolated or estimated stable lines. ----- extrapolated or estimated metastable lines. Ice IV is metastable in the region of stability of ice V: the indicated field for ice IV is inferred from the D_2O system. Ice Ic and vitreous ice are not indicated. /52/.

As we can see, ice occurs in form Ih within the temperature and pressure region where the problematics of this study lies. In the continuation, therefore, the properties of Ih ice only will be discussed. More closely the subject will be ice formed by normally freezing fresh water, in other words the so-called columnar grained ice. On this basis for example snow-ice formed of snow under pressure is left outside this study.

1.3 Structural imperfections of ice crystal

The crystal structure of ice, which was described in Paragraph 1.2 is naturally only theoretical. In ice, as in all other crystalline substances, there are common defects of crystal structure in which the location of atoms or molecules differs from their regular position in the lattice. Such defects are normally classified in three groups: point imperfections (Figure 8), line imperfections (Figure 9) and surface imperfections (for example grain boundaries and stacking faults) (Figure 10).

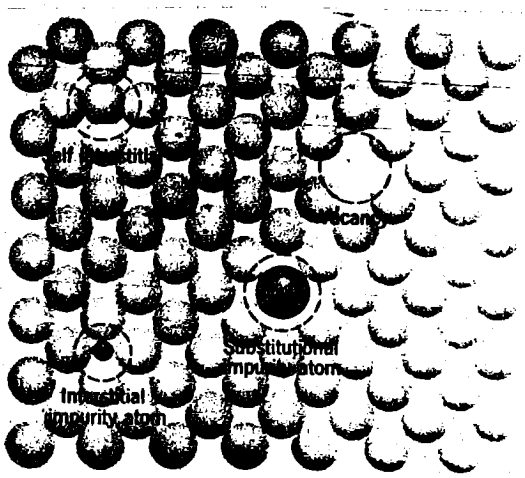

FIGURE 8 :

A two-dimensional representation of a simple crystalline solid, illustrating some of the point imperfections that are possible. /78/

Vacancy and interstitial atom, which can also be atom of another substance, are typical point defects. The movement of the point defect in a material structure is called self-diffusion (vacancy) or diffusion (interstitial impurity atom). The activation energy in the self-diffusion of ice is 62,8 kJ/mol according to Haas /52/ and 52 kJ/mol according to Walker /104/.

From the point of view of the mechanical properties of a material, the most important lattice defect is line imperfection called dislocation. Dislocations in ice were first directly observed by Hayes and Webb (1965) /52/ using transmission X-ray diffraction topography, and screw dislocations were most common (Figure 9b). The screw dislocation causes the crystal structure of ice shear strain which is mainly perpendicular to c-axis. Under certain circumstances, also edge dislocations and partial dislocations have been discovered in ice /52/.

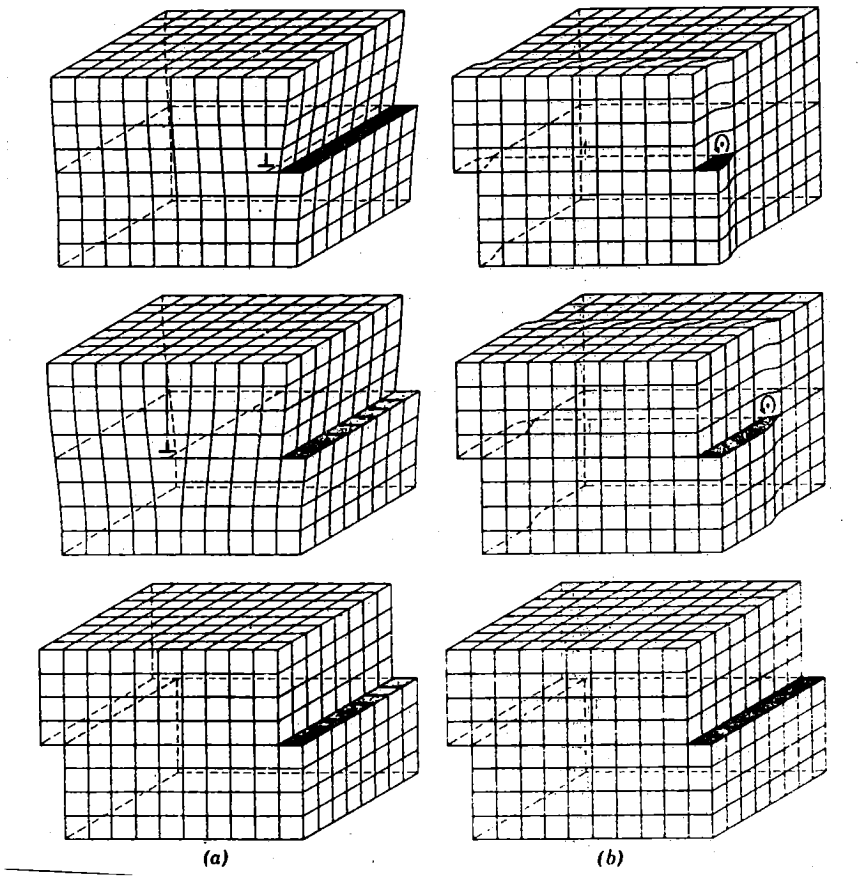

FIGURE 9 :

(a) Slip resulting from the movement (right to left) of a pure edge dislocation through a simple cubic lattice. (b) Slip resulting from the movement (front to back) of a pure screw dislocation through a simple cubic lattice. The dislocations in (a) and (b) have the same Burgers vector so they result in the same amount and direction of slip. /78/

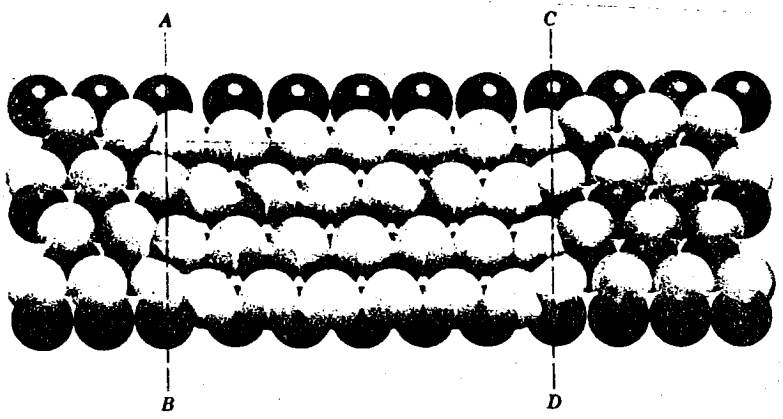

FIGURE 10 :

A view normal to a stacking fault between the lines AB and CD on a close-packed plane, in a HCP (hexagonal closed packed crystal) ice. If the stacking fault is viewed as resulting from the dissociation of a dislocation into two partials. AB and DC are the lines of the partial dislocations. /78/

It has been noted that besides external load, the dislocations may occur also because of the thermal stresses developing during the crystal crowth /46/.

Yosida and Wakahama (1962) studied dislocations and faults in ice using mechanical models. They predicted that in addition to the perfect dislocations and partial dislocations stacking faults (Figure 10) should be possible in ice. But in the work by Hayes and Webb there was no evidence found for the existence of stacking faults. /52/.

In addition to the actual lattice imperfections described above the occurence of some kind of local defects is characteristic of ice. The reason for these is that the hydrogen protons are not located in the lattice structure according to the Bernal-Fowlwe rules (see Page14). A failure of the first Bernal-Fowler rule corresponds to an ionic defect (Figure 11 a and b) and the failure of the second rule is called a Bjerrum defect (Figure 11 c and d). /28/.

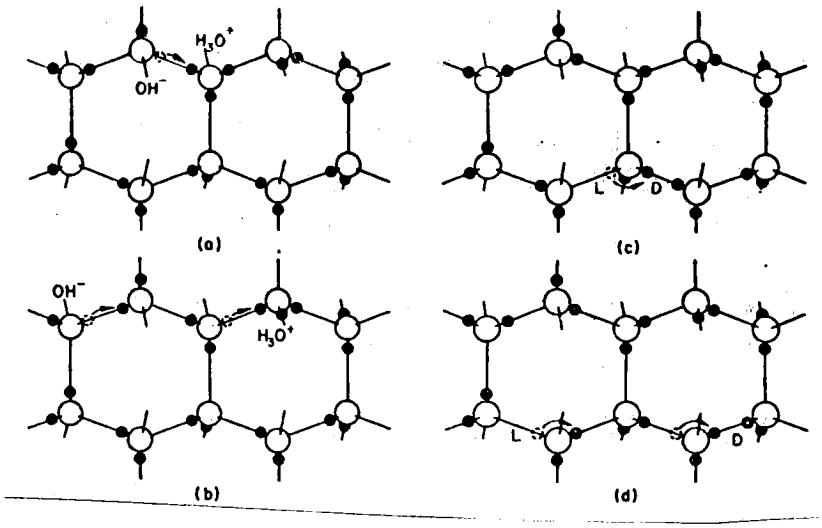

FIGURE 11 :

Diagram to indicate creation and movement of electrical point defects in ice. In (a) the movement of a proton from the position shown with an open circle creates a positive and a negative ion, and (b) shows how the movement of a proton along a bond can make the ions migrate. (c) Shows how a movement of a proton around an oxygen atom can create an L defect and a D defect, and (d) shows how this defect can also migrate. Note that movement of the protons is to the right in all cases, but that the movement of the ions in (b) leaves the water molecules oriented with the protons to their left, while the movement of L and D defects in (d) leaves them with protons to their right. /28/

Decomposing of water molecules to OH^- and H_3O^+ ion is typical for the ionization defect. The developing of the defect requires an energy of 1,570 x 10^{-19}J. On the contrary, during the formation of the Bjerrum defect the structure of the H_2O molecule remains unchanged. The vacancy formed during the rotation of the molecule is called by Bjerrum L (Leer) - defect. Correspondingly the defect caused by the interstitial atom is indicated with D (Doppelt). The energy required for the Bjerrum pair defect is, according to Gränicher, 1,089 x 10^{-19}J /7, 8, 28, 37/.

In single and polycrystals of ice Ih, large cracks were mechanically produced by del Pennino, Loria, Mantovani and Mazzega along prismatic planes. At the same time large potential changes (up to 40 volt) were measured on the surface of the sample. It is pointed out that such a phenomenon may take part in thunderstorm electrification. /88/.

Lately, the research on the crystal structure and especially the structural defects of ice has taken a long step forwards. The possibilities provided by the scanning electron microscope have essentially helped the studying of dislocations /13, 49, 65, 91, 92/.

The above has treated the defects of the crystal structure of ice. Their formation and their influence on the physical properties of ice, especially to its mechanical properties, shall be studied later in connection with the mechanism of deformation.

1.4 Some aspects about natural ice

In the normal freezing of water (for example in lakes), ice crystals are formed around impurities suspended in the water, where the energy required to form stabile nuclei is lower than in the neighbourhood. Thus the randomly oriented crystals form a layer of ice on the water which grows downwards in the direction of the heat gradient. The potential energy of the molecules being at its lowest in the basal plane of the ice crystal, the crystals tend to form so that the c-axis is perpendicular to the direction of growth (Figure 12). The size of the crystals has been found to grow downwards along the growing direction of the ice cover. The reason is that the neighbouring crystals tend to limit the growth of the crystal; the c-axes of different crystals are never completely parallel. Therefore the diameter of ice crystals varies from a few millimeters to several centimeters. The size of the crystals can be studied easily by cutting a thin section of the ice and examining it under polarized light /69/.

Usually the arrangement of the crystal structure is merely local by character. Then the crystals arranged in the same way can form a crystallite with each other. It has been found that the boundaries between crystallites are different when compared with the boundaries between the crystals in a crystallite. There are much less inclusions on the boundaries of crystals than on those of crystallites, where obviously plenty of impurities are collected. This can be clearly seen for example in the fact that the melting of ice always begins at the boundaries of crystallites. The thin water film which Faraday discovered as early as in the 19th century probably has its own signification to the formation of the joint between different crystallites. Fletcher suggests that for temperatures above about 268 K a clean ice surface may be covered by a quasi-liquid layer whose thickness is of order 1...4 nm. /20/.

The formation of the so-called columnar grained ice only has been described in the above. Depending on the circumstances (temperature, pressure, chemical constitution of ice, movement of water), structurally very different kinds of ice may be formed /40/. This paper however will mainly concentrate on the study of the columnar grained ice. Table 1 shows the classification of different kinds of ice by Michel and Ramseier /37/.

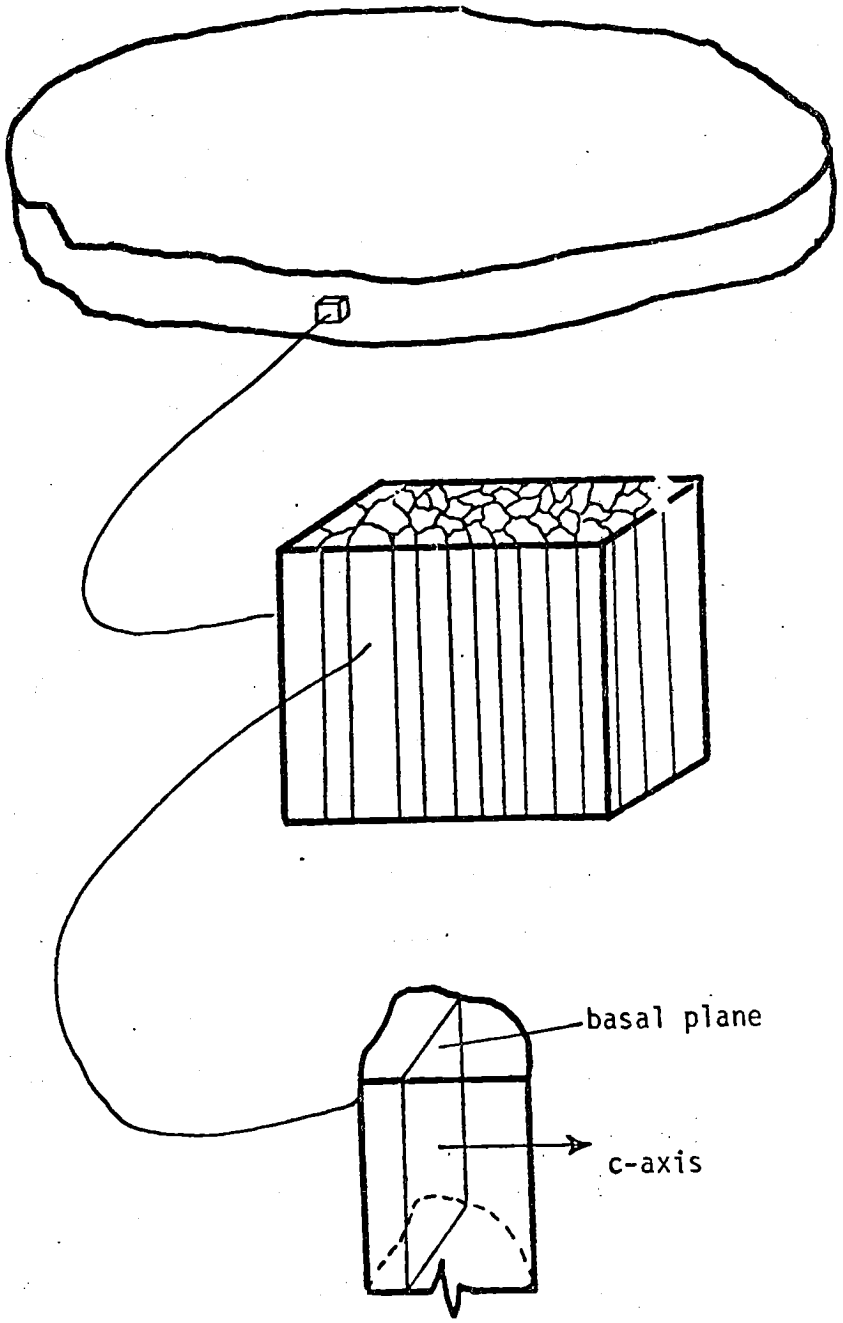

FIGURE 12 : Grain structure in an ice sheet /75/

TABLE 1 : Genetic classification of ice /37/

Primary Ice (ice formed initially)

P1 c-axis preferred vertical; crystal size large to extra large; crystal boundaries of irregular shape.

P2 c-axis orientation random to preferred vertical superimposed on random; crystal size medium to extra large; crystal shape tabular or needle.

P3 Ice cover initiated by frazil; c-axis orientation random; crystal size small to medium; crystal shape equiaxed and tabular.

P4 Ice cover initiated by snow; c-axis orientation random; crystal size small to medium; crystal shape equiaxed.

Secondary Ice (developed from primary ice)

S1 Columnar-grained; c-axis vertical orientation; crystal size increases with depth and is usually large to extra large; grain shape irregular.

S2 Columnar-grained; c-axes tend to become perpendicular to long direction of columns with growth; crystal size small to large increasing more rapidly with depth than type S1.

Tertiary Ice

T1 Snow ice; c-axis orientation random; grains equiaxed; grain size small to medium.

Grain Size

small	Grain diameter	less than	1 mm
medium		between	1 and 5 mm
large		between	5 and 20 mm
very large		greater than	20 mm

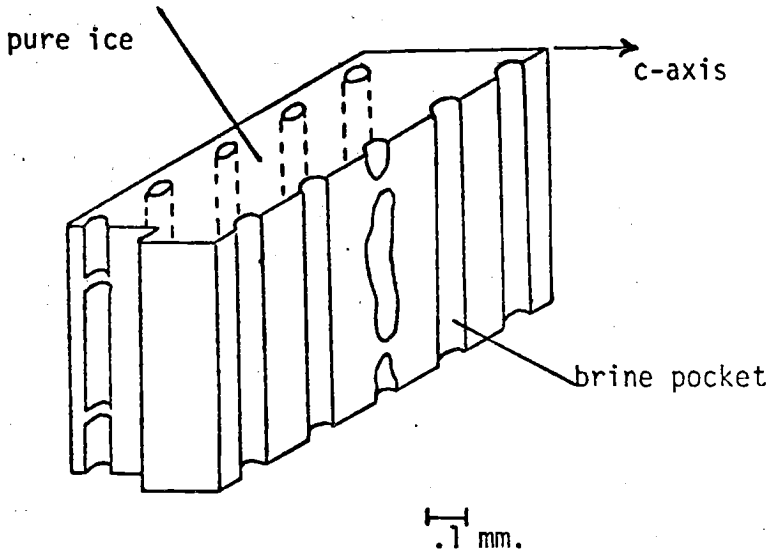

FIGURE 13 : Geometric model of brine pockets /75/

The sea ice differs from what has been mentioned above in that the unarranged surface layer is thicker compared with lake ice and vertical macroscopic cavities are formed in the ice, which contain brine, crystallized salts and air (Figure 13). At the microstructural level the solid component of sea ice is fresh water ice. /75, 106/.

As a summary of the structure of ice some characteristic features can be mentioned:

- Water forms solid phases (different types of ice) more than any other known substance.

- Ice occures generally near its melting point (especially type Ih).

- The crystals of ice are relatively large compared with the crystals of other crystalline materials.

- Despite the open lattice structure of ice, it is able to form solid solutions with very few inorganic compounds, such as HF, NH_3 and NH_4F. A consequence of the incorporation of these molecules into the lattice is that Bjerrum defects are also generated. /104/. Such impurities as do not form a stabile compound with ice gather gradually and form pores and cavities in the ice (compare with the sea ice structure in Figure 13).

2 MECHANICAL PROPERTIES OF ICE

2.1 Dislocations in ice

When an external load acts on a crystalline material, either elastic or plastic deformation occurs. During elastic deformation the atoms change their location so that equilibrium between external forces and forces between the atoms is reached. Then after releasing the external load the deformation returns to its original state. In the plastic deformation, on the other hand, the order of atoms changes and a permanent deformation arises.

Thus a necessary condition for plastic deformation is that the influence of the external load exceeds the activation energy of the strain process concerned.

In the main, the plastic formation of a crystal takes place mainly so that the different parts of the crystal slip with regard to each other along slip planes. By each crystal type this translational slip has an activation energy of different magnitude depending on the slip plane. In ice the translational slip occures easiest in the basal plane of the crystal, which is perpendicular to the c-axis.

Consequently, the plastic deformation in material is caused by internal, thermally activated molecular processes. And because the relaxation times for some significant atomic processes in crystals are so long that complete equilibrium is seldom achieved, the creep of crystalline materials can be easily understood. According to Arrhenius the following experimental general equation is valid for such a deformation process i /104/:

$$\dot{\gamma}_i = f_i \exp\left(\frac{-Q_i}{RT}\right) \qquad (1)$$

where $\dot{\gamma}_i$ is e.g. velocity of the translational slip, $f_i = f_i(T, \tau, str)$ is a frequence factor and is in turn dependent on the absolute temperature T, the applied stress τ, and some substructural details. $Q_i = Q(T, \tau, str)$ is the activation energy. Usually the deformation is caused by many simultaneous molecular processes. If the processes are sequential the observed strain rate in steady state will refer to the slowest process. If they are independent the observed strain rate will be given by $\dot{\gamma} = \Sigma_i \dot{\gamma}_i$. At high homologous temperatures ($T/T_m \approx 1$) the low activation energy process will have short relaxation time and will occur readily and further deformation will depend on processes having higher activation energies.

For most metals the activation energy of creep has been found nearly constant at the temperature region between o,5 T_m and T_m. Then the activation energy of creep, Q_c, has been experimentally determined using the empirical equation

$$\dot{\varepsilon}_s = A\, \sigma^n \exp\left(\frac{-Qc}{RT}\right) \qquad (2)$$

where $\dot{\varepsilon}_s$ is the steady state creep rate, σ is stress, Q_c is the activation energy for creep and n is a constant having value between 3 and 5. Constant A is often taken temperature dependent.

In their closer studies of the mechanism of translational slip Taylor, Orowan and Polanyi, in 1934, arrived at the dislocation theory according to which the translational slip does not happen simultaneously on all slip planes but in a successive wave as figure 9 clearly shows. Especially in studies of metals the dislocation theory has been found to agree well with the observations about the mechanism of strain. However, not until 1965 did Hayes and Webb discover the occurence of dislocations in the ice crystal. Later especially the development of the applications

of the electron microscope has made it possible to study the deformation properties of polycrystalline ice successfully. Thereby it has been found out that the pure translational slip on the basal plane is not sufficient to explain the plastic deformation of polycrystalline ice. The stress concentrations which grow on grain boundaries cause slip on the prism planes as well. Kink bands are also observed within the grains.

When examining the movement of a dislocation in the ice crystal it is interesting to study the meaning of the Bjerrum and ionization defects. Since the structure of the ideal ice crystal is fully arranged only when a H_2O molecule is concerned, but partly random in respect to hydrogen atoms, it is obvious that the passing of a dislocation in a defectless crystal causes changes to the location of protons against the Bernal-Fowler rules. The top of Figure 14 shows a part of a defectless structure through which the dislocation shall pass (the centre diagram). The final result is a crystal structure which is formed when the lower part of the crystal moves to a new equilibrium position. A Bjerrum defect has been created in the structure; a D-defect on BC´and an L-defect on CD´. If the hydrogen atoms move so that no Bjerrum defects are created, the result looks like Figure 15. But in this case a ionization defect (H_3O^+ at C and OH^- at C´) has been created in the structure.

In his article /28/ Glen proposes an estimation for the stress, which causes such a passage of the dislocation that Bjerrum or ionization defects are created in the lattice structures. Glen assumes that the orientation of a bond in the ice structure is random. But as was stated in the bottom of Page 14, this is not quite true. However it is easy to see that this restriction means that such an estimate will underestimate the true number of defects. On this presumption it can be seen that in a defectless

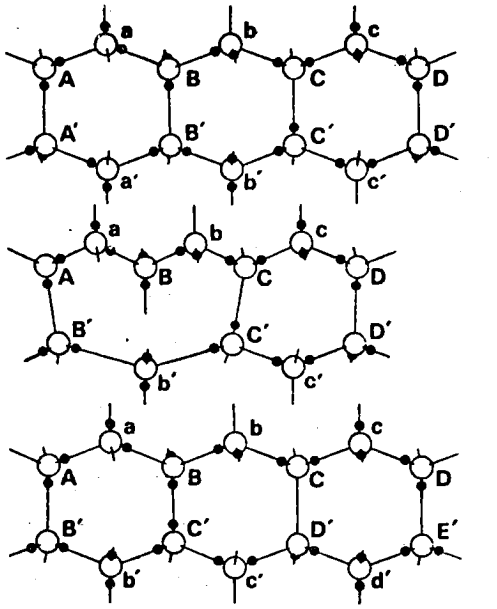

FIGURE 14 :

A portion of an ice lattice showing the point defects which would be created by the passage of a dislocation. The lattice at the top obeys the Bernal-Fowler rules, but the passage of a dislocation, as shown in the centre diagram, would create defects which can be seen in the bottom diagram - a D-defect on BC´ and an L-defect on CD´ /28/.

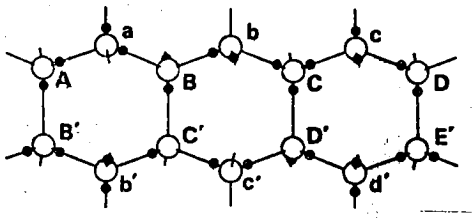

FIGURE 15 :

Alternative end state for the passage of the dislocation shown in Figure 14 if the hydrogen atoms move along their bonds to prevent the creation of Bjerrum defects. Note the negative ionic state at C´ and the positive ionic state at C /28/.

structure the construction of two adjacent parallel hydrogen bonds is consistent with a probability of 0,5 (the oxygen atom is at the same end of the bond). Also exactly half of the bonds would have Bjerrum defects after movement of the

dislocation. The energy needed to create the Bjerrum pair defect is 1,089 x 10^{-19}J (see Page 11) and consequently for one defect 0,545 x 10^{-19}J are required. And because only half of the bonds create Bjerrum defect, the energy required is 0,272 x 10^{-19}J per bond. Further, the amount of bonds per unit area of the basal plane is according to an elementary geometric calculation $(\sqrt{3}\ a_o^2/2)^{-1}$. If the Burgers vector is marked with b and the shear stress required for the passage of dislocation σ, we have

$$\sigma \times b = \frac{0{,}272 \times 10^{-19}\text{J}}{\frac{\sqrt{3}}{2}\ a_o^2} \Longrightarrow \sigma = \frac{0{,}545 \times 10^{-19}\text{J}}{\sqrt{3}\ a_o^2\ b} \qquad (3)$$

Glen supposes the magnitude of the Burgers vector to be equal to the lattice parameter a_o, from which we obtain σ = 341 MPa. However according to many experiments, the shear strength of ice is of the magnitude 0,1 MPa. If we look at the formation of an ionization defect, the energy required is 0,785 x 10^{-19}J per bond, and so we get an even higher value for σ. Accordingly it can be assumed with reason that the hydrogen atoms are reoriented by thermally activated point defects ahead of the dislocation. Thus the velocity of dislocations depends essentially on the transformation of the H_2O - molecule in such a way that the dislocation can pass. Formation of kinks (sensitive to stress) and a low velocity are characteristic to this type of dislocation passage. In the same way it can be explained that the effect of impurities on the properties of ice is caused by the Bjerrum and ionization defects.

In next two chapters the mechanisms of plastic deformation in ideal ice will be studied. The experimental models presented in them are associated with experiments made with fresh water ice. Thus the mechanical properties of sea ice will be left outside this study (the models for the fresh water ice may be partly adapted to the sea ice especially when the salt content is low). These are treated e.g. in the study The mechanical properties of sea ice by Weeks and Assur /106/.

2.2 Plastic deformation of ice single crystal

A single crystal of ice is supposed to be deformed mainly plastically owing to the passages of dislocations in the lattice structure. During experiments all investigators have observed a steady increase in the creep rate with time, and in constant strain rate experiments a yield point is observed. This phenomenon can be examined by Johnston's dislocation multiplication theory /104/ which Jones and Glen have applied to ice /58/.

According to Johnston's theory (which has been applied to LiF) a crystal originally contains some moving dislocations which have been created by for example thermal stresses during the formation of the crystal. The deformation rate caused by the moving dislocations can be presented according to Cottrell /58/ in the form

$$\dot{\varepsilon} = b\,\rho(\varepsilon)\,v\,(\tau) \qquad (4)$$

where b is the Burgers vector of the dislocation, ρ is dislocation density and v is dislocation velocity, which is function of shear stress. We can see that the smaller the ρ is at the time zero, the higher is the yield point. On the other hand, during the passage of the dislocation ρ increases (Frank-Read's dislocation source) so that the constant strain rate requires a smaller shear stress. This can be seen as exceeding of yield point. In creep experiments the stress is constant and thus also the velocity of dislocations is constant. The number of dislocations grows rapidly at the beginning of the experiment and $\dot{\varepsilon}$ becomes higher (primary or transient creep) until equilibrium is reached, and the number of rising dislocations is the same as that of disappearing dislocations (ρ is constant) and $\dot{\varepsilon}$ is constant (secondary or steady-state creep). In practice it is difficult to get the stress to be constant and therefore most creep experiments are performed

using constant load. That is why in tension tests, for instance, the stress increases because of the deformations in the test piece, the velocity of dislocations becomes higher and ρ remains nearly constant. This is tertiar creep, in which $\dot{\varepsilon}$ increases rapidly before the final break. With metals the tertiar creep is only seldom observed during compression tests. On the contrary especially in polycrystalline ice the tertiar creep is caused by changes in the crystal structure, e.g. recrystallization and not so much by the deformation of the test piece. In this case the tertiar creep can be created also in constant stress tests.

In an ice crystal dislocations pass most easily on the basal plane (basal glide or easy glide). This phenomenon has been studied e.g. by Jones and Glen /58/. The results of their creep tests (tension tests) showed that there was no clear work-hardening and that shear strain on the basal plane with time obeyed the equation

$$\varepsilon = a\, t^{m} \qquad (5)$$

(when ε is between 0,3 % and 4 %)

where a and m are constants.

Also many other investigators /75/ realizing that there was no observable steady state creep attempted to express the strain as a function of time for a given stress in the form (5). Constant a is often function of temperature and stress level. In their compression tests Griggs and Coles obtained for exponent m the value 2,0 on a temperature range between 272 K and 255 K and under a stress between 0,2 MPa and 1,4 MPa. On the basis of their tests Higashi, Koinuma and Mae /47, 48/ also arrived at the same conclusion that ice crystals do not work-harden. They also observed that Johnston's theory can be applied to ice.

If in equation (5) the exponent m = 1,5, we see that $\dot{\varepsilon}/\varepsilon^{1/3}$ is a constant which depends on the shear stress acting on the basal plane of the crystal. Jones and Glen /58/ studied this correlation applying the model

$$(\dot{\varepsilon}/\varepsilon^{1/3}) = (\sigma/\sigma_o)^n \qquad (6)$$

when σ_o is constant. The values for m and n obtained on the basis of their tests are presented in Table 2. It shows, that parameter m does not depend on temperature.

TABLE 2 : Parameters m and n in eq. (5) and (6)

T(K)	m	n	
223	1,5 ± 0,2	1...4	when σ = 0,1...0,6 MPa
213	1,4	1...4	
203	1,6	2,3	independent on σ

The article by Jones and Glen however contains no estimation of the suitability of the model to temperatures near the melting point of ice.

It could perhaps be pointed out that better correlation with the test results was obtained using model

$$\log (\dot{\varepsilon}/\varepsilon^{1/3}) = a + b \log \sigma + c (\log \sigma)^2 \qquad (7)$$

where a, b and c are constants.

For activation energy of basal glide Jones and Glen /58/ propose the values

(65 ± 3) kJ/mol between 263 K and 223 K
(40 ± 2) kJ/mol between 223 K and 183 K.

To study the velocity and density of dislocations in ice Jones and Glen /58/ performed also constant strain rate experiments by compressing ice cylinders and applying to the results the model based on the equation (4) developed by Johnston for LiF. In this way the dislocation density ρ was found to be 5×10^{9} m^{-2} and the dislocation velocity $1,5 \times 10^{-8}$ m/s at the moment of yielding and $0,21 \times 18^{-8}$ m/s after the yielding. The strain rate which corresponds to the values mentioned above was $2,7 \times 10^{-7}$ s^{-1}. The low values obtained for the dislocation velocity are probably explained by the fact that the arrangement of Bjerrum defects limits the passage of dislocation in the lattice, as mentioned in Chapter 1.

In their study Readey and Kingery /91/ made among others the following conclusions. Firstly, there was no preferred crystallographic slip direction or work hardening observed, secondly, annealing after deformation has no effect on subsequent deformation behavior of ice, and thirdly, it is proposed that the observed plastic deformation of ice results from glide of dislocations whose velocity is limited by a temperature activated process.

Nakaya /52/ observed that mean distance of the gliding layers (slip bands) on the basal plane is about 60 nm. It is clear therefore that not all of the molecular layers parallel to the basal plane are involved in the slip.

The plastic deformation in ice can naturally occur also in other directions than on the basal plane. Such deformation is called non-basal glide (or hard glide). The most obvious difference between basal and non-basal glide are firstly the yielding stress which in the hard glide is nearly 20-fold compared with the easy glide, and secondly the work hardening is considerable in non-basal glide, which is understandable with the hexagonal crystal structure. Though, the activation energy of creep has nevertheless been observed to be of same magnitude in both cases. Therefore the exponent n in the Arrhenius equation (2) has the value 6,5 in the hard glide creep. The corresponding value for the basal glide creep is 1,5.

Taking into account the essential importance of the Bjerrum and ionization defects in the passage of dislocations, the effect of dissolved impurities on basal glide is easy to understand. Jones and Glen /57/ discovered that at 203 K small amounts of dissolved hydrogen fluoride (HF) have a softening effect, ammonia (NH_3) produces a slight hardening and ammonium fluoride (NH_4F) has no apparent effect. The effect of HF to the creep rate can be expressed with the equation

$$\dot{\varepsilon} = \text{constant} \cdot c^{0,62} \qquad (8)$$

where c is the concentration of HF as ppm. For example tap water and once distilled water may contain 1 ppm and 0,5 ppm of fluorine respectively.

2.3 Plastic deformation of polycrystalline ice

The plastic deformation of polycrystalline ice is a much more complicated process than that of single ice crystals. The reason is that the crystals of polycrystalline ice are arranged as separate grains nearly randomly and the size of the crystals and direction of the c-axis vary. The studies have shown that plastic deformation of polycrystalline ice near the melting point is controlled by non-basal slip and that the creep rate of polycrystalline ice is $10^2 \ldots 10^3$ times slower than that of single crystals oriented for easy glide /101/.

In the 1950's, Glen /27, 52/ performed compression creep tests with polycrystalline ice at different temperatures and stress levels. He found some work hardening, where the creep was comparable to the cube-root of time. At stresses over 0,4 MPa tertiary creep was observed. Glen suggested that the decelerating creep which occurs during the transient creep of polycrystalline ice is due to progressive interference between grains with different orientations and

the reacceleration which occurs in tertiary creep is caused by recrystallization which produces grains oriented more favourably for glide. For the creep rate in the secondary creep Glen proposes the following equations

$$\dot{\varepsilon}_s = A(T)\ \sigma^n \qquad ;\ n = 3...4$$

$$\dot{\varepsilon}_s = B(\sigma)\ \exp \frac{-135}{RT} \tag{9}$$

$$\begin{cases} T = 260{,}2\ K...271{,}5\ K \\ \sigma = 0{,}1...1\ MPa \end{cases}$$

Steinemann /52/ proposes an extension to Glen's model including in the exponent n both the stress level and the temperature

$$\dot{\varepsilon}_s = \text{constant} \cdot \exp\left(\frac{-Q_c}{RT}\right)\ \sigma^{[n_o + f(\sigma,T)]} \tag{10}$$

In Steinemann's opinion, too, the recrystallization is an important factor in the plastic deformation of multi-crystalline ice.

Shumskii /32, 52/ considers that a number of mechanisms act in the deformation of polycrystalline ice. These mechanisms, which become important in turn as the creep rate increases, are: basal slip, slight disturbances of the crystal lattice, grain growth and grain boundary migration, distortion of the crystal lattice, polygonization and primary recrystallization, grain boundary sliding, fracture and pressure melting. Naturally, it is impossible to control this many deformation processes with one model. It is obvious, anyway, that the number and importance of the different processes decrease when the crystals become more arranged and the size of the crystals grows.

This is why most scientists have chosen to apply the Arrhenius model (2) to secondary creep rate. The dependence of exponent n (often assumed to be about 3 for polycrystalline ice) on the stress has been studied in several experiments /104/. On low stress levels ($\sigma << 0{,}1$ MPa) the deformation only seldom exceeds 0,1 % and the creep is still transient even with long experiment times. Transient creep implies that a dislocation mechanism is operative since the strain rate should be independent of strain in Newtonian flow ($n = 1$) where the rate controlling process is the migration of vacancies along a stress gradient (Herring-Nabarro creep). Only Steinemann has performed at low stress levels experiments long enough to create secondary creep. On the stress level below 0,1 MPa exponent n is nearly 2 which suggests that both dislocation glide and vacancy creep are contributing to the observed creep rate, and that at sufficiently low stresses (below 0,01 MPa) Newtonian creep is rate controlling.

The study of Barnes, Tabor and Walker about the creep of polycrystalline ice /3, 100, 104/ is very interesting. They performed compression tests with cylindrical test pieces which were made of distilled and ion-exchanged water (conductivity $0{,}5 \times 10^{-4}$ Sm^{-1} and less than 5×10^{-3} kg/m^3 dissolved solids). The density of the ice was more than 910 kg/m^3 and the grain size between 1 and 2 mm. The accuracy of the test temperature was about 10^{-1} K.

In their study Barnes, Tabor and Walker started from the assumption that the total strain before the tertiary creep caused by recrystallization can be expressed as function of time by superposition of the elastic strain, the primary creep and the secondary creep. Then the Cottrell - Aytek equation can be applied

$$\varepsilon = \varepsilon_o + \beta\, t^{1/3} + \dot{\varepsilon}_s t \qquad (11)$$

where ε_o is the instantaneous strain, β a suitable constant and $\dot{\varepsilon}_s$ the true secondary creep rate. The term $\beta t^{1/3}$ describes the transient creep which dominates the equation

when t is small, while $\dot{\varepsilon}_s t$, the steady-state creep, represents the final flow rate which is approached asymptotically. The secondary creep rate of ice can be described by an Arrhenius type of equation (2). The secondary creep rate can be expressed also in the form presented by Garofalo

$$\dot{\varepsilon}_s = A' (\sinh \alpha\sigma)^n \exp (-Q/RT) \qquad (12)$$

where A' and α are suitable constants. The values (Figure 16) obtained experimentally for equations (12) and (2) are shown in Table 3, where we can see that the value of exponent n is about 3 independently of the temperature and stress level (sinh-model). On the other hand it is interesting to note that the activation energy changes when the temperature exceeds 265 K.

On the basis of their experiments Barnes, Tabor and Walker suggested that different mechanisms dominate in the deformation of polycrystalline ice at different temperatures and stresses.

1° The microcreep regime (deformation at temperatures below 263 K)

The creep behavior is dominated by basal glide of dislocations and not by dislocation climb. This is the same mechanism as controls creep in single crystals and the mobility of the dislocations is probably determined by the concentration of point defects (see Page 29...31). However Glen's theory /28/ does not explain the great difference between the creep of the single ice crystal and polycrystalline ice. According to Weertman /52/ the difference in the creep rates of polycrystalline ice and single crystals of ice oriented for easy glide is due to the fact that the resolved shear stress on the basal plane of any grain in a polycrystalline mass is less than the applied stress.

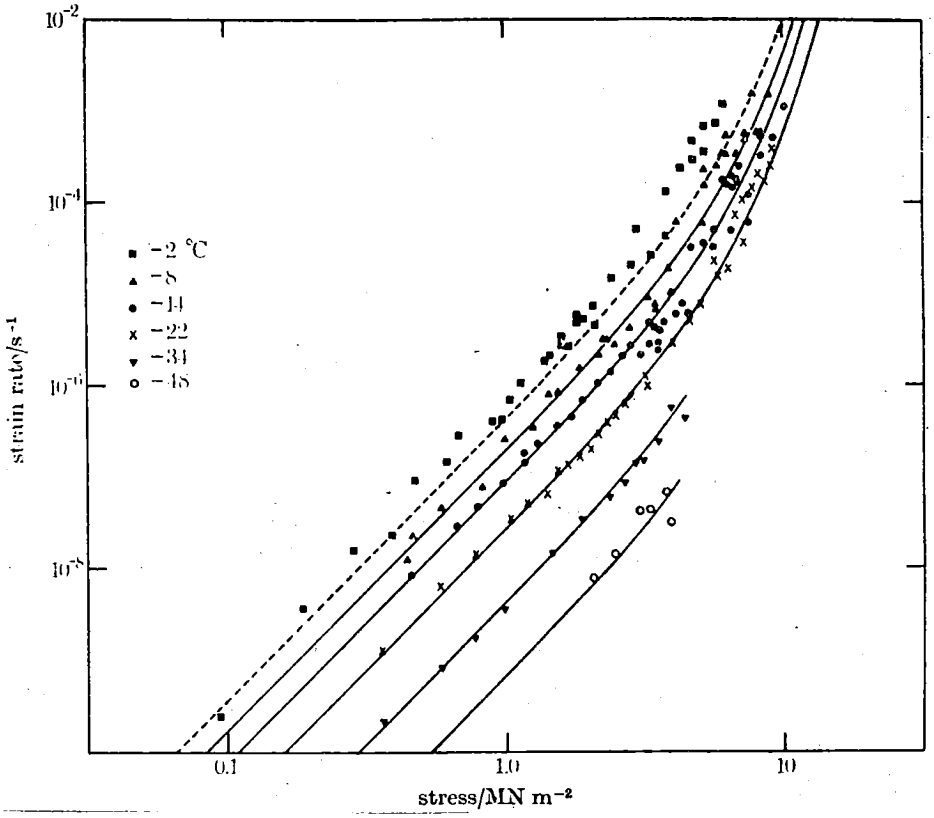

FIGURE 16 :

Secondary creep rate plotted against the applied stress on logarithmic coordinates. The curves are calculated sinh functions based on all the experimental points between -8 and -48°C. It can be seen that the calculated curve for -2°C (shown as a broken line in the figure) lies well below the experimental points obtained at -2°C, indicating that the ice is creeping faster than would have been predicted by extrapolation from lower temperatures. /3/

TABLE 3 : DEFORMATION OF POLYCRYSTALLINE ICE.
ANALYSIS OF SECONDARY CREEP /3/

whole stress range: $\dot{\epsilon}_s = A'(\sinh\alpha\sigma)^n \exp(-Q/RT)$

A'/s^{-1}	α/MN^{-1} m^2	n	Q/kJ mol^{-1}	temperature range °C
4.60×10^{18}	0.279	3.14	120.0	−2 to −8
3.14×10^{10}	0.254	3.08	78.1	−8 to −14
1.88×10^{10}	0.282	2.92	78.1	−14 to −22
2.72×10^{10}	0.262	3.05	78.1	−8 to −45

low stress range: power law region $\dot{\epsilon}_s = A\sigma^n \exp(-Q/RT)$ $\sigma \leq 2.8$MPa

A/s^{-1} (MN^{-1} m^2)^n	n	Q/kJ mol^{-1}	temperature range °C
1.68×10^{17}	3.16	121.4	−2 to −8
6.50×10^{8}	3.01	78.6	−8 to −14
7.56×10^{8}	2.98	78.8	−14 to −22
2.25×10^{8}	3.11	76.4	−22 to −34
2.23×10^{8}	3.18	67.3	−34 to −45
9.72×10^{7}	3.08	74.5	−8 to −45
2.32×10^{18}	3.08	72.8	−8 to −45†

† Including modulus correction

2° The grain boundary regime (deformation at temperatures between 263 K and 270 K)

The measurements of Barnes and Tabor on the hardness and creep of polycrystalline ice indicate that ice becomes significantly softer and the creep rate is greater than that predicted by extrapolation from lower temperatures. There appear to be two processes involved: the formation of liquid at the grain boundaries and grain boundary sliding (see Page 22).

3° The pressure melting regime (above 270 K)

The strain in this region can be devided in three groups: the actual creep which is obtained by extrapolating from lower temperatures, the effect of the surface pressure caused by the load on the lowering of the melting point of ice and grain boundary melting. In their article /2/ Barnes and Tabor assume that for ice colder than 271,8 K the pressure required to produce plastic deformation is not sufficient to produce pressure melting.

Gold /32/ suggests the following mechanisms for the plastic deformation of ice: slip bands, grain boundary migration, small angle boundaries, kink bands, distortion of grain boundaries, crack formation, cavities in the region of grain boundaries and the intersection of slip planes and subboundaries, recovery and recrystallization. Of these specially the formation and growth of cracks have been widely studied by Gold /31, 32, 37/.

In the experiments of Gold it was observed that cracks begin to form during creep when the constant compressive stress exceeds about 0,6 MPa. For stresses less than 1 MPa, the cracking activity was confined primarly to the primary creep stage. When the stress was greater than about 1,2 MPa, crack formation brought on the failure condition before the secondary creep stage could be established. Gold found that cracking activity was essentially random and made observations on the probability distributions for crack density, width and orientation.

3 EXPERIMENTAL STUDIES OF MECHANICAL PROPERTIES OF ICE

3.1 General aspects

Plenty of studies have been made on the mechanical properties of both single ice crystals and polycrystalline ice. Usually the polycrystalline ice has been prepared so that snow or crushed ice has been strewn on the surface of freezing distilled water. Thus a randomly oriented crystal structure with crystal size 1...2 mm is achieved. In some studies, including this one, polycrystalline ice has been made by letting water freeze free in a sufficiently large vessel. Then the c-axes of crystals are randomly oriented in the horizontal plane of the sheet. For preparation of single ice crystals, a Bridgman technique /92/ is usually applied. In some studies natural ice has also been used.

To study the compression, tension and shear strength of ice mainly the following experiments are used:

(i) Uniaxial compression test /2, 3, 30, 31, 37, 57, 58, 92, 96, 103, 104/

These have been generally performed on cylinders or rectangular prisms having a height to width ratio between 2 and 3. Some investigators have also used cubes.

(ii) Uniaxial tensile test /45, 47, 55, 56, 57, 58, 91/

In axial tension experiments, the fixing of the test piece to the loading apparatus usually poses problems. Therefore tension strength of ice has been studied also in experiments (iii)...(v).

(iii) Flexural test /48, 62, 64/

(iv) Ring test and Brazil test /6, 82, 83, 95/

(v) In-situ cantilever test /10, 42, 95/

(vi) Shear test /102/

The following inequation seems to be the rule for different tension tests /75/

$$\sigma_{(iv)} > \sigma_{(iii)} > \sigma_{(ii)} > \sigma_{(v)} \qquad (13)$$

Wide scatter of results is characteristic to all strength experiments of ice. The reason is first of all the dependence of the results on the following factors: loading rate, test temperature and relative humidity, grain structure of test ice (also the chemical composition of the water), stress and temperature history (freezing and preparation of test piece induces initial stresses and strains in ice), sample size (scale effect). Besides those, the study of sea ice also involves other variables such as salinity, brine drainage, solid salt reinforcement and age of ice (e.g. loss of brine).

In early 1972 the study on different ice loads and mechanical properties of ice were started in Department of Structural Engineering of Helsinki University of Technology. Since studies on the strength, deformations, movements and loads of ice also imply studies on the thermoviscoelastical peoperties of ice, it was considered necessary, in addition to litterature studies, to try to develop a mathematical model for the thermorheological properties of ice with laboratory experiments. The next chapters will therefore deal with the creep experiment system developed during the above project and with the results of a series of tests made in 1976. In addition the experimental arrangement is described with photographs in Appendix 2.

3.2 The experimental procedure

3.21 Test specimens

Creep and strength tests were performed by compressing cylindrical pieces with a diameter of about 75 mm and a height of about 160 mm.

The test pieces were made of tap water ice. According the water analysis (Appendix 3) the conductivity of the tap water was 26,3 mSm^{-1} and the evaporation residue 270×10^{-3} kg/m^3. It is interesting to observe that the corresponding values for melted ice were 1,3 mSm^{-1} and 32×10^{-3} kg/m^3. The air content of the water was reduced by warming the water to 333 K before freezing. The use of distilled water was deliberately avoided when preparing the test pieces (contrary to many scientists), in order to better simulate the circumstances of nature. A small comparative test series was performed with lake water ice, and because the results showed no difference it was desided for practical reasons to use only tap water ice.

Water cooled in the open air was brought into a temperature of 263 K in 40 x 50 x 30 cm^3 plastic vessels. The bottom and sides of the vessels were thermally isolated, with the purpose of simulating the freezing process of nature which develops downwards from the water surface. The c-axes are then perpendicular to the long axes of the ice columns and randomly oriented in the horizontal plane of the ice sheet. Freezing time was 10 days, during which a sufficiently thick layer of airless ice was formed in the vessel. The pressure developing under the ice layer during freezing was not released though it caused plenty of air pores on the bottom of the ice layer, because the airless ice layer was still sufficient for preparation of test specimens (Figure 17).

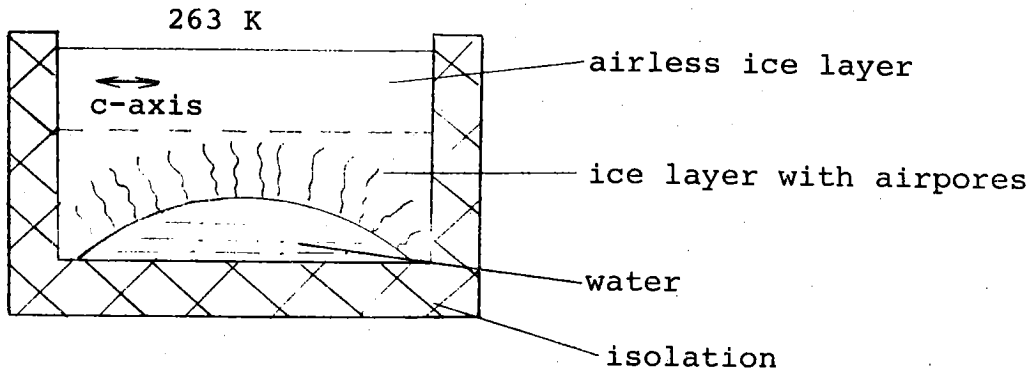

FIGURE 17 : Freezing vessel after 10 days

The ice was sawn with a manual saw to six blocks, from which the test pieces were bored thermally with resistance wire. The boring time was about 10 min per test piece. During boring the surface of the test piece naturally melted a little and that caused rearrangement of crystal structure on the sides of test piece. Its effect on the results was not taken into account.

The thermally bored test pieces were kept at the experiment temperature for 24 hours before they were trimmed with a band saw. The trimmed pieces were loaded after 24 hours. In this way the sufficient balancing time for the temperature of the test pieces was ensured.

The following measurements were made for test piece: diameter at three points (Figure 18), height and weight P. The precission of measurements was 0,1 mm and 0,1 g. The density ρ of every test piece was calculated on the basis of the measured values. The results of the measurements and the densities of the test pieces are shown in Appendices 3 and 4 and a summary is given in Table 4.

$$\rho = \frac{12}{\pi} \frac{P}{H \Sigma D_i^2} \quad ; \ (i = 1, 2, 3) \qquad (14)$$

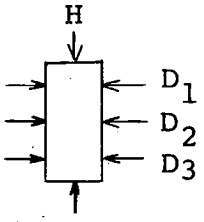

FIGURE 18 : Dimensions of test pieces

TABLE 4 : Precissioness of the sizes of test pieces

T	$\bar{P}$	s	$\bar{H}$	s	$\bar{D}_1$	s	$\bar{D}_2$	s	$\bar{D}_3$	s	$\bar{\rho}$	s	n
Strength test specimens													
268	612,0	15,5	159,7	0,4	72,9	1,1	72,9	0,9	73,0	1,3	918	6	61
263	622,9	13,2	160,2	0,6	73,5	0,9	73,6	0,9	73,4	1,1	916	8	55
253	615,9	11,7	156,6	2,2	73,5	0,7	73,7	0,4	73,7	0,6	924	5	31
Creep test specimens													
271	624,1	16,0	159,7	0,6	73,4	0,8	73,6	0,8	73,4	1,4	922	8	26
268	616,5	10,7	160,3	1,0	73,4	0,6	73,1	0,8	72,5	0,9	918	10	32
263	610,8	17,3	159,9	1,8	72,8	1,2	72,9	1,2	72,8	1,3	917	7	36
253	632,5	4,5	159,3	0,8	73,5	0,7	74,0	0,3	74,1	0,3	926	5	12

The dependence of ice density on temperature can be expressed e.g. according to Pauling /87/

$$\rho = \{917,0 + (273 - T)\ \frac{1}{10\ K}\ \}\ kg/m^3 \qquad (15)$$

which means that the test pieces are nearly airless ice.

The test pieces were bored nearly perpendicularily to the growth direction of ice. It can therefore be supposed that the applied stress is perpendicular to the long axis of the ice columns and in the plane of the c-axis. In the crystal analyses the crystal size was found large (see Table 1). Though there were too few crystal analyses to study reliably the crystal size and direction of c-axis.

3.22 Test conditions

Creep tests were performed in a freezing room, the temperature accuracy of which was more than 1 K. The relative humidity of the test room air varied between 75...86 %. Owing to the technics of the freezing room (continuous cold air blow) also evaporation of the test pieces was examined. Figure 19a shows the evaporation of the test specimens kept in the test room without cover as weight-% and as function of time. Figure 19b shows the effect of a plastic cover built around the loading apparatus to prevent evaporation. There we can see that in ordinary 24 h test the weight loss caused by evaporation in the test piece is about 0,4 %. In addition during experiments longer than 24 h the individual test pieces were also covered with a thin plastic film.

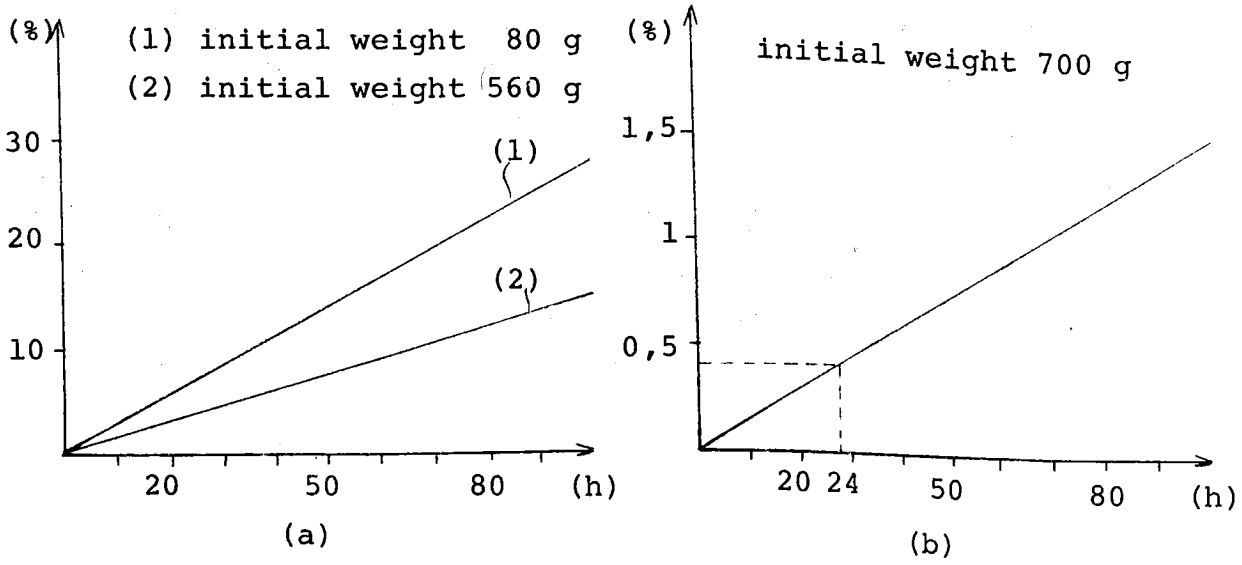

FIGURE 19 : The evaporation of ice (T = 265 K)

3.23 Test apparatus

Strength tests were made with an ordinary hydraulic press (max. power 1 MN, accuracy 100 N) with constant loading rate. The compression machine was located outside the freezing room.

For creep experiments a lever arm apparatus was constructed (Figure 20). With the apparatus four test pieces could be loaded simultaneously with constant load. The loading apparatus was isolated from the floor of the freezing room with a vibration dampener and placed under a plastic cover to prevent evaporation.

The test piece was placed between two steel plates so that the upper plate was joined with a hinge to the loading apparatus. No attempts were made to eliminate the friction between the test piece and the steel plates but the plates were covered with cloth to prevent the test piece from slipping. This naturally caused some transversal deformation near the ends of the test piece, but because the creep strain was measured in the middle of the test specimen it can be assumed that the interference did not reach the measuring area.

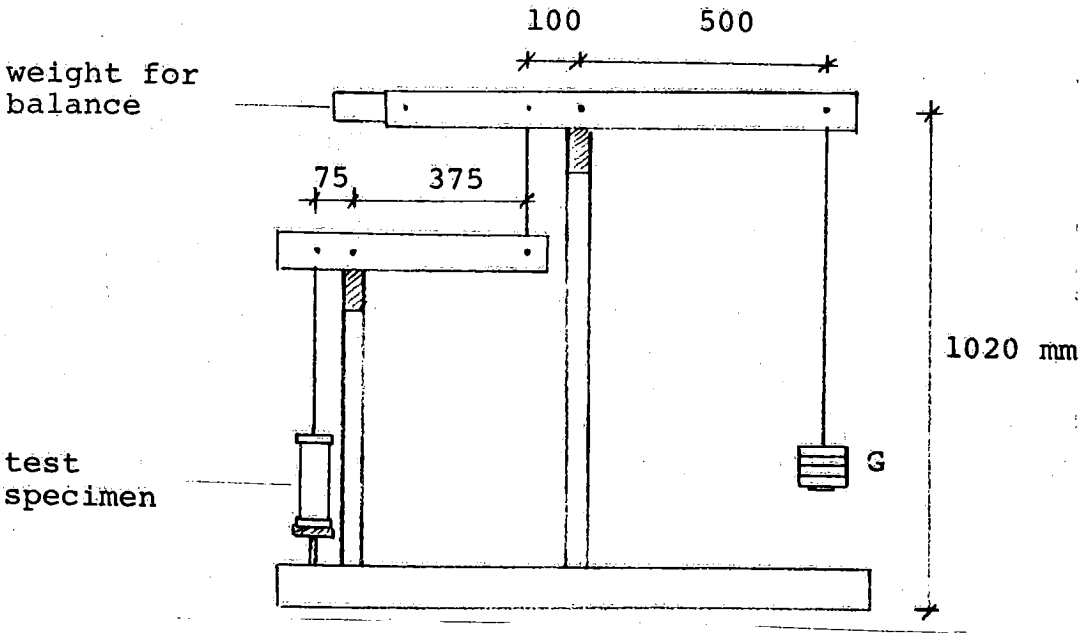

FIGURE 20 : Test apparatus for creep tests

The axial strain of the test piece was measured with a measuring frame (Figure 21) fixed to the specimen, using an inductive strain gauge. Measured values were registered automatically with a datalogger on punched tape at certain intervals (see Table 5). The data tapes were further treated with HP 2000 F time-sharing computer and result curves were drawn with a plotter.

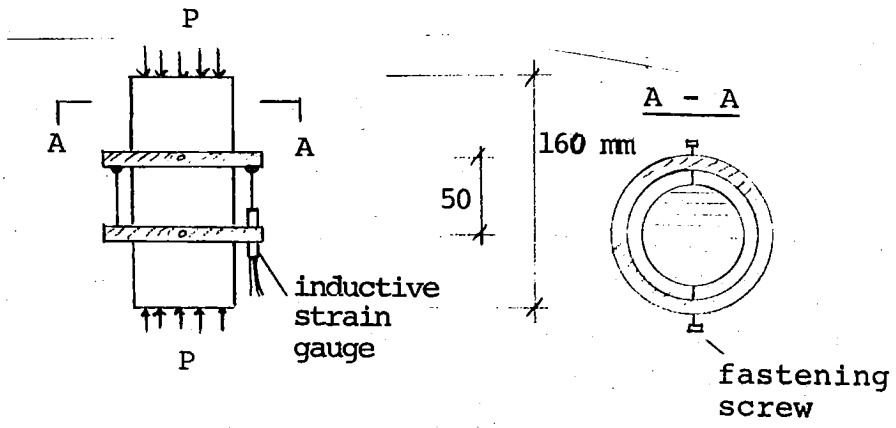

FIGURE 21 : Strain measuring system

TABLE 5 : Time intervals in data logging

Time	Interval
beginning + 30 s	2 s
... 5 min	10 s
...15 min	20 s
...30 min	1 min
...1,5 h	5 min
1,5 h...	20 min

The developed measuring system could only measure axial strain whereas the rotation and slipping of the test piece could not be measured. If the measuring rings would have been fixed to the ice separately with three fixing screws

and the strain would have been measured with three gauges, better results could obviously have been obtained. On the other hand at low stress levels, as in this test series, the loading in the direction of the c-axis causes mainly axial strain.

Corresponding compression test apparatuses have been used e.g. by Gold /33, 37/ and Walker /104/.

Figure 22 is a scheme of the creep test arrangement, the form of the test specimen and the measuring system used by Gold. The measuring frames are fixed to the test piece through freezing. The creep is measured with two inductive gauges. Owing to the form of the test piece the stress condition is obviously not as axial as in the case of cylindrical test specimens. On the other hand with rectangular test specimens the preparation of the test piece and the fixing of the measuring gauge are easier than with cylindrical test specimens.

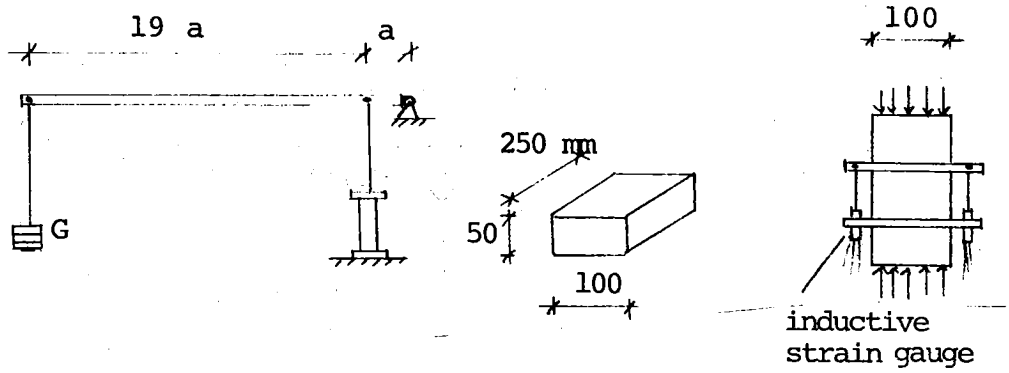

FIGURE 22 : Gold's experimental arrangement

The loading apparatus used by Walker is shown in Figure 23. The strain growing in the cylindrical test piece is measured from the movement of the loading frame. By this means the results of course are not as reliable as when the creep is measured straigth from the test piece, even if the former method attempts to eliminate the friction between ice and loading apparatus.

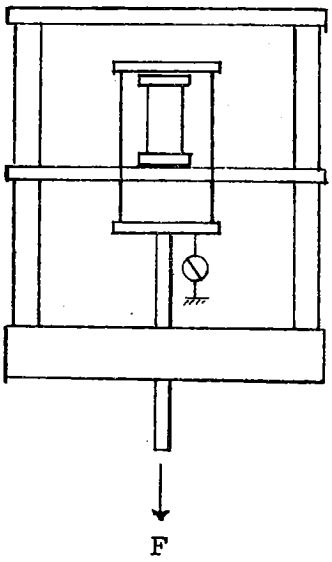

FIGURE 23 : Walker's experimental arrangement

3.24 Estimation of errors

3.241 Variation of form of cross-section the test specimen

In a creep test the stress level developing in the test specimen varied depending on the accuracy of the weights (G) used in the test apparatus and that of the middle diameter (D_2) of the test piece. The stress level changed of course also with the creep because of the transversal deformation in test piece, but in this study only engineering stress was used. When calculating the stress level in creep tests only the value of diameter D_2 was used, because the strain was measured in the middle of the test piece. The variation of the diameter of the test piece was caused by variations in the melting of the test cylinder on different sides of the bore during the thermal boring. Table 6 contains the results of the measurements performed with four test pieces.

TABLE 6 : Variation of the diameter D_2

	1	2	3	4
$D_2(\phi = 0)$	72,4	73,5	73,1	73,4
$D_2(\phi = \pi/4)$	73,4	73,2	73,2	73,1
$D_2(\phi = \pi/2)$	72,1	72,9	73,0	72,6
$D_2(\phi = 3\pi/4)$	73,3	71,9	72,1	72,4
$\bar{D}_2$	72,80	72,88	72,85	72,88
s mm	0,65	0,69	0,51	0,46

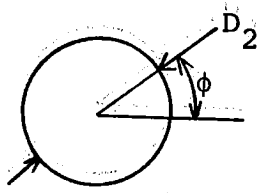

Thus -1,5 % and +1,0 % could be taken as maximum error for variation of the diameter D_2. The measuring accuracy was then also taken into consideration.

The state of stress of the test specimen was calculated with the formula

$$\sigma = \frac{4\,F}{\pi D_2^2} \tag{16}$$

where F was the force which affected the test piece and was caused by the weights G

$$F = 25\ g\ G \tag{17}$$

For proportional error was obtained

$$\frac{\Delta\sigma}{\sigma} = \frac{\Delta G}{G} - 2 \cdot \frac{\Delta D_2}{D_2} \tag{18}$$

For the fault caused by the weights ($\Delta G/G$) values depending on the nominal stress level (or magnitude of weights) were obtained. The minimum and maximum errors for every nominal stress level are noted in Table 7.

TABLE 7 : Errors in nominal stress levels

Stress level (MPa)		$\frac{\Delta G}{G}$ (%)	$\frac{\Delta \sigma}{\sigma}$ (%)
0.1	min	-1,09	-3,09
	max	+0,51	+3,51
0.2	min	-1,09	-3,09
	max	+0,51	+3,51
0.5	min	-0,21	-2,21
	max	+0,15	+3,15
0.7	min	-0,08	-2,08
	max	+0,11	+3,11

3.242 Variation of test temperature

The accuracy of the temperature of the freezing room during the tests was more than 1 K. Before an experiment the temperature was allowed to stabilize for 2 hours. During the experiment the temperature was measured with a Pt-resistance thermometer and registered with a plotter. It was observed that deviation from the test temperature was 1 K at the most and that the change of temperature happened without exception so that the temperature was again back at the test value within 1 hour. Such deviations of temperature occured during the same experiment four times at the most. Thus the effect of the temperature variation on the test results can only be seen as small bends in the creep curves, and the variation of the temperature had no effect on the initial elasticity modulus.

The thermal expansion coefficient for ice can according to Butkovich /11/ be presented in the form

$$\alpha = (52{,}52 + 0{,}1852\ t + 0{,}00885\ t^2 + 0{,}000237\ t^3) \times 10^{-6} \qquad (19)$$

$$(t) = {}^{o}C$$

This can be considered as an average coefficient of linear thermal expansion for all types of ice with a maximum standard deviation of $\pm 0{,}8 \times 10^{-6}\ K^{-1}$ at any temperature to 243 K.

Consequently, the maximum value for the thermal expansion of a test piece is obtained at 271 K which, when the temperature changes 1 K, is

$$\Delta\varepsilon_1 = 52{,}18 \times 10^{-6} = 0{,}052\ ‰ \tag{20}$$

The effect of the temperature change on the strain gauge and other electronic measuring devices causes the following error of the strain

$$\Delta\varepsilon_2 = 1{,}6 \times 10^{-3}\ ‰ \tag{21}$$

As combined effect we obtain

$$\Delta\varepsilon_T = \Delta\varepsilon_1 + \Delta\varepsilon_2 = 0{,}054\ ‰ \tag{22}$$

3.243 Effect of evaporation of test specimen

Evaporation of the test piece was measured to be 0,4 weight-% during a 24 hours test. If evaporation per unit area of cylinder barrel is considered constant, we obtain

$$\frac{\Delta V}{V} = \underbrace{\frac{\Delta H}{H}}_{\approx 0} + 2 \cdot \frac{\Delta D}{D} = -0{,}4\ \%$$

$$\Longrightarrow \frac{\Delta D}{D} = -0{,}2\ \% \tag{23}$$

$$(18) \Longrightarrow \frac{\Delta\sigma}{\sigma} = +0{,}4\ \%$$

In experiments longer than 24 hours, evaporation was not significant because the test pieces were covered with plastic film.

3.3 Failure tests

The purpose of the short test series was to study approximately the failure strength of the ice used in creep tests. It is important to note the inaccuracy of these experiments which was mainly due to the unsuitability of the loading apparatus for so small loads. However the magnitudes of the strengths are probably reliable and comparable with each other.

Ice cylinders were compressed in the direction of the c-axis of the crystal with 1 MN hydraulic loading machine variating the loading rate in different tests (in each test the loading rate was constant). Besides the break load also the time needed to break the test piece was measured (starting at the moment when the force began to grow and ending when the force did not grow any more). Owing to the uncertain failure moment the accuracy of the timing was only 1 s.

The compression apparatus was located in a room where the temperature could not be regulated sufficiently. The test pieces were brought from the freezing room where the temperature was either 268 K, 263 K or 253 K and placed between the precooled compression plates in the compression machine. We can however assume that during the experiments the mean temperature of the test specimens was very close to the desired test temperature.

The dimensions of the test pieces and the results of the experiments are presented in Appendix 4.

The strength of each test specimen was calculated using the smallest cross section area.

$$\sigma_M = \frac{4}{\pi} \frac{F_M}{\min \{ D_i^2 \}} \quad ; \; i = 1, 2, 3 \tag{24}$$

where F_M is the break load measured.

Table 8 contains a summary of the results of all the failure strength tests classified according to loading times. The clearly differing values were left out (indicated with x in Appendix 4) and averages and deviations shown in Table 9 were obtained for failure strengths. The corresponding values are presented in Figures 24a...c.

TABLE 8 : Strength values (all tests)

	T = 268 K			T = 263 K			T = 253 K		
t_M(s)	$\bar{\sigma}_M$	s	n	$\bar{\sigma}_M$(MPa)	s	n (kpl)	$\bar{\sigma}_M$	s	n
0... 2	1,198	0,485	10	1,073	0,397	10	0,001	0,528	6
3... 5	1,151	0,705	14	2,275	1,100	10	1,688	0,931	5
6... 8	2,159	0,541	2	2,722	0,895	10	1,999	1,002	2
9...11	1,574	0,608	8	2,923	0,994	7	1,851	0,932	4
12...14	1,998	0,568	7	3,263	1,913	4	1,626	-	1
15...25	2,277	0,614	14	2,474	1,384	5	2,087	0,644	10
26...46	1,940	0,279	5 60	3,357	0,527	5 51	2,401	1,014	3 30

TABLE 9 : Strength values σ^*_M

$$\bar{\sigma}_M - s \leq \sigma^*_M \leq \bar{\sigma}_M + s$$

	T = 268 K			T = 263 K			T = 253 K		
t_m	$\bar{\sigma}^*_M$	s'	n'	$\bar{\sigma}^*_M$	s'	n'	$\bar{\sigma}^*_M$	s'	n'
0... 2	1,222	0,303	6	1,022	0,228	7	1,177	0,338	5
3... 5	1,167	0,390	9	2,264	0,617	6	1,331	0,553	4
6... 8	2,159	0,541	2	2,577	0,458	8	1,991	1,002	2
9...11	1,673	0,352	6	3,350	0,348	4	1,851	0,932	4
12...14	2,314	0,209	5	3,094	1,320	2	1,626	-	1
15...25	2,362	0,258	9	2,374	0,916	3	1,786	0,340	6
26...46	1,963	0,068	3 40	3,195	0,442	4 34	2,968	0,366	2 24

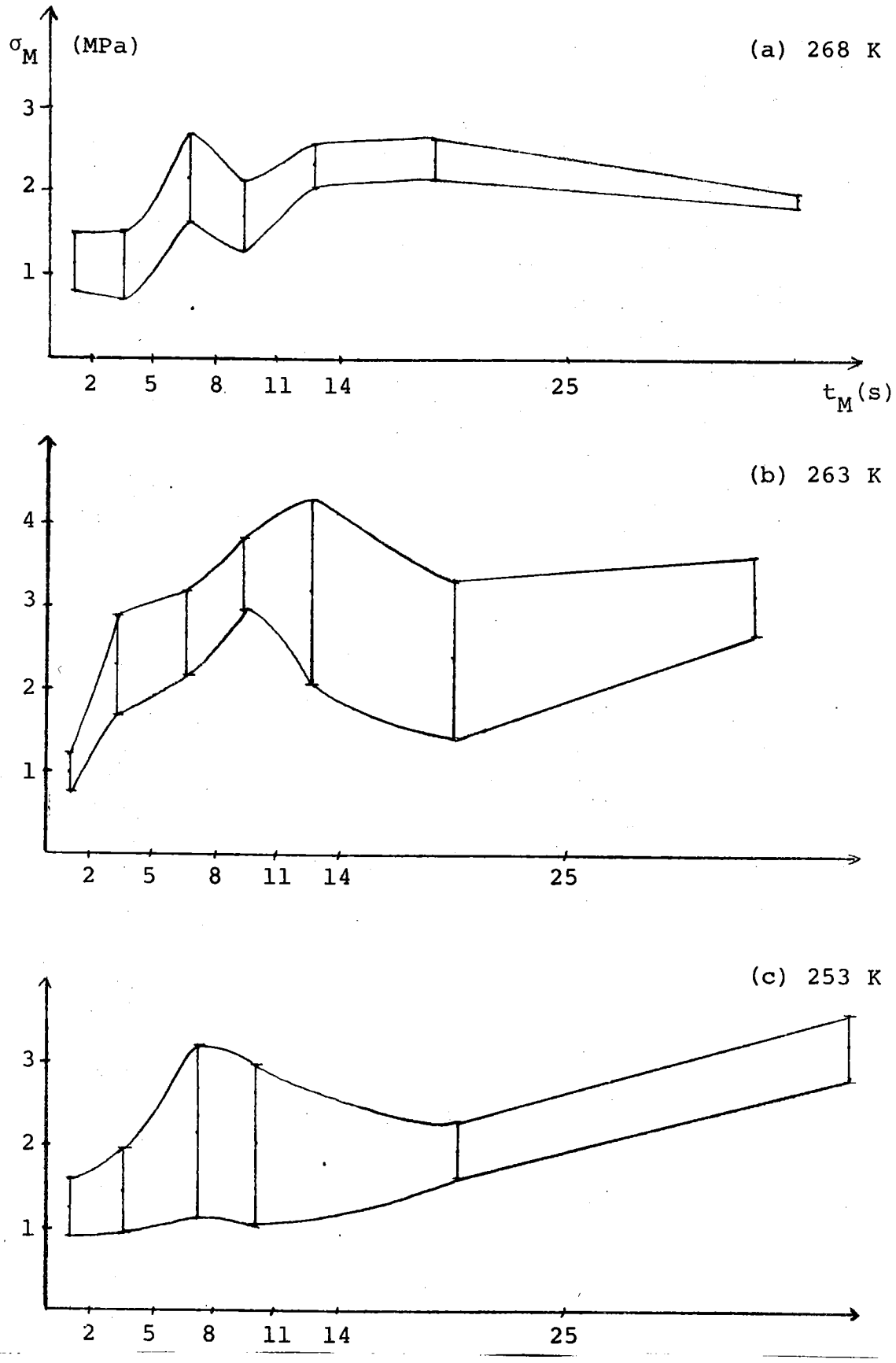

FIGURE 24 : Compressive strength of test ice

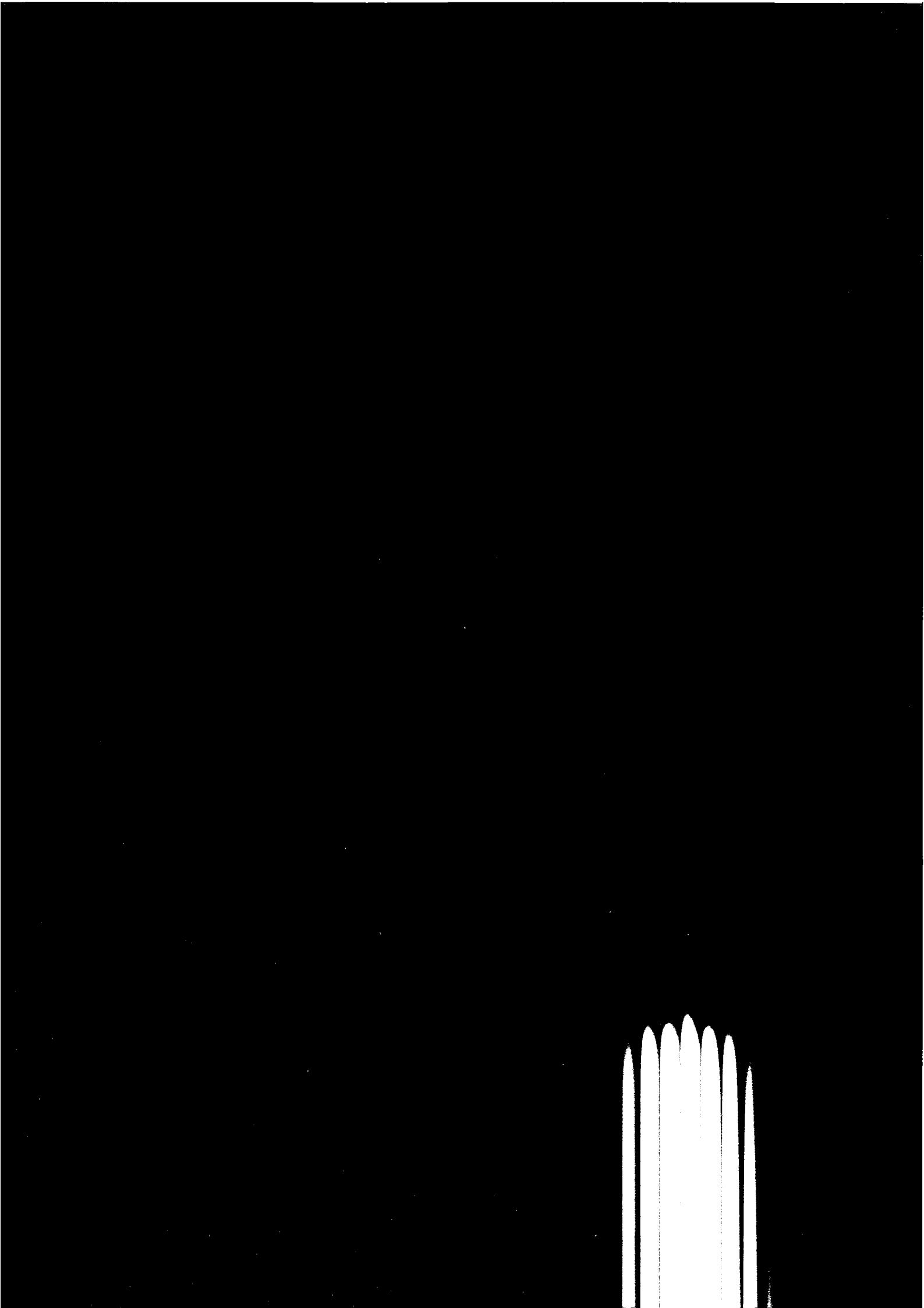

The factors which mainly affect the failure strength of ice are crystal size (larger grained ice yields higher strength values), rate of loading (the maximum of the fracture strength value is such that both an increase and decrease of the loading rate reduce the failure strength; the loading rate corresponding to the maximum value obviously depends on the temperature (see Figure 24)) and temperature (Figures 25 and 26).

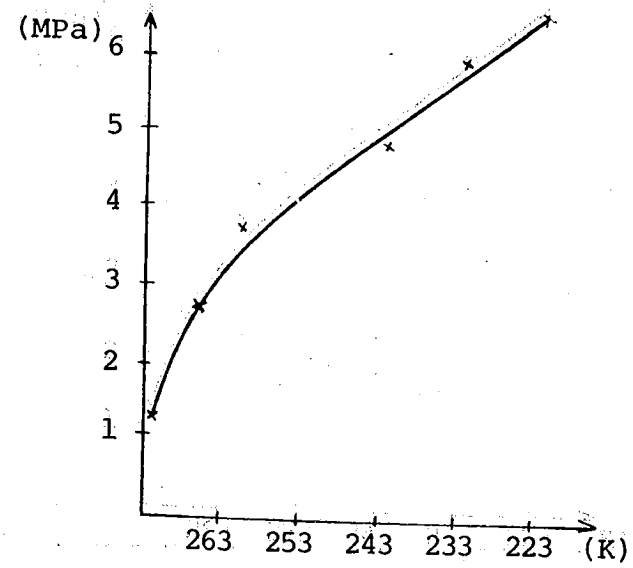

FIGURE 25 : Compressive strength /75/

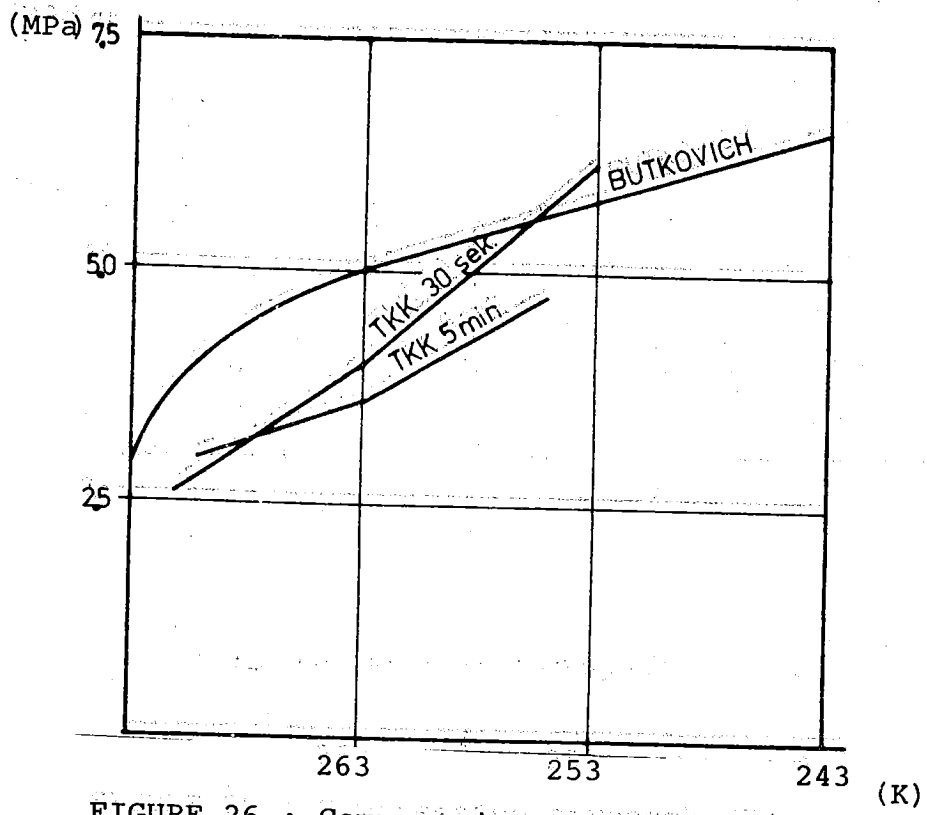

FIGURE 26 : Compressive strength /72/
(TKK means tests earlier made in HUT)

The main rupture types observed in the experiments are in Figure 27 (see also Appendix 6).

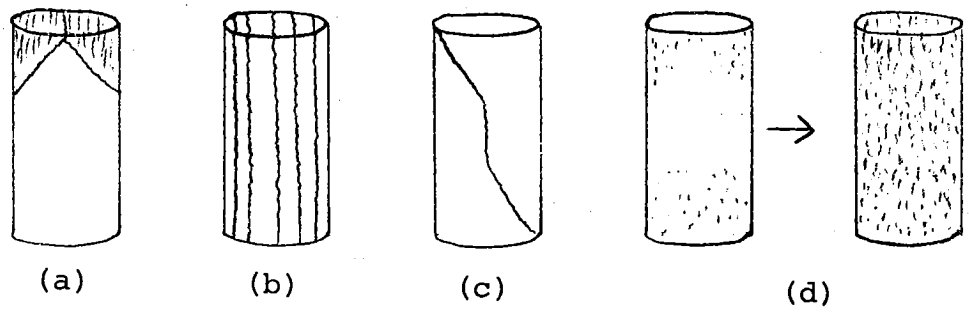

FIGURE 27 : Rupture types observed (b and d were most common)

Rupture tests made with specimens at 253 K failed partly because of difficulties in the preparation of test pieces. Small values of failure strength are obviously due to that the peak of failure strength moves by decreasing of temperature to longer loading times and long enough tests were not made at 253 K to observe this peak. Also the big difference in temperatures of the test piece and the test room have some effect on poor results, because it causes thermal stresses in the ice. The failure at 253 K was clearly more brittle than at other test temperatures. This was seen also in other connections, e.g. by preparation of test specimens.

3.4 Creep tests

In the creep tests deformation caused by compression loading occuring in columnar-grained fresh water ice in the direction of the c-axis was studied as function of time, temperature and stress level. The tests were made at temperatures 271 K, 268 K, 263 K and 253 K. Stress levels were 0,1 MPa, 0,2 MPa, 0,5 MPa and 0,7 MPa. Loading time

was mainly 24 hours. Some 60 hours long tests were however also made and correspondingly in some cases a test had to be interrupted in less than 10 hours. The choice of 24 hours for experiment time was due to the normal day and night rhytm, which usually limits the loads caused by thermal expansion on structures to 24 hours. The low stress levels were chosen because the static ice pressures observed in nature are according to measurements 0,1...1 MPa. The temperatures were chosen so that as many deformation processes as possible (compare Pages 39... 41) would be created.

The dimensions of every test specimen and the initial Young's modulus E_o, which was calculated on the basis of deformation corresponding to the moment 1...2 s, are presented in Appendix 5. The table also includes mention of the ice quality (1-contains plenty of air; 3-no air) and the smoothness of the ends of each test piece (1-ends are slanting or cracked; 3-ends are good).

A summary of the values of E_o for every stress level and temperature is given in Table 10. It shows that the dependence of the initial Young's modulus on the temperature was rather small at temperatures above 263 K but that at 253 K E_o was clearly greater than at other temperatures. The initial Young's modulus is presented by stress levels because at the beginning of the experiment the maximum of stress was achieved in about 2 seconds independently of the stress level ($\dot{\sigma}$ is thus 0,05...0,35 MPa/s). It seems, however, that this had no effect on the values of E_o.

In Figure 28 are given, for the sake of comparison, the values that Bogorodskii /70/ obtained for the initial Young's modulus of fresh-water ice.

TABLE 10 : Young's modulus E_o at time 1...2 s

T(K)		$\bar{E}_o$ (MPa)	s(MPa)	n
271	0,1	9890,6	2443,9	4
	0,2	9375,5	3306,9	10
	0,5	7630,2	1091,2	9
	0,7	8777,7	1004,6	3
	TOT.	8781,7	2435,2	26
268	0,1	7631,8	707,8	7
	0,2	7338,6	696,3	7
	0,5	8615,9	1030,3	7
	0,7	6474,3	1893,4	11
	TOT.	7385,4	1484,2	32
263	0,1	10867,3	4972,3	10
	0,2	8061,7	2865,2	7
	0,5	8069,6	1884,6	12
	0,7	6152,5	1383,3	7
	TOT.	8472,4	3466,1	36
253	0,2	16862,9	9371,7	4
	0,5	12009,9	3955,9	4
	0,7	12430,9	5932,3	4
	TOT.	13767,9	6563,3	12

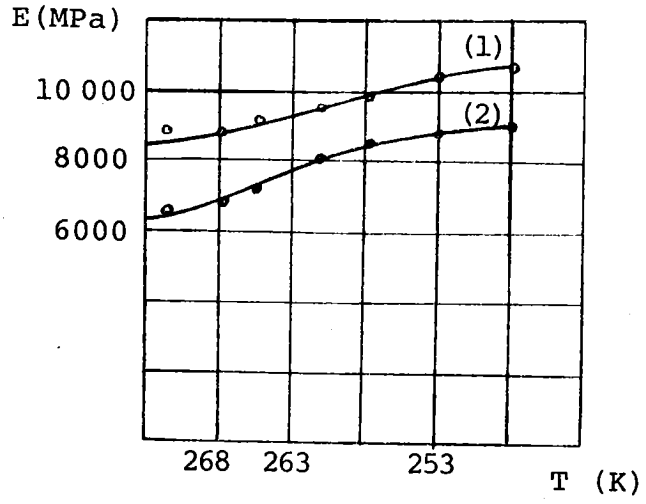

(1)
ρ = 918 kg/m^3

(2)
ρ = 890 kg/m^3

FIGURE 28 : Young's modulus E /70/

The results of the creep tests are presented graphically in (log ε, log t) -scale in Appendix 7.

Appendix 8 contains the most typical curves from the different test results and some comparison between the effect of the stress level at a constant temperature and correspondingly the effect of temperature at a constant stress level. The following curves are presented in the comparison:

271 K	1, 13, 23, 25
268 K	31, 39, 41, 56
263 K	59, 72, 76, 90
253 K	97, 102, 105
0,2 MPa	10, 39, 74, 95
0,5 MPa	23, 44, 76, 102
0,7 MPa	25, 56, 90, 105

For the stress level 0,1 MPa it is not possible to present a clear comparison because of the small deformations.

It may be that the wide scattering which is typical of the ice tests does not appear very clearly from the figures of Appendix 7. Therefore the results of parallel tests 76...83 (263 K, 0,5 MPa) are plotted in (ε, t)-scale in Figure 29 as an example. It shows that the strain was still mainly primary creep where the differences between the deformation mechanisms of different test pieces can be observed most clearly. Probably there would not be quite so great a scattering in the rate of secondary creep.

The results of the experiments at 271 K; 1 (0,1 MPa), 13 (0,2 MPa), 17 and 19 (0,5 MPa) and 25 (0,7 MPa) are presented in Figure 30. The situation in the figure was charasteristic of all the experiments. The three lowest

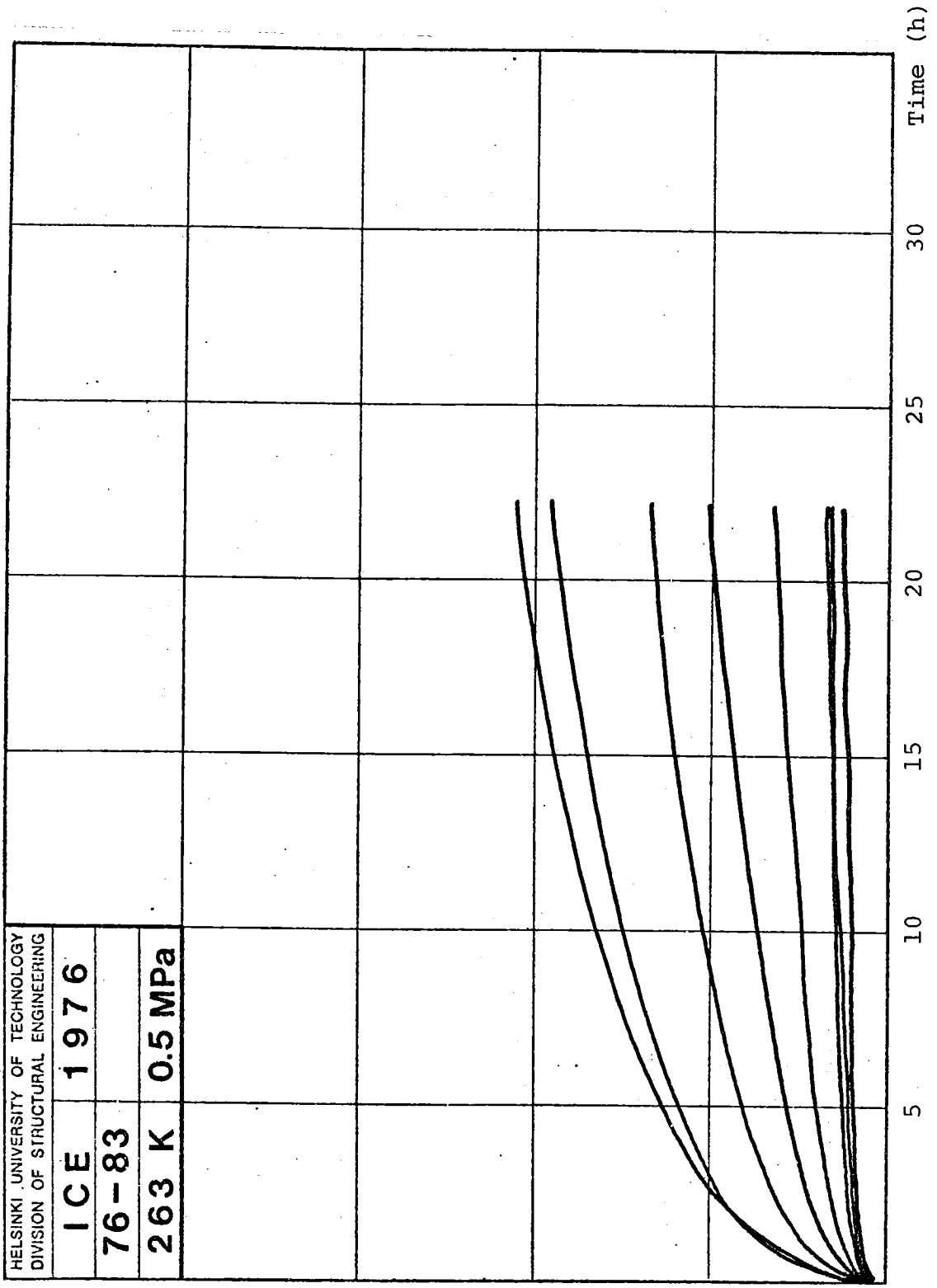

FIGURE 29 : Creep tests 76...83

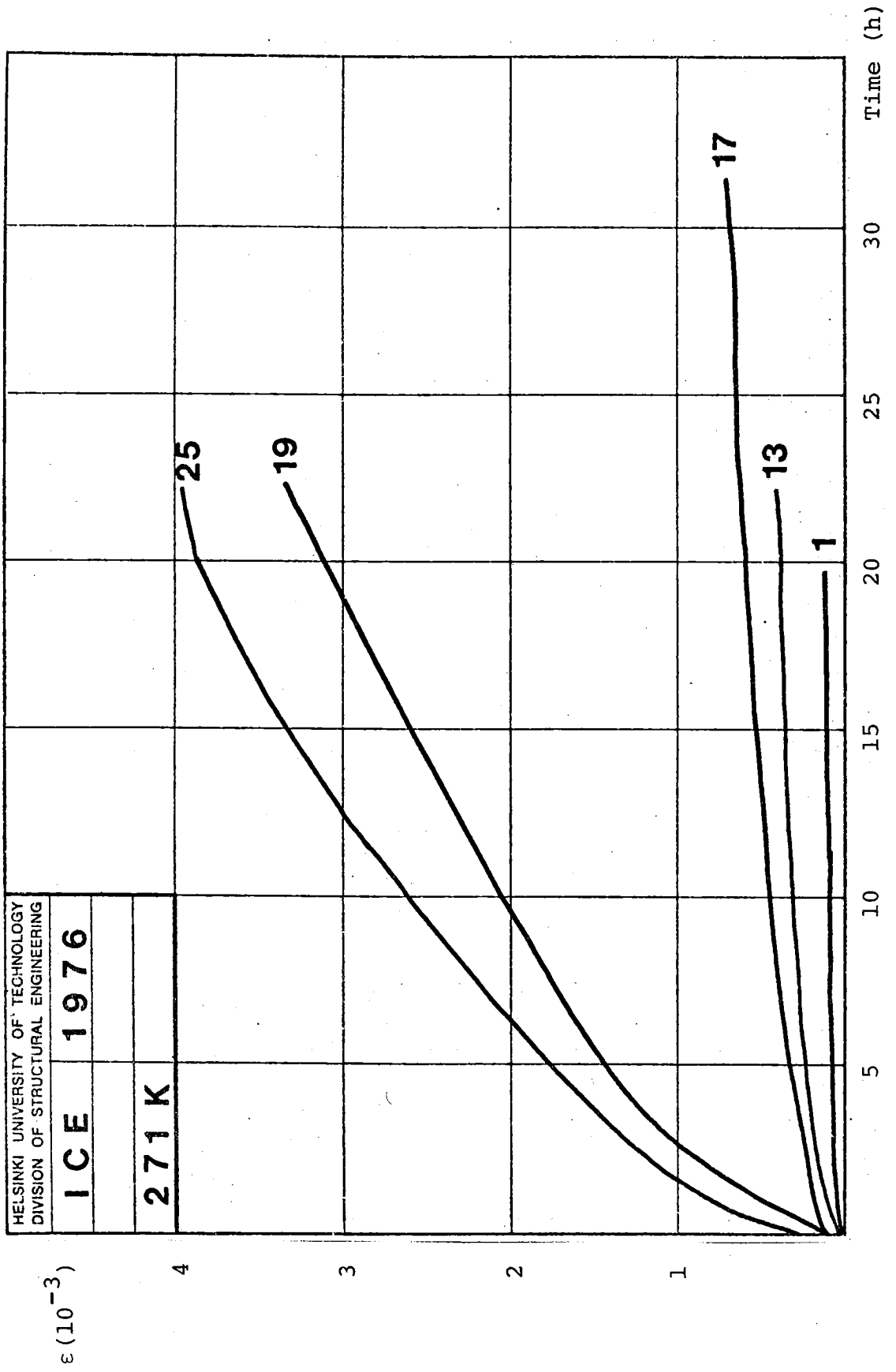

FIGURE 30 : Some creep curves at 271 K

curves (1, 13, 17) clearly describe the hard glide creep. The deformation presented by curve 19 differed completely from the creep in test 17 of the same stress level. The deformation was clearly easy glide and secondary creep had begun already after about 10 hours.

At further increase of the stress level (Curve 25) the deformation mechanism obviously again differed from that of other test pieces.

It was in fact the wide scatter which formed the greatest difficulty in the analysis of the test results. The most important reason probably was that the c-axis was not always exactly parallel with the loading direction. Due to the randomnes of the inertial structure of ice, there were many different mechanisms participating the deformation of a test piece, each of them in a different way sensitive to the stress level and the temperature (cf. Chapter 1.23). Faults in the experiment technology naturally had their effect on the scatter as well. Because of the wide scatter the linearity of the creep could not be reliably observed on the basis of the test results.

In spite of the wide scatter some obvious dependence on the stress level and temperature can be observed in the test results (cf. Appendix 8 and Figure 31). Figure 31 presents the results of the tests made on the stress level 0,7 MPa and at the temperatures 271 K (24...26), 268 K (52...54) and 253 K (103...106). The dependence of different creep curve spectra on the temperature is obvious.

The small values measured for the strain were typical for the test series. Besides the loading direction this resulted from the large crystal size of the test pieces and the great density of the ice. Figure 32 illustrates for the sake of comparison some characteristic creep curves of a test series /43/ made earlier at HUT.

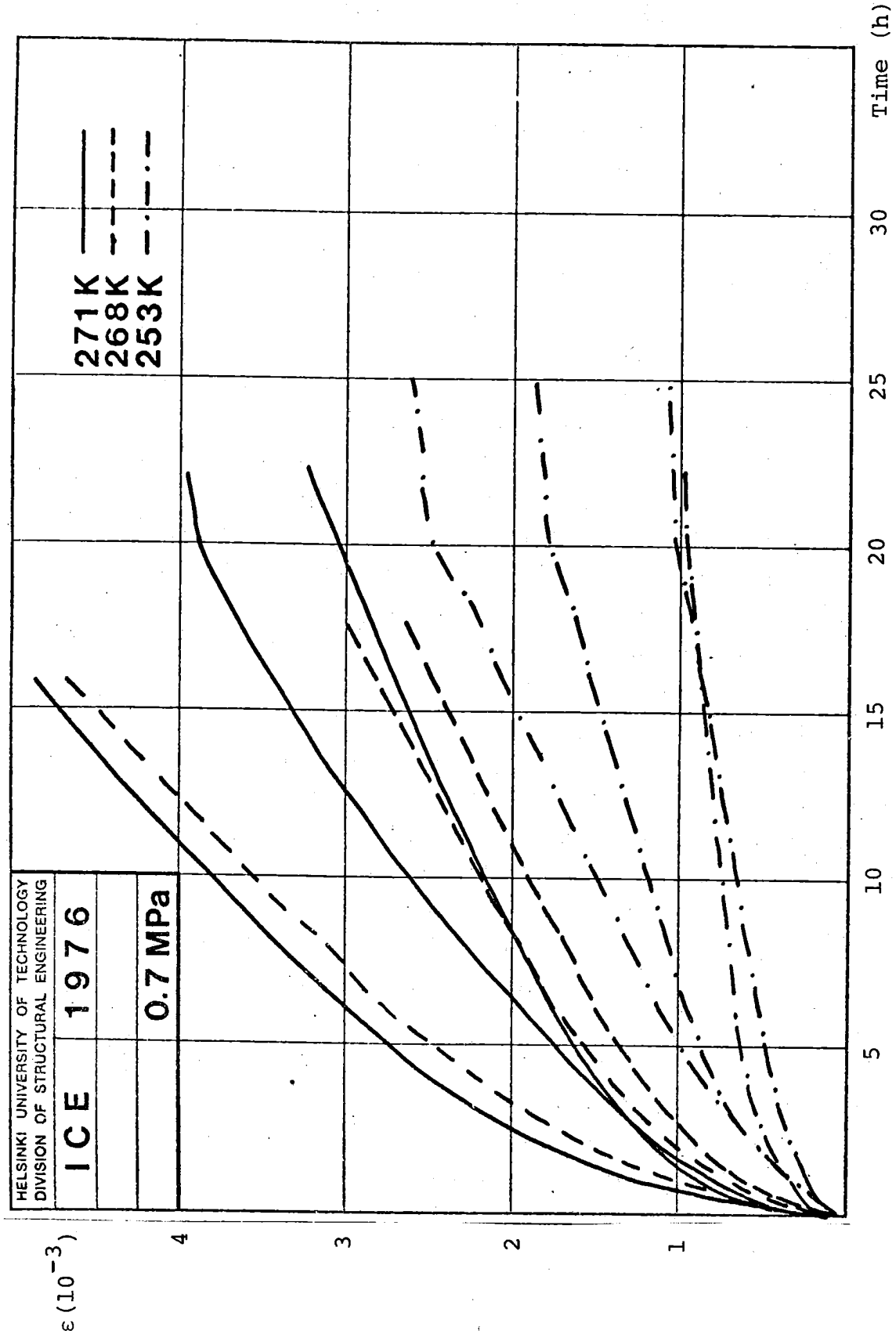

FIGURE 31 : Creep curves at stress level 0,7 MPa

The great difference in the results is mainly due to a different experimental technique. In the earlier test serie the strain was measured from the levers of the loading apparatus and not straight from the test piece. The ice also contained much more air (density was 870...910 kg/m^3) than the ice in the present tests.

Figure 33 presents the test results obtained by Gold /33/ at a temperature of (263,5 ± 0,5) K on different stress levels. The figure also illustrates the effect of reloading on the creep behavior of ice. The experiments were made with the arrangement shown in Figure 22 using columnar-grained ice and loading in the direction of the c-axis.

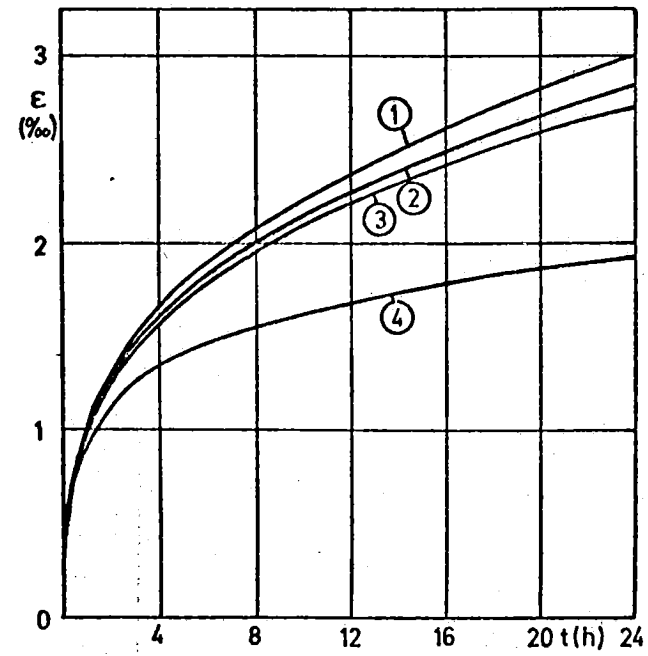

1 T = 271 K ; σ = 0,31 MPa
2 T = 268 K ; σ = 0,32 MPa
3 T = 261 K ; σ = 0,32 MPa
4 T = 248 K ; σ = 0,32 Mpa

FIGURE 32 : Creep curves of tap water ice /73/

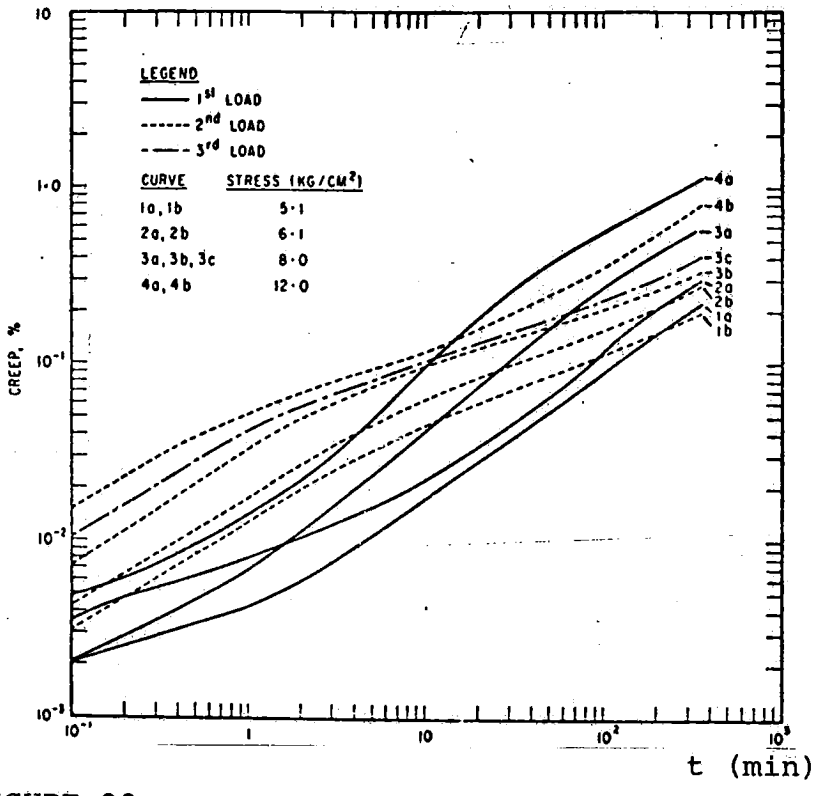

FIGURE 33 :

Time-dependence of creep of multigrained, columnar ice during first loading and reloading /33/

Gold observed /31/ that for the ice and conditions of loading used in compressive creep experiments an initial increasing creep rate with time was sometimes observed (Figure 34 a). Also Krausz /64/ made the same observation in his experiments. It has however been found, that when a test specimen is reloaded /32, 33/, the creep is always of the common type (Figure 34 b). Gold does not, however, give any reason for such unusual kind of creep. It should be noted that creep like that in Figure 34a was not observed during this study. It is true that the reason may be the low stress levels used, for Gold /31/ observed unusual creep behavior only at stress levels higher than 1,5 MPa.

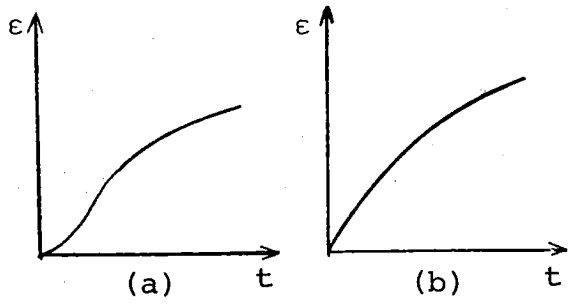

FIGURE 34 :
The two types of behavior observed in the creep tests on columnar-grained ice /64/

Many scientists have in their studies presented experimental values only for the rate of secondary creep and proper (ε, t) -test curves can hardly be found in publications. In this study the stress levels were too low and the loading times too short to observe secondary creep more than occasionally. Comparison of the results with other studies is also made difficult by the fact that the results are essentially dependent not only on the experimental arrangement but also the crystal structure of ice (especially the grain size) and the size of the test pieces.

In many experiments some cracking occured at the start of the test or during it. Especially in tests at 253 K cracks tended to form when the loading was started. Cracks occured only at stress levels 0,5 MPa and 0,7 MPa. Figure 35 illustrates the most common types of cracking. Frequent cracking at the ends of a test piece was obviously due to unsufficient trimming of the test piece, because of which stress peaks were created. Creep curves for specimens which cracked during loading before creep have not been included in Appendix 7.

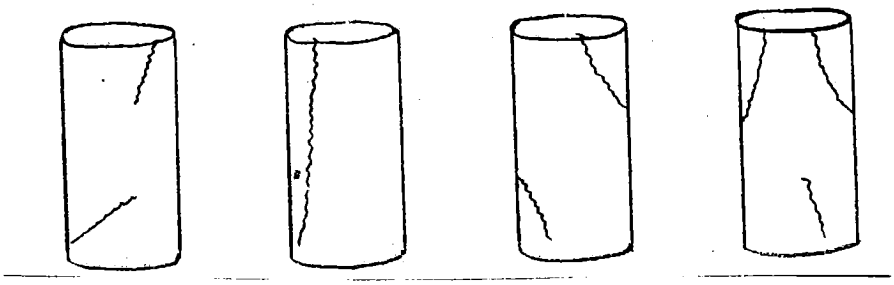

FIGURE 35 : Some types of cracking of test pieces

Few actual creep ruptures were observed at temperatures 271 K and 268 K and at stresses 0,72...0,75 MPa. The rupture almost always occured as shown in Figure 36 (see also Appendix 6).

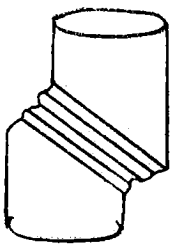

FIGURE 36 : A creep rupture type of test cylinder

4 CREEP MODELS FOR ICE

4.1 Models in litterature

For creep at constant temperature the following creep function is defined

$$D(t, T_o, \sigma_o) = \frac{\varepsilon(t, T_o, \sigma_o)}{\sigma_o} \tag{25}$$

The creep formulas (compression tests) presented for ice in litterature (Appendix 1) can in principle be classified into two groups in which the deformation obeys power law concerning either stress or the time.

In a general case the strain before tertiar creep can be expressed with Cottrell - Aytek formula (11)

$$\varepsilon(t, T, \sigma) = \varepsilon_o(T, \sigma) + \beta(T, \sigma)t^{n(T, \sigma)} + \dot{\varepsilon}_s(T, \sigma)t \tag{26}$$

which gives for creep function

$$D(t, T_o, \sigma_o) = \frac{1}{E_o(T_o)} + \frac{\beta(T_o, \sigma_o)}{\sigma_o} t^{n(T_o, \sigma_o)} + \frac{\dot{\varepsilon}_s(T_o, \sigma_o)}{\sigma_o} t \tag{27}$$

If in equation (27) the initial strain and the secondary creep are disregarded, the following function is obtained for easy glide creep

$$D(t, T_o, \sigma_o) = B(T_o, \sigma_o)\ t^{n(T_o, \sigma_o)} \tag{28}$$

Correspondingly, if the secondary creep is disregarded, which is possible at low stress levels and with short loading times, we obtain

$$D(t, T_o, \sigma_o) = A(T_o) + B(T_o, \sigma_o)\ t^{n(T_o, \sigma_o)} \tag{29}$$

Another creep model found in the litterature has the form

$$D(t, T_o, \sigma_o) = A(T_o, t)\ \sigma_o^{m(T_o, \sigma_o)} \tag{30}$$

which is obtained on the basis the formula (9) presented by Glen. The time dependence of the constant A has usually been formulated implicitely.

Naturally the constants β and $\dot{\varepsilon}_s$ in the model (27) can be dependent on the stress also according to the power law. $\dot{\varepsilon}_s$ has often the form (2) or (12).

According to many scientists the above creep models (27) and (30) applied to ice are nonlinear in respect to the stress. This nonlinearity in the model (27) is mainly included in the formula of the secondary creep. In question of primary creep only, the model (29) has been found to be only slightly nonlinear.

4.2 Models used in this work

In creep studies of metals e.g. the following equations have been often /26/ used to describe the strain

$$\varepsilon = \varepsilon_o + \beta t^m + \dot{\varepsilon}_s t \tag{31}$$

$$\varepsilon = \varepsilon_o + \varepsilon_t(1 - e^{-rt}) + \dot{\varepsilon}_s t \tag{32}$$

where ε_o is the elastic strain, ε_t the limiting transient creep strain, $\dot{\varepsilon}_s$ the secondary creep rate and β, m and r are suitably choosen constants which in a general case are dependent on the stress level and temperature.

It has been observed that the models (31) and (32) can succesfully be applied in particular for hcp-crystalline metals.

Though the above creep equations are empirical by character, they can be derived from usual formulas of reaction kinetics /74/. The model (31) is obtained straight by modifying the reaction rate of a single reaction and correspondingly the primary creep in the model (32) is obtained studying reactions in series.

In this work the creep of polycrystalline ice was studied at so low stress levels and with so short loading times that there was good reason to assume the creep to be mainly primary and linear in respect to the stress. Because of the wide scatter of the test results the linearity of the creep can however not be seen in the creep curves.

Models derived from equations (31) and (32) were tested with the creep data disregarding the secondary creep.

$$D(t, T_o, \sigma_o) = a_1(T_o) + b_1(T_o)\, t^{n_1(T_o)} \tag{33}$$

$$D(t, T_o, \sigma_o) = a_2(T_o) - b_2(T_o)\, e^{n_2(T_o)t} \tag{34}$$

As a special case of the model (33) also a Andrade -type model with exponent $n_1 = 1/3$ was studied.

Model (34) is also known as the Kelvin-Voigt model.

Besides the above models also a phenomenological model (35) developed by Mäkeläinen for glassy polymers /79/ was tested

$$\log D(t, T_o, \sigma_o) = a_3(T_o, \sigma_o) + b_3(T_o, \sigma_o) * \operatorname{arsinh}\left[\log\left(n_3(T_o, \sigma_o)\, t\right)\right] \tag{35}$$

The model can be also nonlinear in respect to the stress level.

The above creep functions are valid only when the temperature is constant. In models (33) and (34) the change in temperature can be taken into account with the so called shift hypothesis /59, 73/. The temperature dependence of the model (35), the so called stretch hypothesis, has been presented by Mäkeläinen /79/.

The fitnes of the models with the experimental data was studied with a modified method of least squares. The error functional is then minimized.

$$Erf = \sum_{i=1}^{k} \{D_t(t_i) - D_m(t_i, T_o)\}^2 \qquad (36)$$

where $D_t(t_i)$ is the value at time t_i calculated with the theoretical creep model and $D_m(t_i, T_o)$ is the corresponding creep data at temperature T_o. In the minimizing the simple heuristical interation was used. The calculations were performed with Univac-1108 computer.

The suitability of the model was tested with the so called relative deviation

$$s_r = \left\{ \frac{1}{k-1} \sum_{i=1}^{k} \left[\frac{D_t(t_i) - D_m(t_i, T_o)}{D_m(t_i, T_o)} \right]^2 \right\}^{1/2} \qquad (37)$$

In formulas (36) and (37) k indicates the number of data points used. The points were selected uniformly in respect to log t using the linear interpolation.

Appendix 9 contains the parameters and relative deviations of models (33), (34) and (35) calculated for each experimental creep curve. The number of the data points used is also mentioned.

Table 11 shows the averages and deviations of the relative deviations (defined in equation (37)) obtained with the models studied. The values were calculated considering the parameters of models determined for all test curves. It can be clearly seen in the table that the model of Mäkeläinen (35) best describes the group of test points. The model seems to be very flexible. Also the model (33) gives very good results especially at low stress levels. The creep model (34) is considerably poorer than models mentioned above and the Andrade - type model is entirely unsuitable for data points.

The dependence of the parameters of the models studied on the temperature and the stress levels can be seen in Appendix 10, where all those parameters are indicated, which could be fitted in the picture.

The temperature dependence of constant a_1 in model (33), which in the physical sense describes the inverse value of the initial Young's modulus of ice, corresponds rather well to the values of E_o obtained in the experiments. The value of constant n_1 seems to be, independently from temperature, about $0,5 \pm 0,1$. The dependence of the constants of the model (33) on the stress levels can not be observed on the basis of the results, and therefore the use of a linear model is well motivated.

The scattering of the parameters of the creep model (34) is rather wide, which well reflects the unsuitability of the model for the ice studied. By increasing the number of exponential terms better fitnes could doubtless be obtained between the data points and the model.

The scattering of the parameters in the model by Mäkeläinen (35) is rather slight, but the explicit presentation of the temperature and stress dependence of parameters is left outside this study.

			Model (33)		Model (34)		Model (35)		Andrade-model	
T(K)	σ(MPa)	Number of tests	$\bar{S}_{r1}$(%)	s (%)	$\bar{S}_{r2}$(%)	s (%)	$\bar{S}_{r3}$(%)	s (%)	$\bar{S}_{r4}$(%)	s (%)
271	0.1	4	10.11	4.16	17.54	7.26	12.28	2.79	26.71	16.39
	0.2	10	12.51	11.12	13.48	5.90	8.10	4.98	47.20	47.83
	0.5	9	13.77	12.01	28.44	19.23	9.37	5.70	79.63	75.16
	0.7	3	13.73	11.44	66.90	14.55	7.89	1.34	103.76	59.07
268	0.1	7	5.41	3.56	11.46	6.54	11.33	6.32	32.16	15.44
	0.2	7	7.61	7.85	24.52	8.65	5.58	3.86	34.58	36.14
	0.5	7	3.99	2.38	18.34	6.02	6.81	6.02	23.62	35.78
	0.7	11	22.68	38.52	24.12	12.02	15.51	6.36	104.54	53.78
263	0.1	10	2.71	1.32	7.56	2.95	6.14	2.47	13.03	6.47
	0.2	7	13.83	10.43	22.93	9.28	5.77	2.83	30.52	23.10
	0.5	12	8.87	7.22	20.34	12.73	6.37	4.29	27.10	39.11
	0.7	7	9.55	7.64	15.06	13.55	8.54	3.68	43.82	60.48
273	0.2	4	10.51	5.84	10.26	6.60	9.56	4.36	25.33	16.91
	0.5	4	13.34	7.25	12.14	2.79	14.79	5.50	77.47	41.45
	0.7	4	15.40	10.84	21.29	11.72	13.30	5.03	92.98	85.45

TABLE 11 : The averages and deviations of relative deviations obtained with the creep models

5 CONCLUSIONS

The plastic deformation of polycrystalline ice is, depending on the conditions, caused by very different deformation mechanisms, as was seen in Chapter 2. This causes a great scatter in the results of strength and creep tests for ice, which was observed also in this study. Because of the wide scatter it is not possible to present a general model for the creep of ice. For every single test a usable creep model can easily be formed, but it is not very simple to combine the models calculated on the basis of different test results so that the final model is thermodynamically acceptable and suitable for applications. This kind of a model is however under development.

In future this ice study project intends to examine e.g. the following subjects:

1° Expanding of the creep studies for ice so that the effect of long-time and stepwise loading on the creep will be examined.

2° The effect of the crystal structure of ice on the strength and creep properties.

3° Analysis of plastic properties of ice under conditions of cyclic loading.

4° Development of a stochastic creep model for ice.

5° Effects of crack formation and propagation in ice.

6° Study of different static and dynamic ice loads by means of litterature, calculations and measurements in the laboratory and also in nature.

7° Examination of the creep properties of sea ice.

8° Fracture strength of ice and its dependence on the loading rate.

REFERENCES

1. Atkins, A.G., Caddel, R.M., The laws of similitude and crack propagation. Int. J. mech. Sci. 16 (1974) pp. 541...548.

2. Barnes, P., Tabor, D., Plastic flow and pressure melting in the deformation of ice I. Nature 210 (1966) pp. 878... 882.

3. Barnes, P., Tabor, D., Walker, J.C.F., The friction and creep of polycrystalline ice. Proc. R. Soc. Lond. A324 (1971) pp. 127...155.

4. Bass, R., Zur Theorie der mechanischen Relaxation des Eises. Z. Phys. 153 (1958) pp. 16...37.

5. Bass, R., Rossberg, D., Ziegler, G., Die elastischen Konstanten des Eises. Z. Phys. 149 (1957) pp. 199...203.

6. Berger, R.H., Marshall, S.J., Munis, R.H., Fourney, M.E., Holographic technique for measurements of strain. CRREL (U.S. Army Cold Regions Research and Engineering Laboratory, Hanover, New Hampshire) rep. 227, 1975.

7. Bilgram, J.H., Phase equilibria and point defects in ice. Phys. cond. matter 18 (1974) pp. 263...273.

8. Bilgram, J.H., Gränicher, H., Defect equilibria and conduction mechanisms in ice. Phys. cond. matter 18 (1974) pp. 275...291.

9. Brierly, W.H., Calkins, D.J., Dentlartog, S.L., Mellor, M., Veda, H.T., Lock wall deicing with water jets. CRREL spec. rep. 239, 1975.

10. Brown, J.H., Elasticity and strength of sea ice. Ice and snow, Ed. Kingery, MIT Press 1963 pp. 79...106.

11. Butkovich, T.R., Thermal expansion of ice. J. appl. Phys. 30 (1959) pp. 350...353.

12. Clee, T.E., Savage, J.C., Neave, K.G., Internal friction in ice near its melting point. J. Geophys. Res. 74 (1969) pp. 973...980.

13. Cross, J.D., Scanning electron microscopy of evaporating ice. Science 164 (1969) pp. 174...1975.

14. Cutcliffe, J.L., Kingery, W.D., Coble, R.L., Elastic and time-dependent deformation of ice sheets. Ice and snow, Ed. Kingery, MIT Press 1963 pp. 305...310.

15. Dixit, B., Pounder, E.R., The specific heat of saline ice. J. Glaciol. 14 (1975) pp. 459...465.

16. Drouin, M., Static ice force on extended structures. NRC of Canada, Conf. on Ice Pressure, Tech. Mem. No. 92 pp. 95...108.

17. Ehrlich, N.A., Welsh, J.P., Ice and icebreakers. Advanced concepts and techniques in the study of snow and ice resources. Monterey Calif. 1973 pp. 235...243.

18. Enkvist, E. On the ice resistance encountered by ships operating in the continuous mode of ice breaking. Svenska Tekniska Vetenskapsakademien i Finland, report 24, 1972.

19. Eranti, E., Statical ice forces (in Finnish), Helsinki University of Technology, Div. of Struct. Eng. 1976 (not published).

20. Fletcher, N.H., The chemical physics of ice. Cambridge University Press 1970.

21. Ford, T.F., Nichols, O.D., Shear characteristics of ice in bulk, at ice/solid interfaces, and at ice/lubricant/solid interfaces in a laboratory device. US Naval Res. Lab. rep. 5662, 1961.

22. Frankenstein, G.E., Strength of ice sheets. NRC of Canada, Conf. on Ice Pressure, Tech. Mem. No. 92 pp. 79...87.

23. Frankenstein, G.E., Dynamic Young's moduls and flexural strength of sea ice. CRREL, Tech. rep. 222, 1970.

24. Frederking, R., Downdrag loads developed by a floating ice cover: Field experiments. Can. Geotech. J. 11 (1974) pp. 339...347.

25. Frederking, R., Gold, L.W., Experimental study of edge loading of ice plates. Can. Geotech. J. 12 (1975) pp. 456...463.

26. Garofalo, F., Fundamentals of creep and creep-rupture in metals. The Macmillan Company 1965.

27. Glen, J.W., The rheology of ice. Ice and Snow, Ed. Kingery, MIT Press 1963 pp. 3...7.

28. Glen, J.W., The effect of hydrogen disorder on dislocation movement and plastic deformation of ice. Phys. Condens. Mater. 7 (1968) pp. 43...51.

29. Glen, J.W., Structure and point defects of ice: their effect on the electrical and mechanical properties. Sci. Prog., Oxf. 57 (1969) pp. 1...21.

30. Gold, L.W., Some observations on the dependence of strain on stress for ice. Can. J. Phys. 36 (1958) pp. 1265...1275.

31. Gold, L.W., The cracking activity in ice during creep. Can. J. Phys. 38 (1960) pp. 1137...1148.

32. Gold, L.W., Deformation mechanisms in ice. Ice and snow, Ed. Kingery, MIT Press 1963 pp. 8...27.

33. Gold, L.W., The inital creep of columnar-grained ice. Can. J. Phys. 43 (1965) pp. 1414...1434.

34. Gold, L.W., Dependence of crack formation on crystallographic orientation for ice. Can. J. Phys. 44 (1966) pp. 3757...3764.

35. Gold, L.W., Elastic and strength properties of freshwater ice. NRC of Canada, Techn. pap. 283, 1968.

36. Gold, L.W., Observations on the movement of ice at a bridge pier. Proc. Conf. on Ice Pressures against structures. Laval University, Quebec 1966.

37. Gold, L.W., The failure process in columnar-grained ice. PhD Thesis, McGill University, Montreal 1970.

38. Gold, L.W., The failure of ice. NRC of Canada, Res. pap. 516, 1972.

39. Gold, L.W., Black, C.D., Trofimenkof, F., Matz, D., Deflections of plates on elastic foundation. Trans. of the E.I.C. 2 (1958).

40. Gold, L.W., Traetteberg, A., Youg's modulus of ice and ice engineering problems. 2nd Symp. Appl. of Solid Mech. Ontario, Canada 1974.

41. Gosar, P., Theory of the anelastic relaxation of cubic and hexagonal ice. Phil. Mag. 29 (1974) pp. 221...240.

42. Gow, A.J., Langston, D., Flexural strength of lake ice in relation to its growth structure and thermal history. CRREL Res. rep. 349, 1975.

43. Hakari, S., The time and temperature dependence of mechanical properties of ice. (in Finnish). MSc Thesis, Helsinki University of Technology (1973).

44. Hassinen, P., Creep modells for ice (in Finnish). Helsinki University of Technology, Div. of Struct. Eng. 1976 (not published).

45. Hawkes, I., Development and evaluation of an apparatus for the direct tensile testing of ice. CRREL, Spec. rep. 131, 1969.

46. Higashi, A., Growth and perfection of ice crystals. J. Crystal Growth 24/25 (1974) pp. 102...107.

47. Higashi, A., Koinuma, S., Mae, S., Plastic yielding in ice single crystals. Jap. J. appl. Phys. 3 (1964) pp. 610...616.

48. Higashi, A., Koinuma, S., Mae, S., Bending creep of ice single crystals. Jap. J. appl. Phys. 4 (1965) pp. 575...582.

49. Higuchi, K., The etching of ice crystals. Acta Metall. 6 (1958) pp. 636...642.

50. Hirayama, K., Schwarz, J., Wu, H-C., Model technique for the investigation of ice forces on structures. Proc. POAC 2nd confr. Iceland 1973 pp. 332...344.

51. Hobbs, H.A., Cutcliffe, J.L., Kingery, W.D., Effect of creep and temperature gradients of long-time deformation of ice sheets. Ice and Snow, Ed. Kingery, MIT Press (1963) pp. 311...321.

52. Hobbs, P.V., Ice Physics. Clarendon Press, Great Britain 1974.

53. Hutter, K., A general theory for floating ice plates. Arch. Mech. 27 (1975) pp. 617...638.

54. Hutter, K., Floating sea ice plates and the significance of the dependence of the Poisson ratio on brine content. Proc. R. Soc. Lond. A343 (1975) pp. 85...108.

55. Jellinek, H.H.G., Brill, R., Viscoelastic properties of ice. J. appl. Phys. 27 (1956) pp. 1198...1209.

56. Jellinek, H.H.G., Juznic, K., Grain growth of polycrystalline ice under stress. Proc. 5th int. cong. on rheol. pp. 407...419.

57. Jones, S.J., Glen, J.W., The effect of dissolved impurities on the mechanical properties of ice crystals. Phil. Mag. 19 (1969) pp. 13...24.

58. Jones, S.J., Glen, J.W., The mechanical properties of single crystals of pure ice. J. Glaciol. 8 (1969) pp. 463...473.

59. Jumppanen, P., Ice thermal loads against walls of water reservoirs. Proc. POAC 2nd Confr. Iceland 1973 pp. 679...702.

60. Kingery, W.D., French, D.N., Stress-rupture behavior of sea ice. Ice and Snow, Ed. Kingery, MIT Press 1963 pp. 124...129.

61. Kobayashi, T., Ohtake, T., Hexagonal twin prisms of ice. J. Atmos. Sci. 31 (1974) pp. 1377...1383.

62. Krausz, A.S., The creep of ice in bending. NRC of Canada, Res. paper 176, 1963.

63. Krausz, A.S., An experimental investigation of strain relaxation in ice. NRC of Canada, Res. paper 387, 1969.

64. Krausz, A.S., Plastic deformation of fresh-water ice. NRC of Canada, Techn. paper 284, 1968.

65. Kuroiwa, D., Hamilton, W.L., Studies of ice etching and dislocation etch pits. Ice and snow, Ed. Kingery, MIT Press 1963 pp. 34...55.

66. Lamb, D., Scott, W.D., The mechanism of ice crystal growth and habit formation. J. Atmos. Sci. 31 (1974) pp. 570...580.

67. Langham, E.J., Phase equilibria of veins in polycrystalline ice. Can. J. Earth Sci. 11 (1974) pp. 1280...1287.

68. Langleben, M.P., Pounder, E.R., Elastic parameters of sea ice. Ice and Snow, Ed. Kingery, MIT Press 1963 pp. 69...78.

69. Langway Jr., C.C., Ice fabrics and the universal stage. USA SIPRE Techn. rep. 62, 1958.

70 Lavrov, V.V., Deformation and strength if ice (Leningrad 1969). Israel Progr. Sci. Transl. Jerusalem 1971.

71. Legerer, F.J., Discussion contribution regarding improvement potential of ice-navigation. Arctic systems workshop 1975.

72. Leppävuori, E.K.M., The physical properties of ice (in Finnish). Helsinki University of Technology, Div. of Struct. Eng. Publ. 6, 1973.

73. Leppävuori, E.K.M., Ice pressures caused by thermal expansion. MSc Thesis, Helsinki University of Technology 1974.

74. Levenspiel, O., Chemical reaction engineering. John Wiley & Sons, New York 1966.

75. Maser, K.R., An analysis of the small-scale strength testing of ice. MIT, rep. MITSG 72-6, 1972.

76. Meyerhof, G.G., Bearing capacity of floating ice sheets. Trans. Am. Soc. Civ. Eng. 127 (1962) pp. 524...557.

77. Michel, B., Ice pressure on engineering structures. CRREL 1970.

78. Moffatt, W.G., Pearsall, G.W., Wulff, J., The structure and properties of materials. Vol I. John Wiley & Sons, USA 1964.

79. Mäkeläinen, P., On the modelling of long-term thermo-viscoelastic behaviour of glassy polymers. Helsinki University of Technology. Res. pap. 56, 1976.

80. Nevel, D.E., The narrow free infinite wedge on an elastic foundation. USA CRREL Res. rap. 79, 1961.

81. Nevel, D.E., Lifting forces exerted by ice on structures. CRREL.

82. Nevel, D.E., The ring test, Brazil test and strength of sea ice. CRREL 1969.

83. Paige, R.A., Kennedy, R.A., Strength studies of sea ice-effect of load rate of ring tensile strength. Naval civil eng. lab. (USA) techn. rep. R-545, 1967.

84. Palmer, W., On the analysis of floating ice plates. PhD Thesis, New York University 1971.

85. Panfilov, D.F., Experimental investigation of the carrying capacity of an ice cover. Bulletin of AU-Union Sci. Res. Inst. of Hydr. Eng. USSR, 64 (1960) pp. 101...115.

86. Parmerter, R.R., Dimensionless strength parameters for floating ice sheets. Proc. POAC 2nd confr. Iceland 1973 pp. 490...501.

87. Pauling, L., College Chemistry. W.H. Freeman & Co, USA 1964.

88. del Pennino, U., Loria, A., Mantovani, S., Mazzega, E., Polarization phenomena induced by cracks in Ih ice chrystals. Il nuovo cimento 24 (1974) pp. 108...120.

89. Peyton, H.R., Sea ice strength. University of Alaska 1966.

90. Pounder, E.R., The physics of ice. Pergamon Press.

91. Readey, D.W., Kingery, W.D., Plastic deformation of single crystal ice. Acta metall. 12 (1964) pp. 171...178.

92. Readings, C.J., Bartlett, J.T., Slip in single crystals of ice. J. Glaciol. 7 (1968) pp. 479...491.

93. Rekonen, T., Effect of ice on navigation and on navigational aids. XXIIIrd Int. Navig. Cong. Ottawa 1973.

94. Roggensack, W.D., Large Scale laboratory direct shear tests on ice. Can. Geotech. J. 12 (1975) pp. 169...178.

95. Sala, I., Experimental studies on the stress concentration index of sea-ice. IASH publ. 54 pp. 15...19.

96. Sala, I., Olkkonen, E., On the visco-elastic properties of ice and wood.

97. Sarkisov, G.N., Dashevsky, V.G., Malenkov, G.G., The thermodynamics and structure of liquid water. The Monte-Carlo Method. Molecular Phys. 27 (1974) pp. 1249...1269.

98. Savelev, B.A., Manual for the study of the properties of ice. CRREL Draft Transl. 343 1972.

99. Sundararajan, C., Reddy, D.V., Stochastic analysis of ice - structure interaction. Proc. of POAC 2nd Confr. Iceland 1973 pp. 345...353.

100. Tabor, D., Walker, J.C.F., Creep and friction of ice. Nature 228 (1970) pp. 137...139.

101. Tegart, W.J., Non-basal slip as a major deformation process in the creep of polyrystalline ice. J. Glaciol. 5 (1964) pp. 251...254.

102 Tusima, K., Fujii, T., Measurements of shear strength of ice. Low Temp. Sci. A31 (1973) pp. 31...43.

103. Wakahama, G., On the plastic deformation of ice V. Plastic deformation of polycrystalline ice. Low Temp. Sci. A22 (1964) pp. 1...24.

104. Walker, J.C.F., The mechanical properties of ice at high homologous temperatures. PhD Thesis, University of Cambridge 1970.

105. Weeks, W.F., Assur, A., Structural control of the vertical variation of the strength of sea and salt ice. Ice and Snow, Ed. Kingery, MIT Press 1963, pp. 258...276.

106. Weeks, W., Assur, A., The mechanical properties of sea ice. CRREL 1967.

107. Weeks, W.F., Hibler III, W.D., Ackley, S.F., Sea ice: scales, problems and requirements. Advanced concepts and techniques in the study of snow and ice resources, Monterey Calif. 1973 pp. 255...267.

108. Weertman, J., The Eshelby-Schoeck viscous dislocation damping mechanism applied to the steady-state creep of ice. Ice and Snow, Ed. Kingery, MIT Press 1963 pp. 28... 33.

109. Weertman, J., Creep of ice. Physics and Chemistry of Ice, Ed. Whalley, Jones and Gold, Royal Soc. Can. 1973 pp. 320...337.

110. Whalley, E., The O-H distance in ice. Molecular Phys. 28 (1974) pp. 1105...1108.

APPENDIXES

APPENDIX 1

CLASSIFICATION OF LITTERATURE ACCORDING TO SUBJECT
(Compare references on Pages 78...87)

1 ADHESION AND FRICTION OF ICE

3	17	18	21	52
70	72	90	98	100
104				

2 CREEP OF ICE

2	3	14	20	22
27	28	31	32	33
37	40	43	44	47
48	52	55	57	58
60	62	63	64	70
72	73	75	88	90
91	92	96	98	100
101	103	104	106	108
109				

3 ELASTIC PROPERTIES OF ICE

5	6	10	12	17
18	20	22	23	25
30	35	37	40	41
42	45	52	68	70
72	75	82	83	89
90	93	94	95	98
102	105	106		

4 FRACTURE OF ICE

1	22	25	31	32
34	37	38	52	58
60	70	72	75	89
98				

5 ICE PROBLEMS

9	10	14	17	18
19	22	24	25	32
33	36	39	40	50
51	52	53	54	59
71	73	76	77	80
81	82	84	85	86
95	98	99	104	107

6 PHYSICAL PROPERTIES OF ICE (not mechanical properties)

11	15	17	20	29
52	56	70	72	89
90	98			

7 STRUCTURE OF ICE

2	4	7	8	12
13	20	28	29	32
37	40	41	46	49
52	56	57	61	65
66	67	69	70	72
75	77	88	91	92
97	98	103	104	105
106	110			

APPENDIX 2

THE EXPERIMENTAL PROCEDURE FOR CREEP TESTS

1 Freezing of water

2 Sawing of ice block

3 Thermal boring of test specimen

4 Trimming of ends of test specimen

5 Loading apparatus

6 Arrangement for creep measuring

7 Fastening of measure ring

8 Device for output and registering of data

9 Manipulation of creep data

10 Plotting of test results

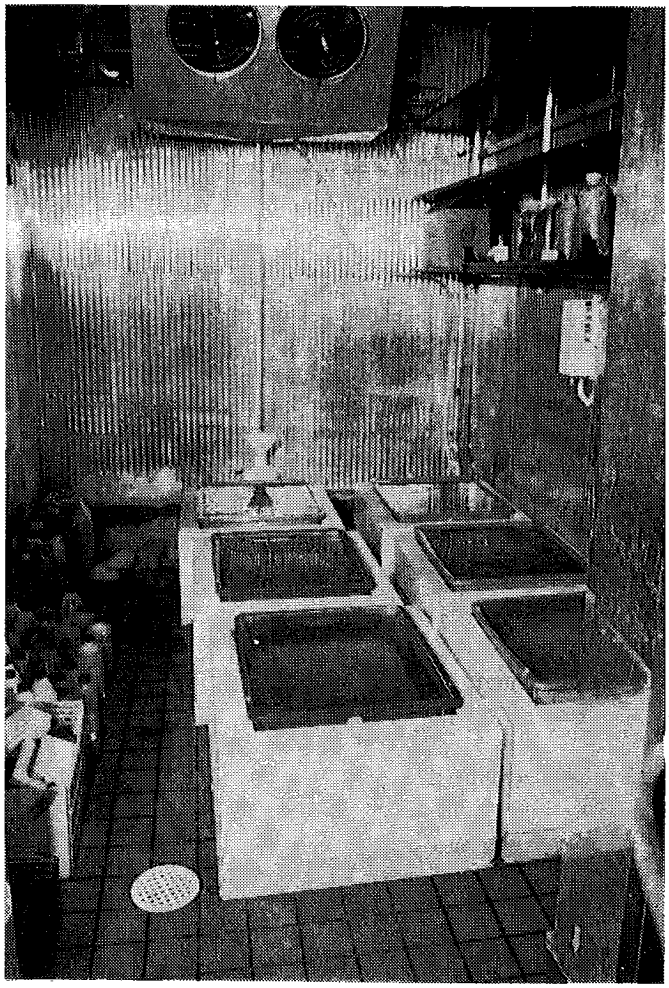

1

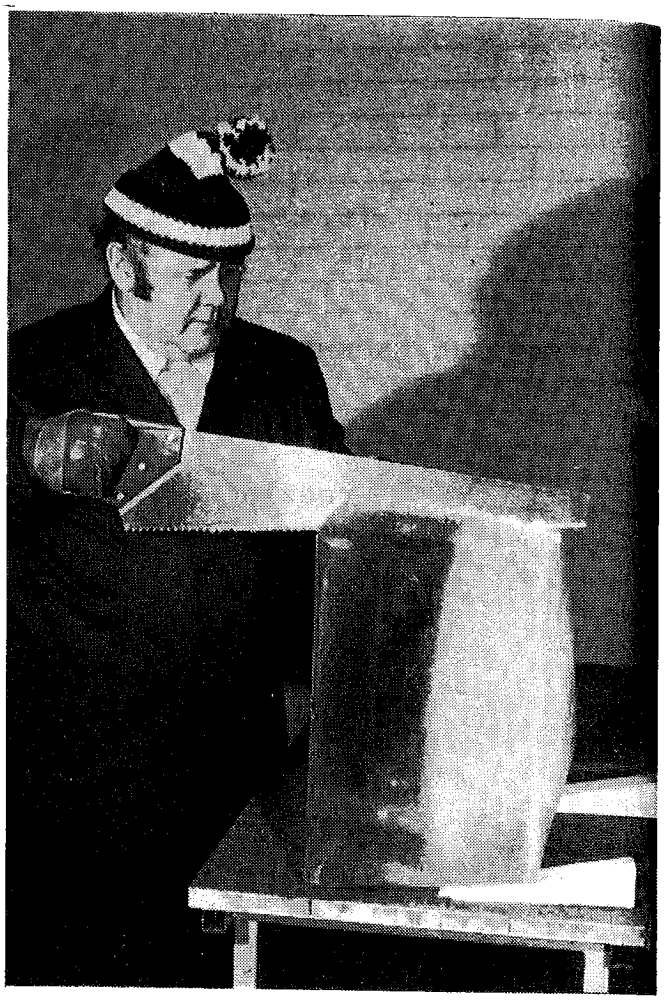

2

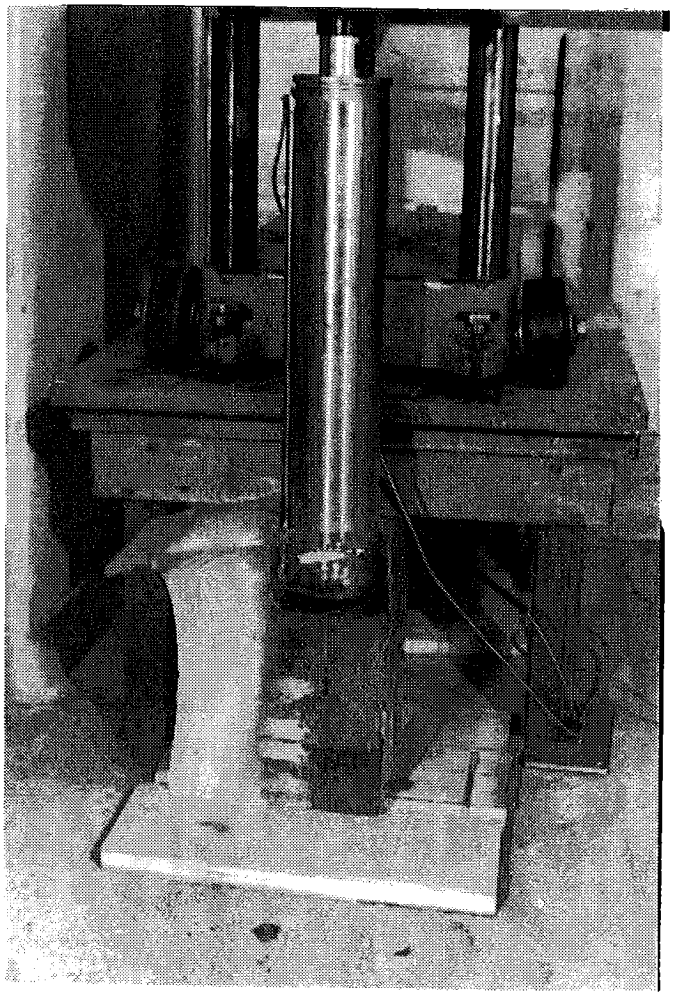

3

4

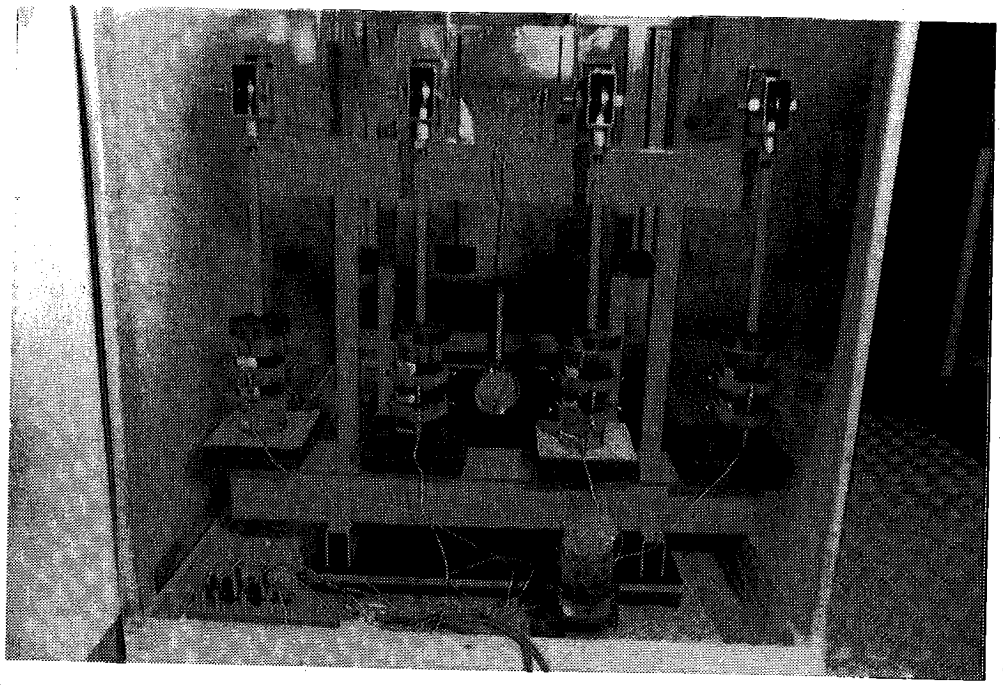

5

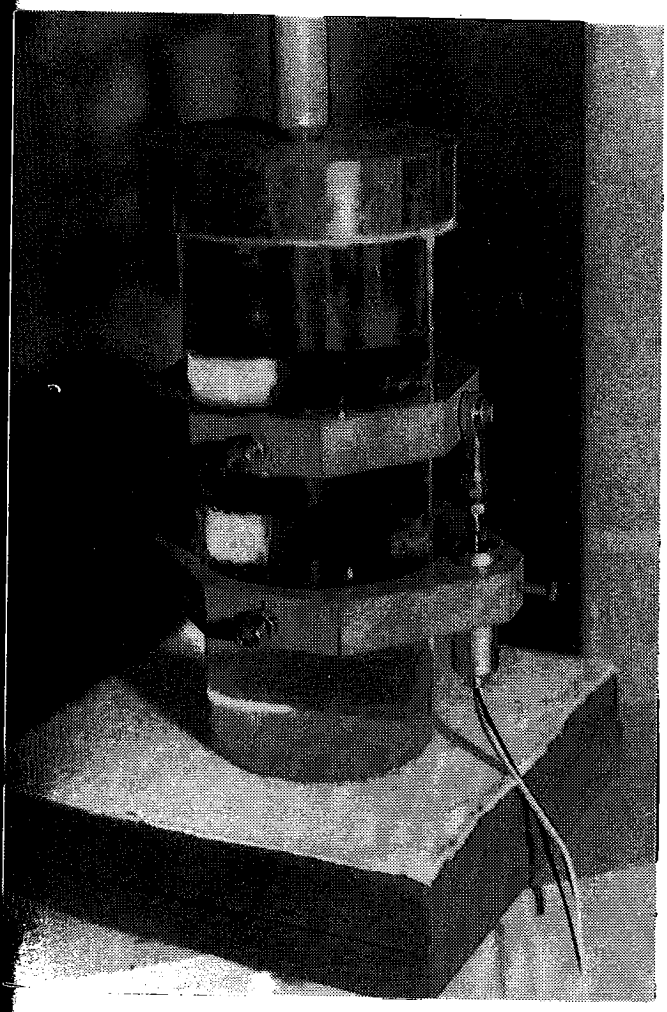

6

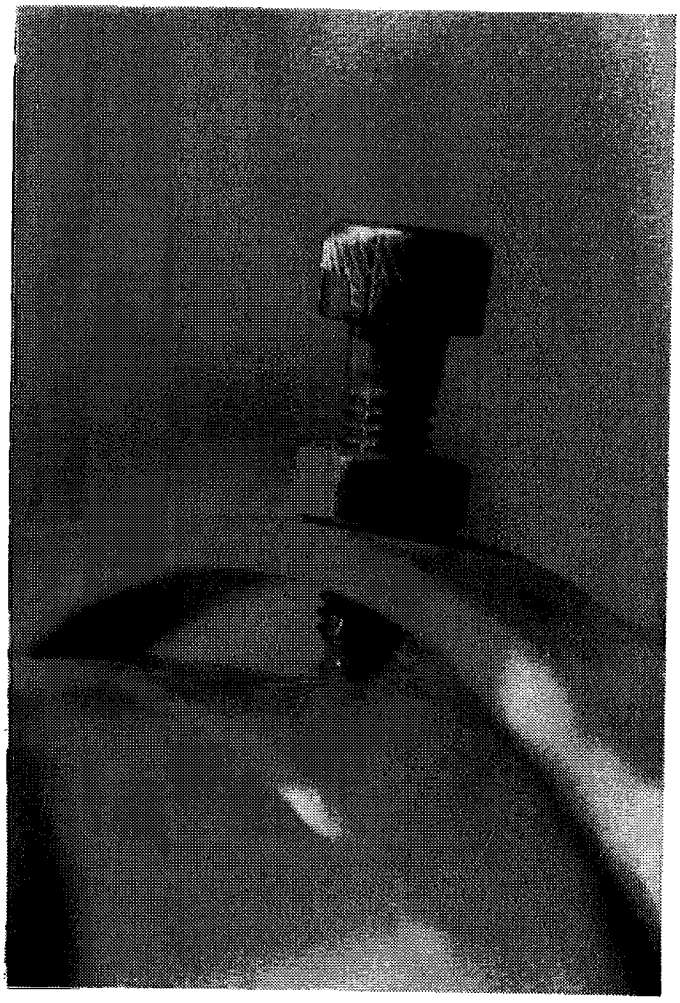

7

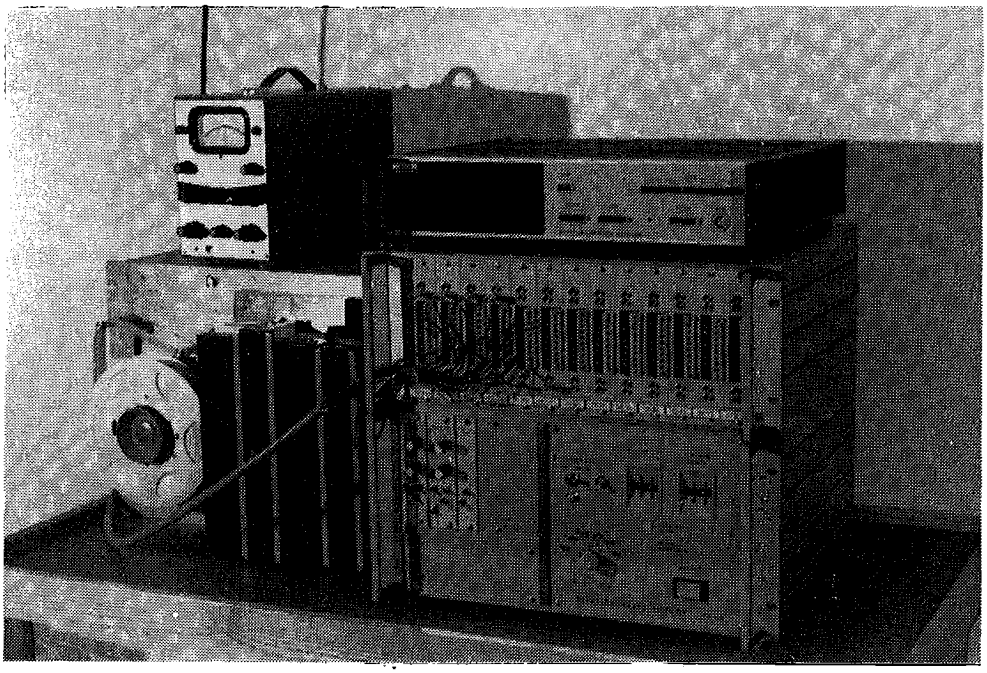

8

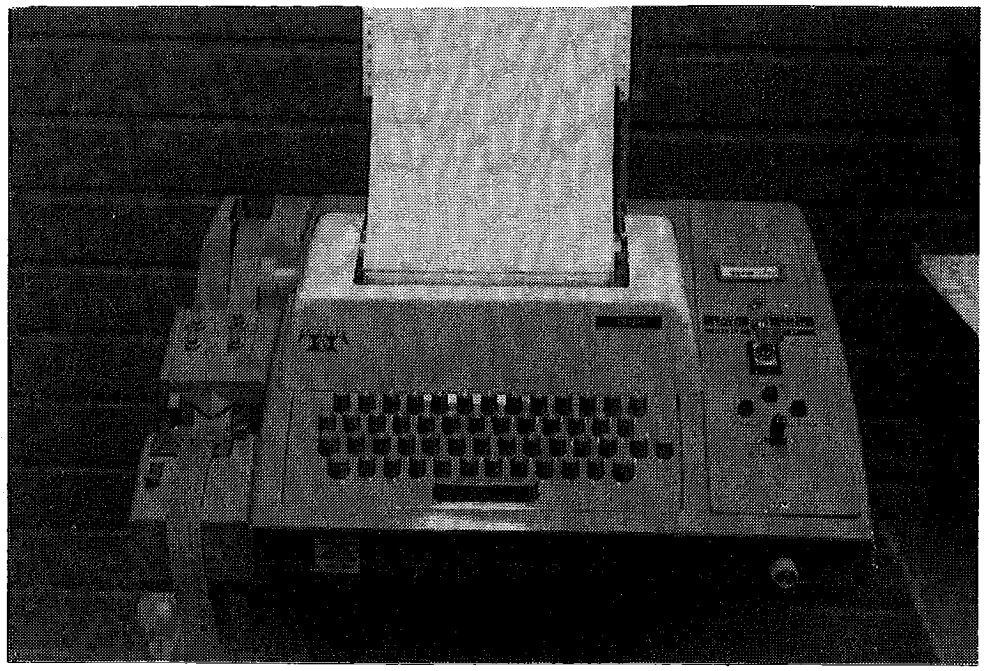

9

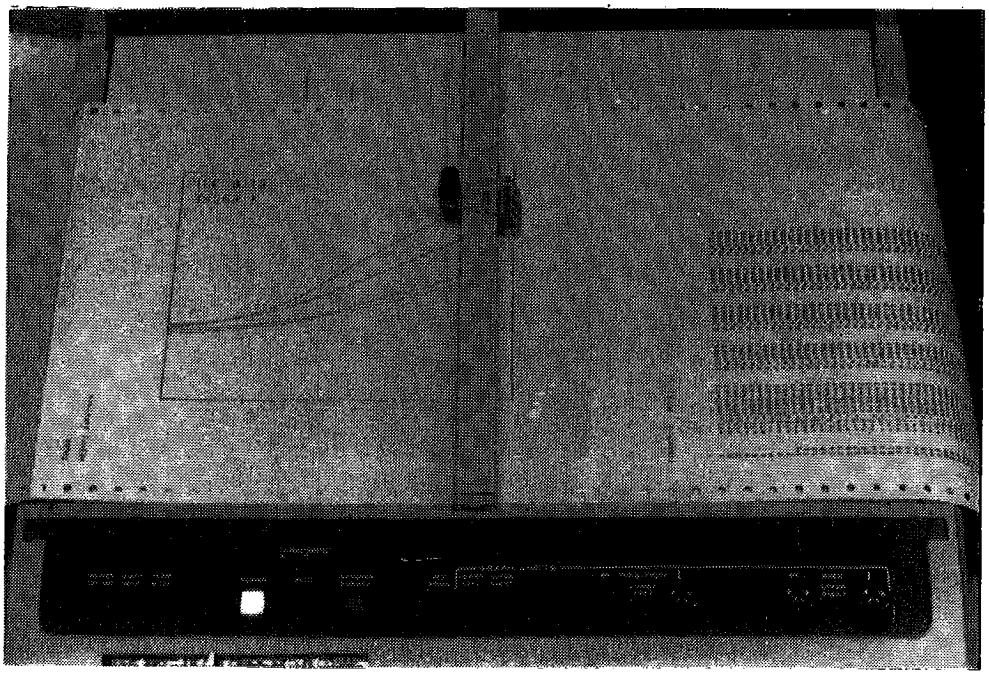

10

APPENDIX 3

WATER ANALYSIS

Number of sample			1	2	3	4
Colour	mg Pt/l		5	<5	<5	5
Conductivity	H_2O mS m^{-1}		1,3	1,4	1,9	26,3
Consumption of	$KMnO_4$ mg/l		5	5	3	7
pH			6,9	8,6	9,1	8,1
Alkalinity, mixed indicator	mval/l		0,03	0,07	0,1	0,65
Bicarbonate	HCO_3	mg/l	1,8	4,1	5,6	39,3
Total iron	Fe	"	0,1	0,1	0,09	0,07
Calsium	Ca	"	1,2	1,6	1,6	29,0
Magnesium	Mg	"	0,5	0,0	0,7	3,9
Potassium	K	"	0,5	0,2	0,0	3,4
Sodium	Na	"	4,1	0,9	1,0	16,5
Ammonium	NH_4	"	0,1	0,1	0,1	0,2
Nitrite	NO_2	µg/l	1	0,6	2	0,2
Nitrate	NO_3	mg/l	0,1	0,0	0,0	6,1
Chloride	Cl	"	1,2	0,7	1,2	20,0
Sulphate	SO_4	"	1,8	0,8	0,6	48
Ortophosphate	P	µg/l	0,7	3,5	1,0	1,0
Total phosphor	P	"	15	13	11	11
Total hardness	°dH		0,28	0,22	0,39	5,0
Bicarbonate hardness	°dH					
Evaporation residue		mg/l	32	39	34	270

Samples: 1 = From the top of the ice piece
2 = From the bottom of the ice piece
} Figure 17
3 = Lake water
4 = Tap water

RESULTS OF FAILURE TESTS

Experiments 1... 55 T = 263 K
Experiments 56...116 T = 268 K
Experiments 117...147 T = 253 K

No.	P(g)	H(mm)	D_1(mm)	D_2(mm)	D_3(mm)	ρ(kg/m^3)	F_M(kN)	σ_M(MPa)	t_M(s)
1	607.5	161.3	73.3	71.6	72.5	913	3.1	0.755	2
2	606.1	160.3	73.6	73.1	72.4	903	3.5	0.833	2
x3	611.1	160.7	73.5	72.8	72.3	912	1.5	0.358	2
4	601.0	160.5	73.6	73.1	72.7	891	3.8	0.885	2
5	601.4	159.3	71.6	72.6	72.9	918	4.8	1.168	2
6	611.5	160.5	73.5	73.0	72.1	914	5.0	1.200	2
x7	614.1	161.0	72.5	73.0	71.6	927	20.0	4.868	6
x8	616.5	160.1	73.4	73.4	72.9	914	15.0	3.522	5
9	605.5	160.9	72.4	73.5	72.9	901	9.8	2.333	7
10	617.1	161.1	73.5	72.7	72.1	922	14.1	3.384	7
11	610.0	160.9	71.4	73.0	72.8	921	13.7	3.353	9
12	611.2	160.8	73.0	72.2	71.2	930	12.5	3.077	5
x13	610.5	160.9	73.4	72.9	72.7	907	9.5	2.243	-
14	607.6	160.7	70.6	73.0	73.3	921	5.5	1.377	2
x15	610.2	160.0	73.4	71.6	71.4	933	5.3	1.297	12
x16	618.9	159.6	73.3	72.9	74.0	916	17.2	4.038	5
x17	610.0	159.5	73.3	72.1	72.0	927	6.6	1.584	2
x18	619.9	160.5	73.4	73.9	73.3	909	5.8	1.343	10
19	609.9	159.4	72.9	73.1	73.1	913	12.8	3.005	8
20	607.6	159.5	72.9	73.1	71.9	919	9.4	2.269	7
21	608.5	159.5	73.1	73.0	72.9	912	9.2	2.160	12
22	615.4	160.2	73.6	73.1	73.2	910	10.4	2.428	5

x23	636.8	160.4	74.4	74.3	73.0	926	7.6	1.780	10
24	637.6	160.5	73.7	74.5	74.0	922	11.2	2.573	8
x25	643.3	160.5	74.2	74.8	73.8	925	7.6	1.741	7
26	632.2	159.8	73.6	74.6	73.5	922	9.5	2.194	6
27	637.1	159.8	74.3	74.4	75.1	912	8.0	1.808	4
28	626.6	160.6	73.0	74.1	73.7	917	4.0	0.937	2
x29	638.8	158.8	74.4	74.3	75.4	918	-	-	-
x30	641.6	160.1	74.3	74.9	75.4	910	3.5	0.791	3
x31	644.3	160.9	74.6	74.0	74.4	923	17.3	3.942	10
x32	641.5	160.7	74.1	75.2	75.2	908	24.5	5.568	13
33	639.7	160.4	74.5	74.9	74.3	913	13.5	3.051	9
34	644.2	161.1	74.5	74.5	75.0	913	15.0	3.372	21
35	637.2	160.3	74.6	74.8	74.9	905	13.2	2.960	46
36	644.0	159.6	74.5	74.9	75.0	918	13.0	2.923	28
37	641.6	160.2	74.4	74.6	74.9	915	13.5	3.043	45
x38	628.6	160.2	73.2	74.3	74.2	915	17.2	4.005	36
39	626.7	160.1	73.9	74.0	73.5	915	6.8	1.571	21
40	619.0	160.0	71.8	73.8	73.3	925	9.0	2.178	22
x41	616.5	160.6	73.6	73.1	73.3	909	18.6	4.343	18
42	617.1	159.7	73.1	73.1	74.0	913	16.5	3.853	34
x43	612.8	159.5	72.4	73.5	72.7	921	3.8	0.905	17
44	625.5	159.6	73.7	74.5	73.8	911	8.0	1.838	4
x45	617.5	160.0	73.0	73.0	73.7	916	-	-	-
46	619.4	160.1	73.3	73.4	73.9	911	12.3	2.856	3
x47	619.3	159.8	73.1	73.5	74.3	910	7.0	1.635	2
x48	628.1	159.8	74.3	72.9	74.6	915	3.5	0.822	4
x49	645.5	160.1	75.3	75.0	74.2	917	-	-	-
50	635.6	159.3	74.8	74.6	74.5	912	7.0	1.574	4
51	625.8	159.6	74.9	73.8	73.6	909	12.2	2.810	8
52	622.1	160.9	73.2	74.0	72.4	919	8.6	2.047	8
53	633.2	160.9	73.0	74.1	75.2	913	17.2	4.027	12
54	633.7	160.8	73.3	74.0	73.6	925	13.6	3.158	9
55	617.5	160.7	73.6	73.6	71.0	925	15.5	3.837	10

56	612.8	159.8	72.2	72.6	73.3	924	3.7	0.886	5
x57	594.5	159.6	71.6	71.7	72.0	921	1.5	0.365	3
x58	596.7	159.5	71.6	72.7	72.0	916	1.0	0.243	4
59	602.3	159.2	72.1	72.4	72.4	922	4.5	1.080	1
60	599.2	159.1	72.2	72.0	72.4	920	3.5	0.842	2
x61	609.5	160.0	73.1	72.4	72.9	915	1.2	0.286	3
62	624.2	159.6	73.0	73.8	73.9	920	5.5	1.288	4
63	607.4	158.8	72.2	72.5	72.5	929	5.7	1.364	5
64	599.2	159.3	72.9	72.0	72.3	914	5.2	1.252	4
x65	595.3	160.1	72.6	71.7	72.3	908	8.6	2.087	5
x66	623.3	158.5	73.8	74.2	74.2	913	10.0	2.291	29
x67	626.2	159.0	73.1	74.0	74.1	922	14.8	3.456	16
68	630.5	159.9	74.0	73.9	74.3	915	11.0	2.513	13
69	632.2	160.0	74.2	74.1	74.0	916	9.5	2.165	18
70	630.2	159.8	73.9	74.0	74.2	916	8.6	1.965	27
71	635.5	159.8	74.0	74.6	74.2	918	12.2	2.780	15
72	613.1	159.7	73.0	72.8	71.8	929	8.4	2.033	15
73	616.1	159.2	73.2	73.6	73.9	910	9.4	2.189	22
x74	634.6	159.6	74.2	74.4	74.8	913	5.5	1.246	15
x75	630.3	159.4	74.1	73.8	74.4	917	5.0	1.145	14
76	633.4	159.7	74.4	74.4	74.5	911	10.0	2.254	23
77	633.1	159.6	74.8	73.9	74.3	914	10.7	2.445	22
x78	599.6	159.9	71.7	72.5	72.3	917	6.2	1.505	18
x79	591.5	159.8	71.9	71.4	72.5	911	5.8	1.420	20
80	612.3	159.5	73.0	73.1	72.5	921	9.3	2.208	22
81	599.4	159.5	72.2	72.3	72.5	915	5.2	1.245	11
82	588.0	159.8	72.4	72.8	68.3	924	6.8	1.819	4
x83	630.7	160.1	73.8	74.2	74.1	915	8.0	1.833	2
84	590.3	160.0	70.8	71.8	71.7	921	3.8	0.946	1
85	588.6	159.7	71.2	71.6	72.7	909	6.3	1.551	1
86	600.4	159.8	71.6	72.2	71.7	927	6.0	1.460	1
87	605.4	159.7	73.4	72.6	71.8	916	6.0	1.452	1
x88	632.3	159.9	74.2	74.3	73.1	923	7.5	1.751	1

89	605.6	159.3	71.7	73.6	70.0	939	1.8	0.458	4
x90	619.0	160.6	73.1	73.1	72.3	925	1.5	0.358	2
x91	609.6	159.4	72.8	72.6	73.4	915	3.0	0.710	2
92	610.0	159.8	73.0	72.6	72.8	917	3.5	0.829	4
x93	619.5	159.3	73.5	73.5	73.8	914	1.5	0.346	10
x94	612.0	160.1	72.7	73.5	71.5	924	-	-	-
95	612.4	159.4	73.7	72.7	73.5	910	5.5	1.298	3
96	612.8	160.0	73.0	73.2	73.8	907	5.6	1.311	5
97	623.8	159.5	73.2	73.5	73.6	923	10.6	2.468	18
x98	564.6	159.9	68.3	71.6	69.3	924	11.2	2.996	19
x99	581.2	160.0	70.9	71.5	70.2	921	6.0	1.519	38
100	625.3	160.0	73.8	73.7	72.6	924	8.0	1.894	30
101	587.1	159.6	72.1	71.0	71.5	915	8.2	2.030	32
x102	604.6	159.2	72.5	72.3	72.4	922	11.0	2.626	3
103	592.0	160.0	70.8	71.5	72.5	919	6.2	1.543	11
104	609.6	159.5	72.6	72.8	74.0	910	7.0	1.657	11
105	613.6	160.2	73.1	72.4	74.3	908	8.5	2.023	10
106	614.2	159.4	73.3	72.8	73.7	914	9.0	2.119	12
107	610.5	159.5	72.7	72.6	74.3	909	7.5	1.776	8
108	628.7	160.1	74.3	73.5	74.5	911	11.0	2.541	8
x109	607.0	159.6	72.1	72.3	74.3	911	9.2	2.208	10
110	614.2	159.6	73.2	72.7	72.7	923	6.0	1.417	10
111	622.0	159.7	74.2	73.0	74.1	911	9.2	2.154	9
112	624.3	160.1	73.5	73.2	72.5	930	9.2	2.184	14
113	630.1	159.8	73.9	73.8	74.4	916	11.2	2.566	12
114	622.4	159.9	74.2	73.4	73.0	917	11.6	2.716	15
x115	612.6	160.7	72.9	72.9	73.2	911	5.4	1.268	13
116	628.2	159.8	74.2	73.6	74.0	916	9.5	2.188	12
x117	618.6	157.5	73.9	73.6	74.0	917	5.9	1.387	19
x118	610.5	156.8	72.6	72.8	73.1	935	12.9	3.116	4
119	620.8	158.2	73.0	73.2	73.8	929	3.9	0.932	9
120	627.3	157.2	73.8	74.1	74.2	927	3.4	0.795	5
121	614.5	156.3	73.6	73.9	74.0	918	4.9	1.152	4

122	615.4	156.9	73.0	73.8	74.3	919	2.5	0.597	2
x123	623.4	158.6	73.4	73.4	73.7	926	0.5	0.118	2
x124	611.3	156.0	73.0	73.5	73.6	927	12.6	3.010	15
125	624.2	157.5	73.8	73.0	74.0	931	6.7	1.601	20
126	599.8	154.4	73.0	73.2	73.9	919	5.4	1.290	6
127	624.0	158.3	74.3	74.1	73.5	917	5.4	1.273	5
128	611.6	157.3	73.1	73.3	73.8	919	7.8	1.859	25
129	613.4	154.4	73.5	73.7	74.1	930	6.9	1.626	12
130	632.0	159.0	73.4	74.5	74.4	922	8.8	2.080	20
x131	625.3	158.4	74.0	74.0	73.7	920	12.6	2.954	25
132	637.5	158.3	74.8	74.4	74.6	921	5.7	1.311	20
133	606.1	157.0	73.1	73.4	71.9	927	11.0	2.709	30
x134	630.0	159.1	73.8	74.2	74.2	919	12.0	2.805	25
135	609.0	155.2	74.2	73.5	73.0	923	13.5	3.226	40
x136	627.6	157.2	73.8	73.9	73.6	934	5.4	1.269	35
137	614.3	157.0	74.2	73.6	72.8	921	9.3	2.234	20
138	629.0	159.2	73.3	73.8	73.4	931	6.9	1.631	20
139	613.5	156.3	73.5	73.7	72.9	928	11.3	2.707	7
140	625.3	157.7	73.7	73.4	74.4	930	10.8	2.552	11
141	610.8	155.7	73.0	73.7	73.4	928	4.9	1.171	9
142	595.2	152.6	73.0	73.6	73.5	923	8.8	2.103	4
143	614.6	156.7	73.8	73.3	73.4	924	11.6	2.749	10
144	595.7	155.5	71.0	74.2	73.2	920	5.4	1.436	2
145	585.8	149.0	73.4	73.8	73.5	925	5.4	1.276	2
146	608.3	153.2	73.9	74.1	74.2	922	5.1	1.189	1
147	618.7	156.6	74.0	73.9	73.6	923	5.9	1.387	1

CREEP TEST SPECIMENS

No.	$P_{(g)}$	H(mm)	D_1 (mm)	D_2 (mm)	D_3 (mm)	ρ (kg/m^3)	T(K)	σ(MPa)	t(h)	E_o(MPa)	Ice quality	Trimming of the ends
1	628.6	159.5	72.5	73.6	74.5	928	271	0.115	20	7644.4	3	2
2	640.7	159.8	74.4	73.8	74.0	931	271	0.115	20	7908.0	3	3
3	633.2	159.6	74.8	74.0	73.8	917	271	0.114	20	12005.0	3	3
4	637.8	159.5	75.0	74.0	73.5	926	271	0.114	20	12005.0	3	2
5	601.3	160.2	72.4	72.5	71.8	916	271	0.238	8	9139.6	3	3
6	569.7	160.9	73.0	72.2	69.6	921	271	0.240	8	7429.8	3	3
7	600.4	160.7	73.1	71.7	71.7	914	271	0.243	8	5553.4	3	3
8	599.0	160.2	73.2	72.4	71.4	910	271	0.238	8	11213.5	2	3
9	637.2	159.5	74.0	74.2	74.2	926	271	0.227	22	11634.2	3	3
10	638.5	159.7	73.2	74.5	74.5	928	271	0.225	22	9576.3	2	3
11	638.6	160.2	73.8	74.2	73.8	929	271	0.227	22	7562.2	3	3
12	625.2	157.8	71.8	73.6	75.0	934	271	0.231	22	17080.0	2	3
13	638.0	160.3	74.2	74.2	74.2	922	271	0.227	22	7438.3	3	3
14	631.2	159.8	72.8	74.0	74.5	924	271	0.228	22	7128.0	3	3
15	602.2	159.9	73.3	72.9	70.8	917	271	0.499	32	6528.6	3	3
16	605.4	160.3	73.0	73.0	72.0	911	271	0.498	32	7271.1	3	3
17	601.1	160.3	73.1	72.8	71.9	906	271	0.501	32	7502.8	2	3
18	604.0	159.6	73.1	72.8	72.4	910	271	0.501	32	5891.9	3	2
19	634.2	159.6	72.2	74.5	74.5	930	271	0.478	22	7137.6	3	3
20	634.5	160.4	74.0	74.2	74.2	916	271	0.482	22	7902.1	3	3
21	635.4	159.6	74.3	73.6	74.0	927	271	0.490	22	9422.8	3	3
22	634.8	159.0	73.2	73.8	74.5	932	271	0.487	22	8702.3	3	3
23	634.3	159.2	74.2	74.2	74.5	919	271	0.482	22	8311.9	2	3
24	628.8	159.0	73.0	74.2	74.0	926	271	0.709	22	9452.8	3	3

25	631.8	159.5	73.2	74.0	74.2	926	271	0.713	22	9257.1	3	3
26	634.4	159.2	74.4	74.2	74.0	921	271	0.709	22	7623.2	3	3
27	608.1	161.3	73.2	73.1	71.5	911	268	0.123	8	7678.0	3	3
28	610.6	160.8	72.9	72.6	72.6	915	268	0.119	8	6722.7	3	3
29	612.4	160.8	72.7	72.6	72.4	921	268	0.119	8	7899.2	3	3
30	602.5	160.8	72.9	71.4	72.3	915	268	0.123	8	8829.2	3	3
31	636.8	159.2	72.5	74.5	74.0	938	268	0.113	8	8037.3	3	3
32	632.5	159.6	74.2	74.0	73.8	921	268	0.114	8	7128.0	3	3
33	635.8	158.5	72.4	74.0	74.6	941	268	0.114	8	7128.0	3	3
34	514.4	161.9	73.3	73.0	71.2	911	268	0.234	22	7684.8	3	2
35	612.1	160.8	73.8	73.4	71.4	913	268	0.232	22	7133.5	3	3
36	616.5	160.5	73.0	73.3	72.0	924	268	0.233	22	6038.2	3	2
37	609.2	161.5	73.5	72.6	71.7	911	268	0.237	20	7073.9	2	2
38	609.4	161.4	73.7	72.9	72.0	905	268	0.235	20	7373.5	3	3
39	611.5	161.4	73.8	72.9	72.2	906	268	0.235	20	7933.5	2	2
40	606.5	160.5	73.0	72.0	72.6	915	268	0.241	20	8133.1	2	3
41	611.2	160.5	72.8	72.2	72.8	920	268	0.509	32	7833.4	2	2
42	609.6	159.5	73.2	73.0	72.8	913	268	0.495	32	9808.9	3	2
43	609.3	158.6	73.5	73.5	71.7	920	268	0.491	32	9270.1	3	2
44	610.1	159.4	73.2	72.2	72.1	927	268	0.509	32	7894.1	2	2
45	615.3	161.5	73.5	72.7	72.8	910	268	0.502	45	8283.6	3	3
46	612.6	160.8	73.7	72.9	71.6	917	268	0.499	45	9889.9	3	3
47	612.1	161.7	73.4	72.7	72.7	906	268	0.502	45	7331.2	3	3
48	611.5	161.2	73.6	72.7	72.7	906	268	0.739	8	7403.7	3	3
49	601.6	160.2	73.1	72.3	71.7	913	268	0.747	8	6021.9	1	2
50	603.0	161.4	72.9	72.4	71.7	909	268	0.745	8	6141.4	2	2
51	608.1	161.2	73.2	72.6	71.0	920	268	0.741	8	6921.0	2	3
52	622.5	159.4	73.8	74.0	72.8	920	268	0.713	18	4882.2	3	3
53	628.8	159.2	74.6	74.2	72.8	922	268	0.709	18	3458.3	2	3
54	633.7	159.2	74.0	74.6	74.6	916	268	0.701	18	4644.9	2	3
55	628.6	159.5	73.0	73.8	73.2	933	268	0.717	20	6635.8	3	3
56	632.9	159.3	74.2	73.8	73.2	930	268	0.717	20	6231.9	3	3
57	632.9	159.0	74.0	73.8	72.5	940	268	0.717	20	10386.4	3	3

58	624.3	159.5	74.5	73.5	73.2	917	268	0.723	20	8500.3	3	3
59	605.3	160.5	73.0	72.4	71.9	915	263	0.118	7	7524.4	2	3
60	614.2	161.3	73.3	73.2	72.1	913	263	0.117	7	11713.9	2	3
61	604.8	160.5	72.7	71.3	72.0	926	263	0.123	7	19046.2	2	3
62	603.1	161.1	71.4	72.3	72.0	922	263	0.119	7	10763.4	2	3
63	614.0	160.2	72.9	72.8	73.8	912	263	0.118	7	5519.3	3	3
64	600.2	160.0	71.9	72.5	72.7	912	263	0.119	7	8704.4	2	2
65	614.0	160.7	72.1	73.4	73.2	915	263	0.116	4	19647.4	2	3
66	615.5	159.7	71.4	73.6	73.1	928	263	0.115	4	5778.9	2	2
67	614.1	160.3	72.3	72.8	73.9	915	263	0.118	4	8269.3	2	2
68	575.4	150.5	72.9	72.5	72.8	920	263	0.119	4	11705.9	2	3
69	574.5	159.0	71.7	68.5	71.1	927	263	0.266	22	12563.7	2	2
70	556.3	159.5	70.0	69.1	68.2	930	263	0.262	22	5813.1	2	3
71	574.0	160.3	68.5	71.5	69.9	931	263	0.244	22	6185.4	2	3
72	615.8	160.5	73.1	73.4	72.9	913	263	0.232	20	6894.8	2	3
73	613.2	159.0	73.9	73.3	72.2	918	263	0.232	20	7981.9	2	3
74	614.1	160.4	74.0	73.3	72.8	906	263	0.232	20	11551.4	2	2
75	616.1	160.3	73.0	73.6	73.2	912	263	0.231	20	5441.4	2	2
76	614.2	160.7	73.5	73.1	72.8	910	263	0.497	22	6910.7	2	3
77	614.9	160.1	73.8	73.8	73.4	901	263	0.487	22	8456.9	2	3
78	622.2	161.7	73.8	73.5	73.2	907	263	0.491	22	7602.6	2	3
79	615.3	159.9	73.1	72.8	73.7	914	263	0.501	22	7704.8	2	2
80	611.1	160.1	73.6	73.0	71.6	919	263	0.498	22	6953.9	2	2
81	612.4	160.3	73.4	73.4	72.0	914	263	0.493	22	6783.6	2	2
82	623.0	162.5	73.5	73.4	71.8	919	263	0.493	22	9208.6	2	2
83	610.2	159.4	73.9	73.4	72.6	907	263	0.493	22	5098.7	2	2
84	616.5	160.3	73.2	73.4	73.6	909	263	0.490	63	11631.6	2	3
85	617.6	160.3	72.8	73.4	72.8	921	263	0.493	8	6419.0	2	3
86	629.0	160.2	73.3	73.7	74.8	915	263	0.489	8	10769.2	2	3
87	620.0	159.4	72.7	72.8	74.3	922	263	0.501	24	2295.8	2	3
88	607.3	160.0	72.4	72.6	72.5	919	263	0.741	22	6969.9	2	3
89	611.0	160.2	72.4	72.7	73.4	915	263	0.739	22	5521.6	1	3
90	623.5	160.5	72.7	73.0	73.5	926	263	0.732	22	7918.5	2	3
91	604.8	160.3	72.1	72.4	73.1	913	263	0.745	22	7676.8	3	3

92	636.5	159.0	74.2	74.5	74.0	925	263	0.703	2	4596.0	2	3
93	636.3	159.0	74.6	74.0	74.0	925	263	0.713	2	4598.0	3	3
94	639.2	160.0	74.2	74.2	74.5	921	263	0.709	2	5787.0	3	3
95	630.6	158.6	73.2	74.0	74.0	931	253	0.228	20	14811.3	3	3
96	637.5	159.3	74.2	74.0	73.8	930	253	0.228	20	10861.6	3	3
97	631.4	158.0	73.0	74.2	74.3	933	253	0.227	20	11120.9	3	2
98	629.0	160.2	72.5	74.2	74.5	919	253	0.227	20	30657.6	3	2
99	631.4	159.7	74.0	73.8	73.8	923	253	0.487	22	9282.5	3	3
100	639.6	159.5	74.0	74.2	74.5	927	253	0.482	22	9270.9	3	3
101	639.0	159.0	74.5	74.6	73.5	929	253	0.477	22	17664.3	2	3
102	636.8	158.8	74.5	74.0	74.5	924	253	0.485	22	11822.0	3	3
103	630.9	160.5	73.4	74.2	73.8	919	253	0.709	25	16879.9	2	3
104	630.5	160.6	73.2	73.2	74.0	926	253	0.729	25	18211.5	3	2
105	627.5	158.6	73.2	73.8	74.4	925	253	0.717	25	7465.3	3	3
106	626.2	158.7	72.5	73.8	74.2	930	253	0.717	25	7166.7	3	3

APPENDIX 6

SOME PHOTOGRAPHS OF ICE FAILURE

1 Failure test specimen

2...8 Creep rupture (T = 271 K and σ = 0,75 PMa)

1

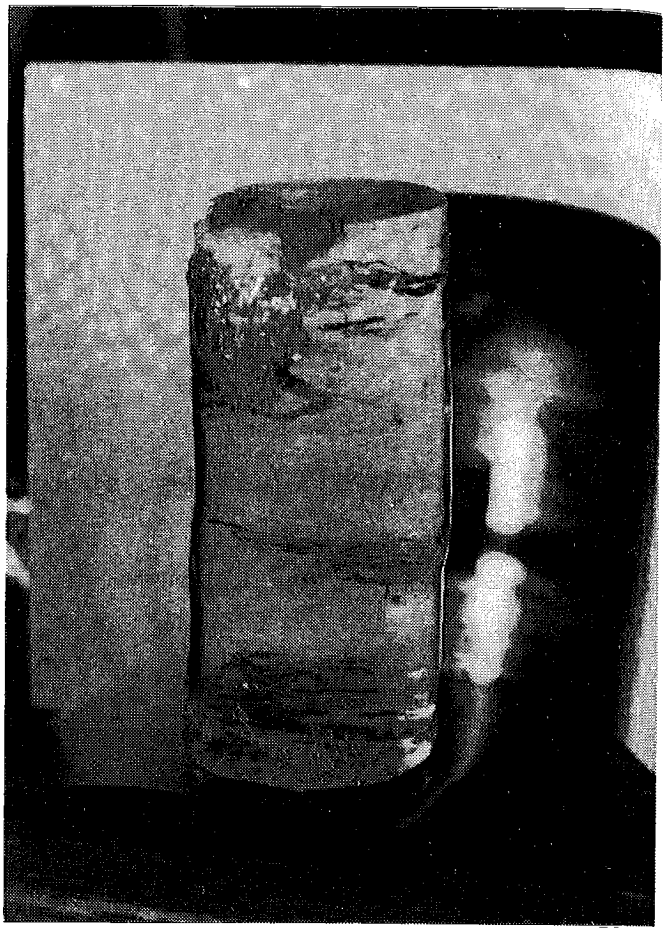

2

3

4

5

6

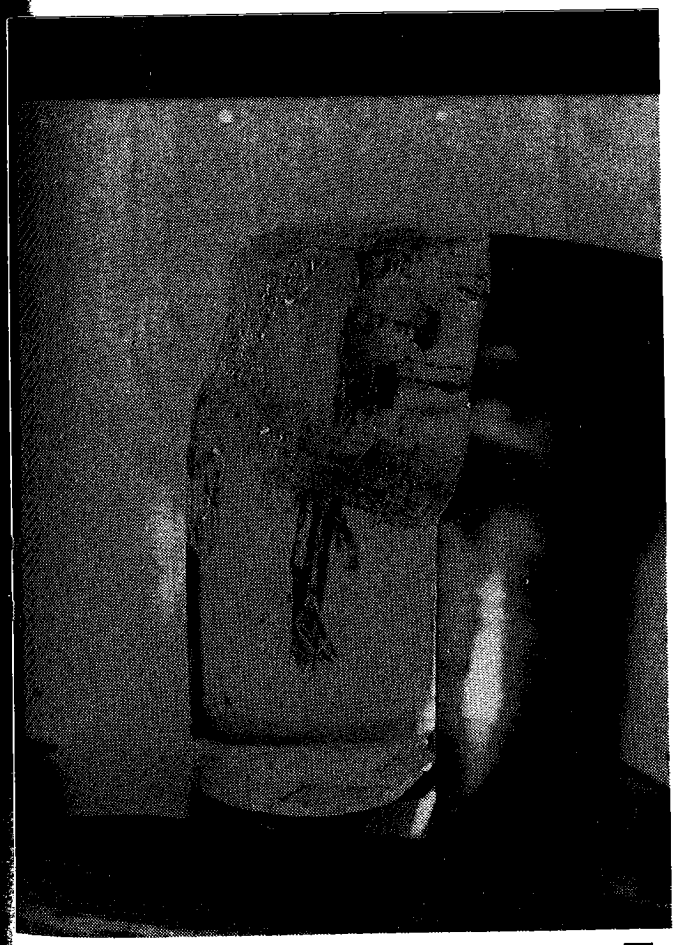

7

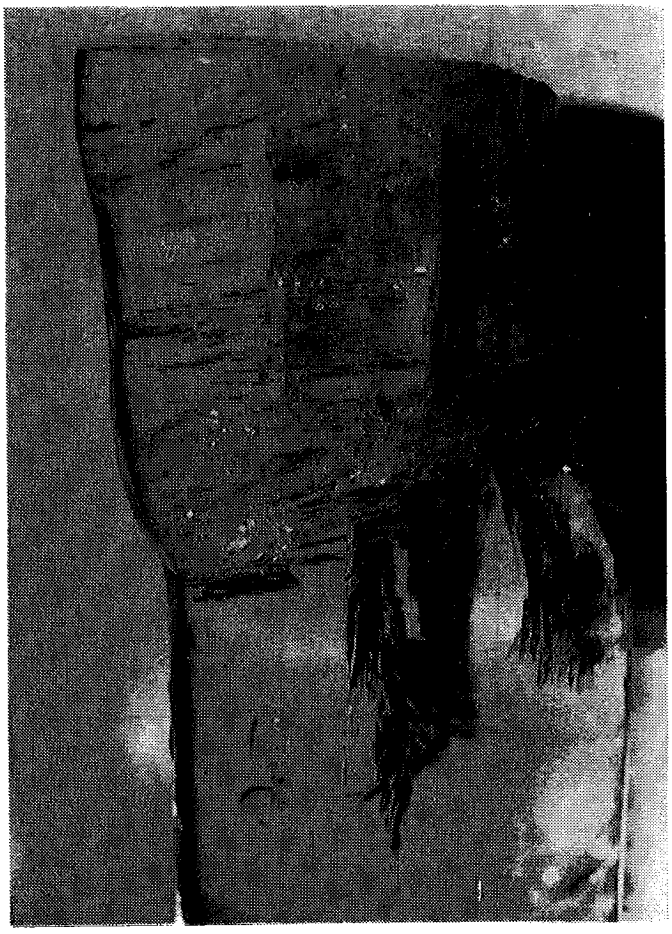

8

APPENDIX 7

CREEP TEST CURVES IN (log ε, log t) - SCALE

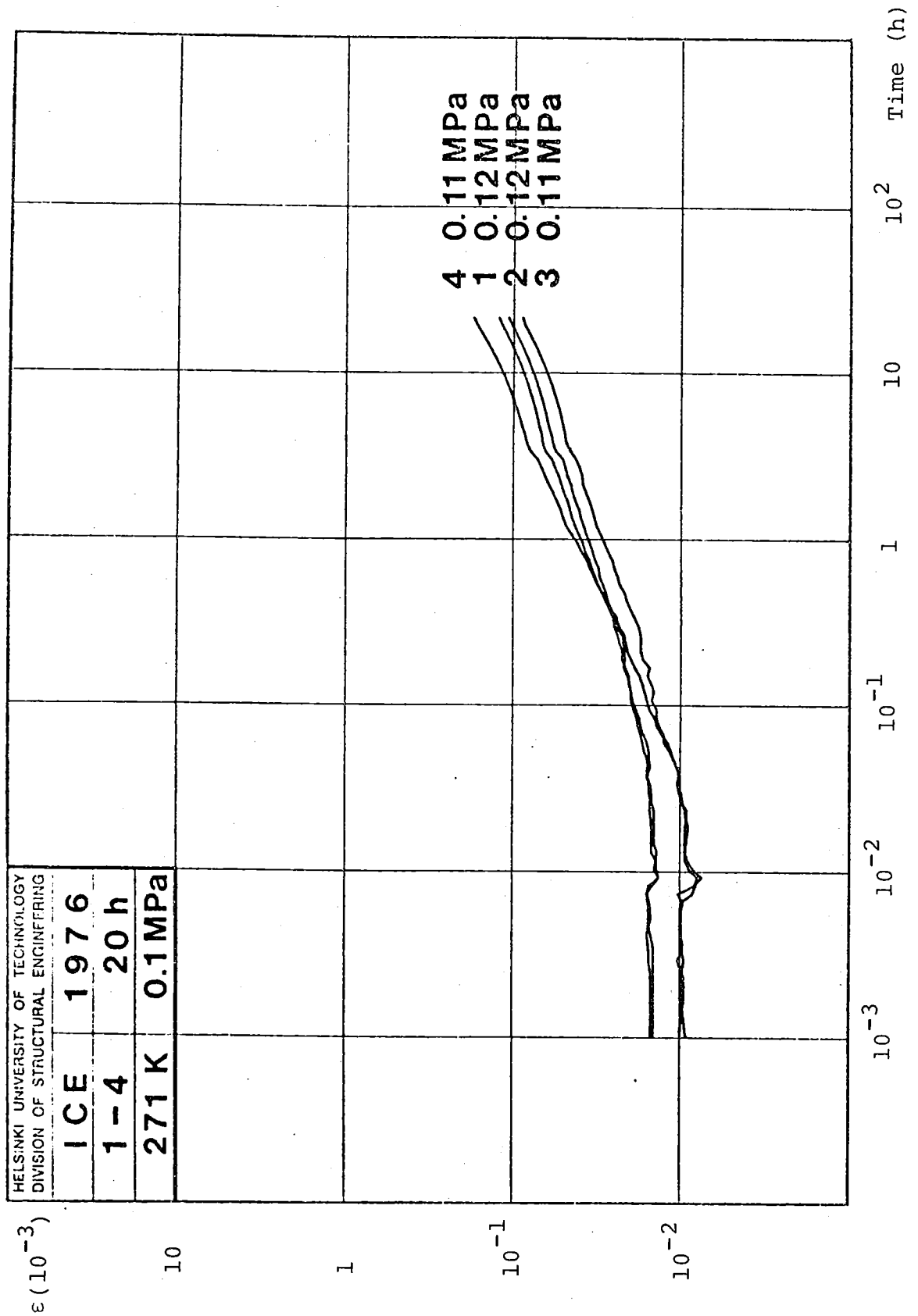
HELSINKI UNIVERSITY OF TECHNOLOGY
DIVISION OF STRUCTURAL ENGINEERING
ICE 1976
1-4 20 h
271 K 0.1 MPa
4 0.11 MPa
1 0.12 MPa
2 0.12 MPa
3 0.11 MPa
ε (10^-3)
10
1
10^-1
10^-2
10^-3
10^-2
10^-1
1
10
10^2
Time (h)

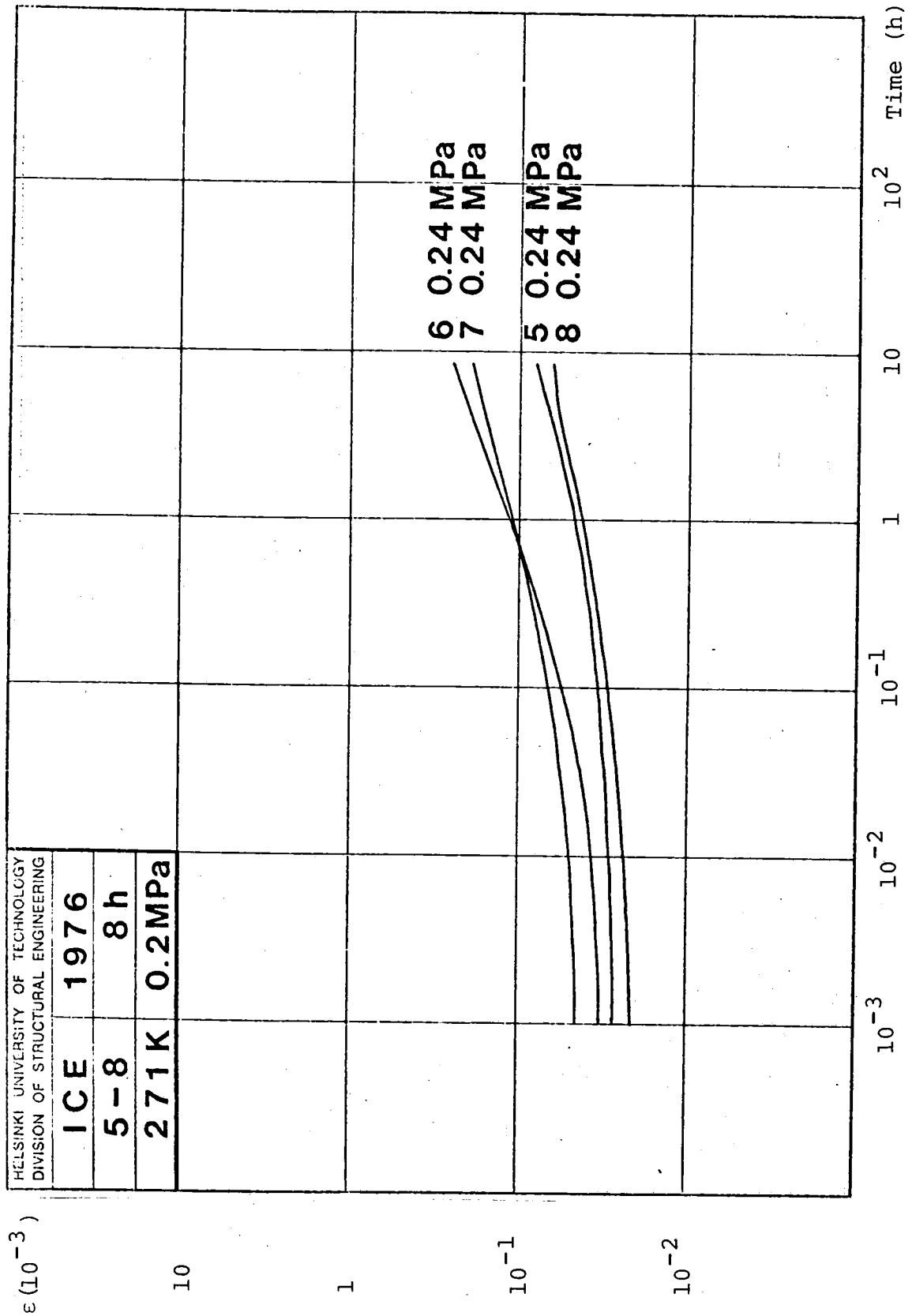
HELSINKI UNIVERSITY OF TECHNOLOGY
DIVISION OF STRUCTURAL ENGINEERING
ICE 1976
5-8 8 h
271K 0.2MPa
6 0.24 MPa
7 0.24 MPa
5 0.24 MPa
8 0.24 MPa
ε (10⁻³)
10
1
10⁻¹
10⁻²
10⁻³
10⁻²
10⁻¹
1
10
10²
Time (h)

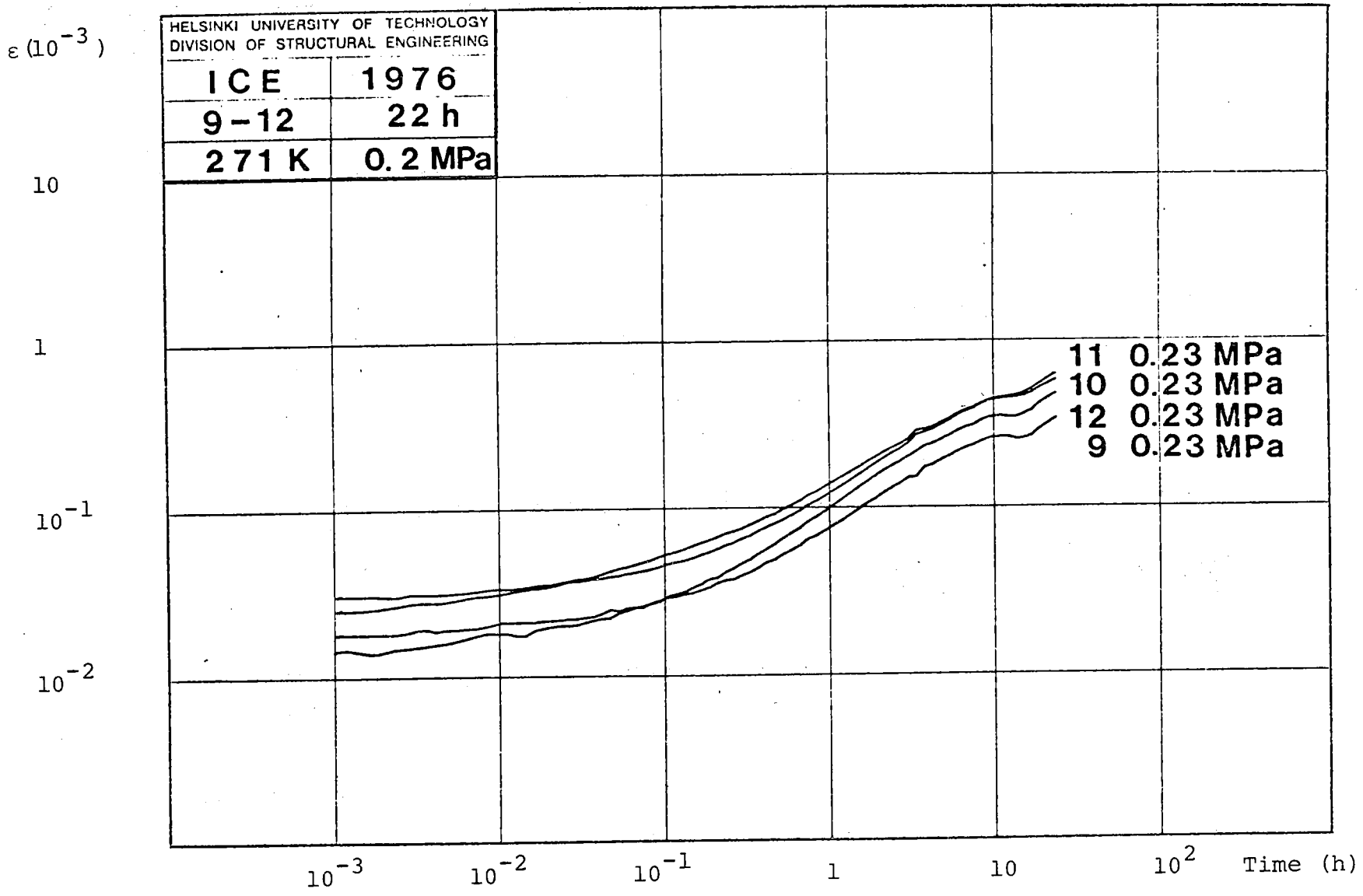
HELSINKI UNIVERSITY OF TECHNOLOGY
DIVISION OF STRUCTURAL ENGINEERING
ICE
1976
9-12
22 h
271 K
0.2 MPa
ε (10^-3)
10
1
10^-1
10^-2
11 0.23 MPa
10 0.23 MPa
12 0.23 MPa
9 0.23 MPa
10^-3
10^-2
10^-1
1
10
10^2
Time (h)

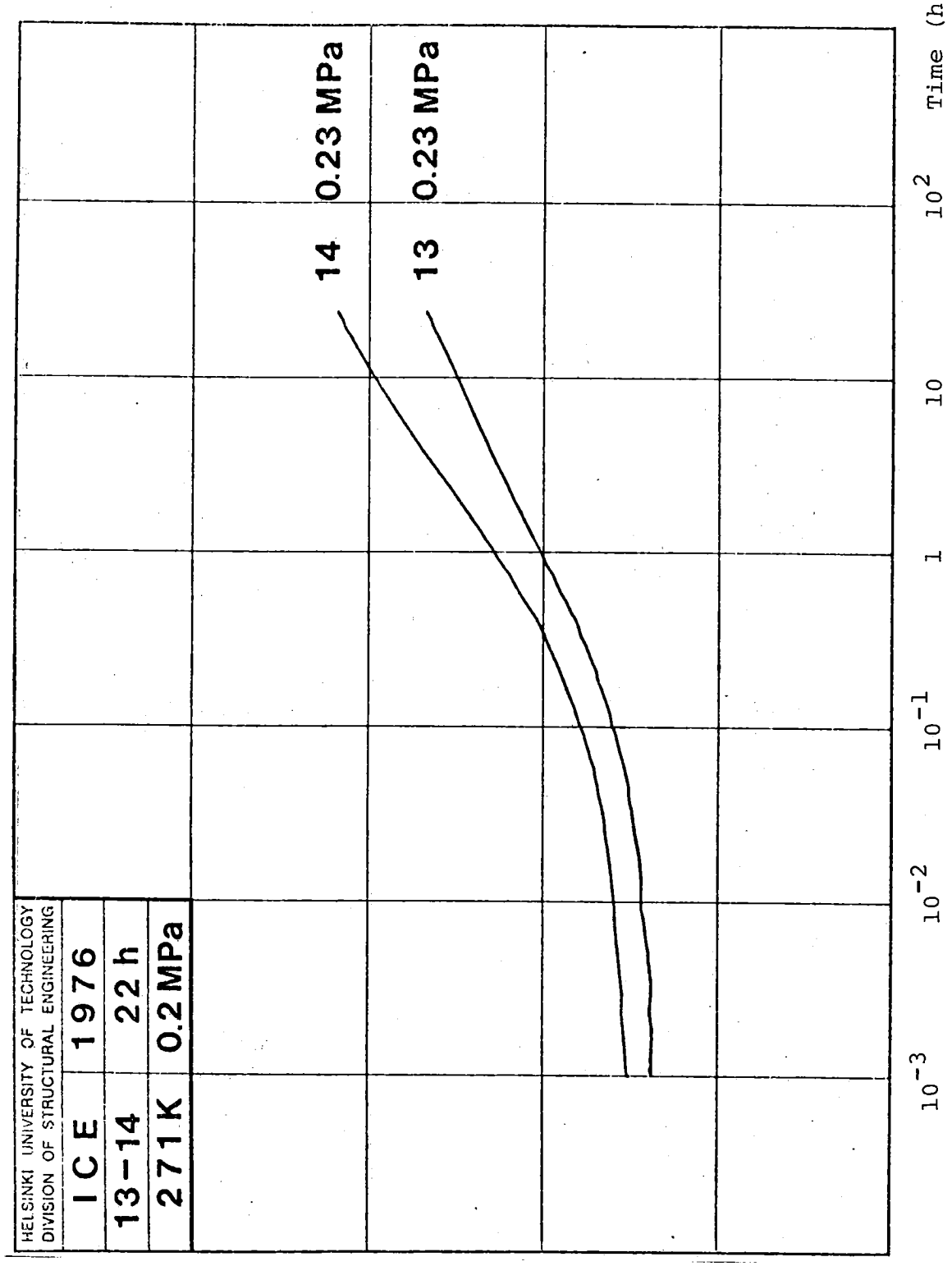
HELSINKI UNIVERSITY OF TECHNOLOGY
DIVISION OF STRUCTURAL ENGINEERING
ICE 1976
13–14 22 h
271 K 0.2 MPa
14 0.23 MPa
13 0.23 MPa
ε (10⁻³)
10
1
10⁻¹
10⁻²
10⁻³
10⁻²
10⁻¹
1
10
10²
Time (h)

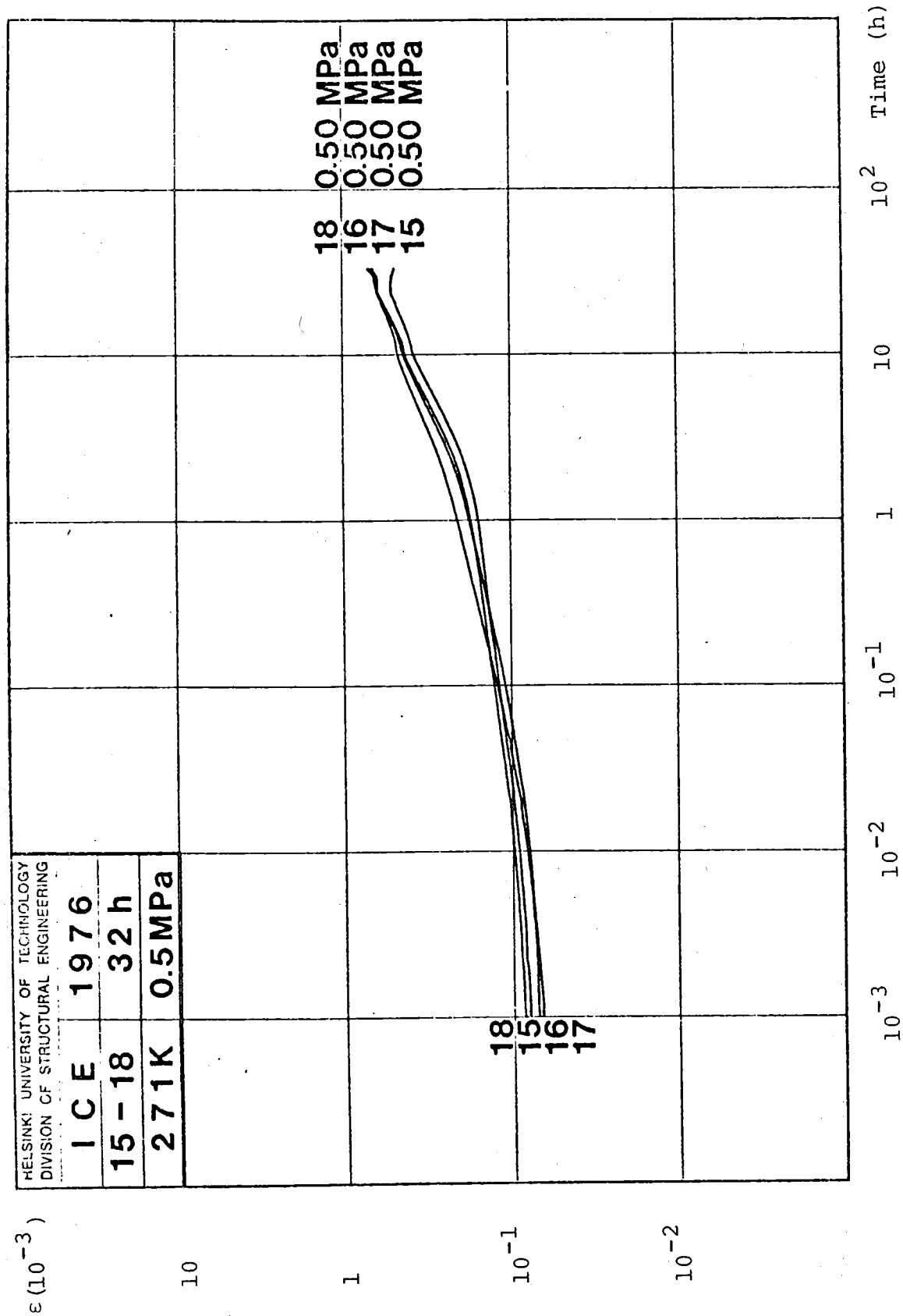
HELSINKI UNIVERSITY OF TECHNOLOGY
DIVISION OF STRUCTURAL ENGINEERING
ICE 1976
15 - 18 32 h
271K 0.5MPa
18 0.50 MPa
16 0.50 MPa
17 0.50 MPa
15 0.50 MPa
18
15
16
17
ε (10⁻³)
10
1
10⁻¹
10⁻²
10⁻³
10⁻²
10⁻¹
1
10
10²
Time (h)

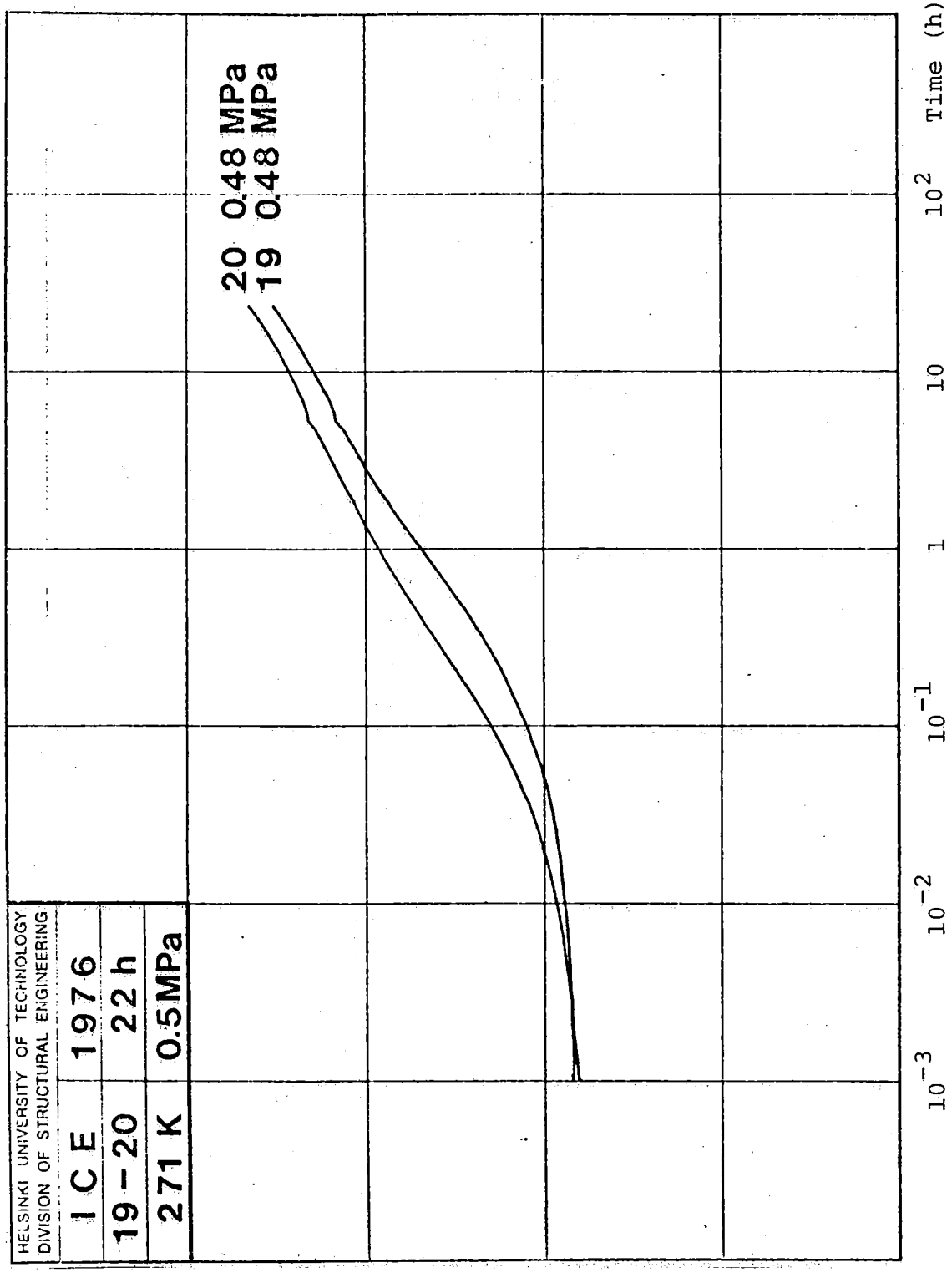
HELSINKI UNIVERSITY OF TECHNOLOGY
DIVISION OF STRUCTURAL ENGINEERING
ICE 1976
19-20 22 h
271 K 0.5MPa
20 0.48 MPa
19 0.48 MPa
ε (10⁻³)
10
1
10⁻¹
10⁻²
10⁻³
10⁻²
10⁻¹
1
10
10²
Time (h)

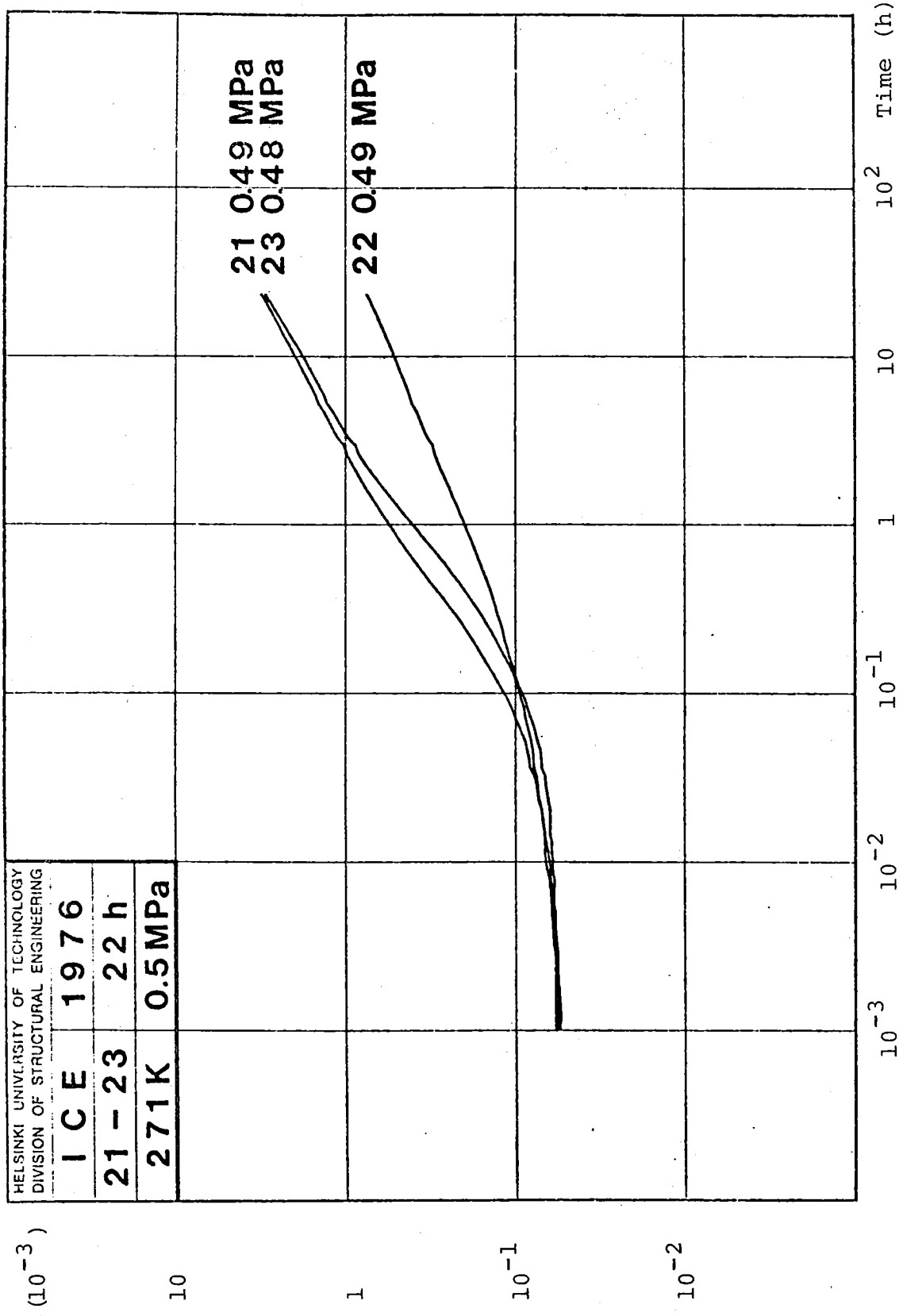
HELSINKI UNIVERSITY OF TECHNOLOGY
DIVISION OF STRUCTURAL ENGINEERING
ICE 1976
21 – 23 22 h
271 K 0.5 MPa
21 0.49 MPa
23 0.48 MPa
22 0.49 MPa
ε (10⁻³)
10
1
10⁻¹
10⁻²
10⁻³
10⁻²
10⁻¹
1
10
10²
Time (h)

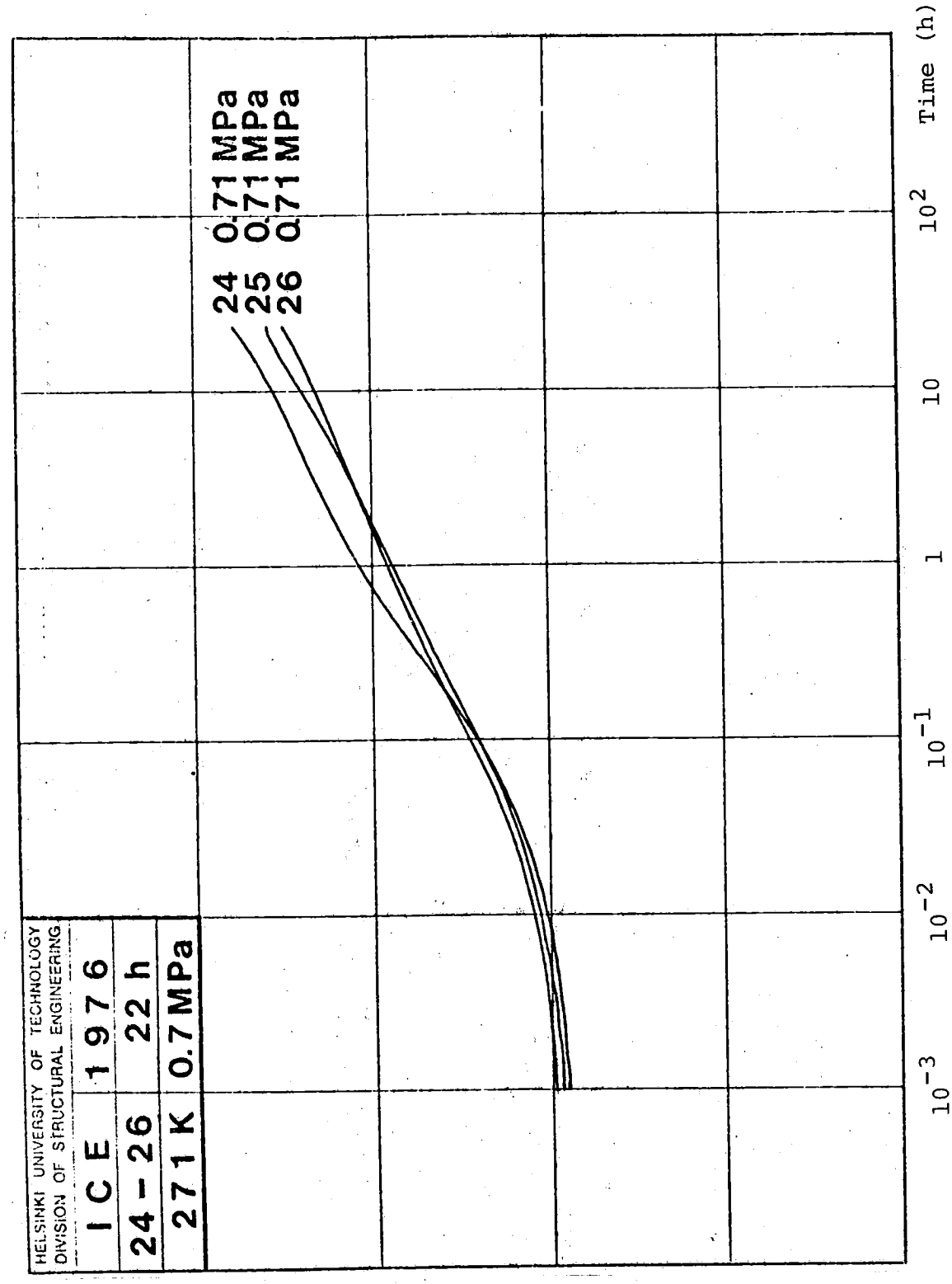
HELSINKI UNIVERSITY OF TECHNOLOGY
DIVISION OF STRUCTURAL ENGINEERING
ICE 1976
24-26 22 h
271 K 0.7 MPa
24 0.71 MPa
25 0.71 MPa
26 0.71 MPa
ε (10⁻³)
10
1
10⁻¹
10⁻²
10⁻³
10⁻²
10⁻¹
1
10
10²
Time (h)

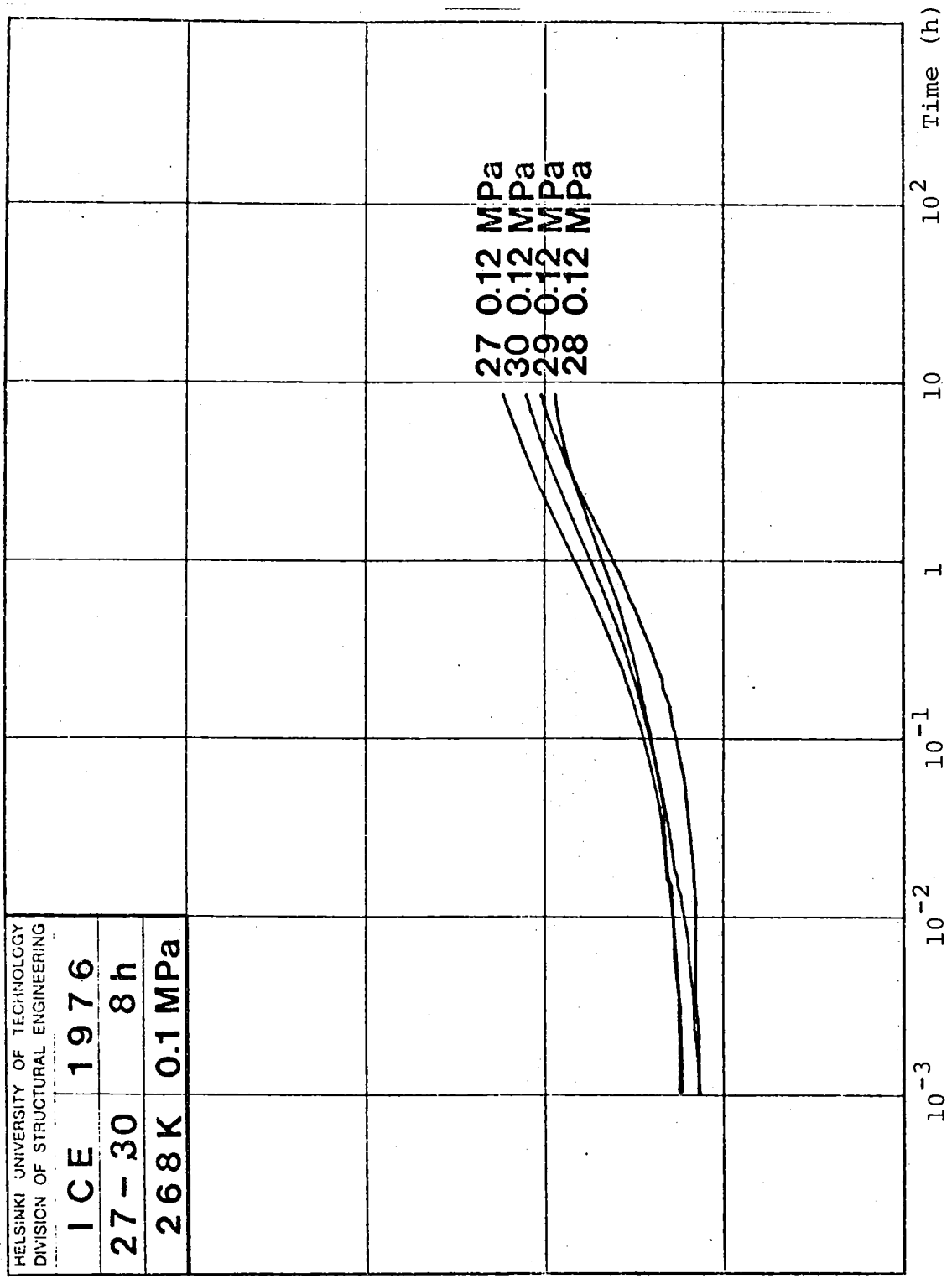
HELSINKI UNIVERSITY OF TECHNOLOGY
DIVISION OF STRUCTURAL ENGINEERING
ICE 1976
27 - 30 8 h
268K 0.1 MPa
27 0.12 MPa
30 0.12 MPa
29 0.12 MPa
28 0.12 MPa
ε (10⁻³)
10
1
10⁻¹
10⁻²
10⁻³
10⁻²
10⁻¹
1
10
10²
Time (h)

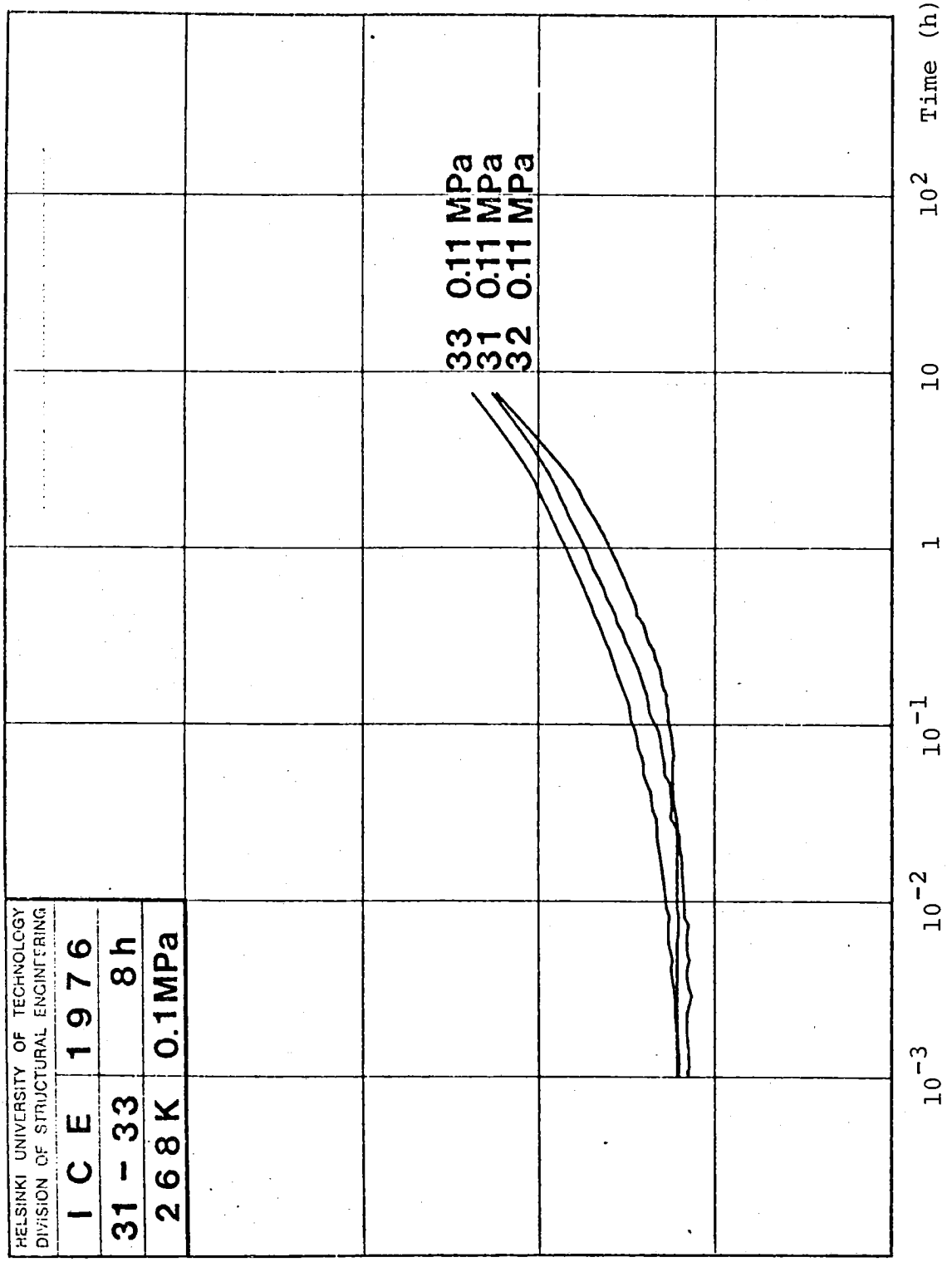
HELSINKI UNIVERSITY OF TECHNOLOGY
DIVISION OF STRUCTURAL ENGINEERING
ICE 1976
31 - 33 8h
268K 0.1MPa
33 0.11 MPa
31 0.11 MPa
32 0.11 MPa
ε (10⁻³)
10
1
10⁻¹
10⁻²
10⁻³
10⁻²
10⁻¹
1
10
10²
Time (h)

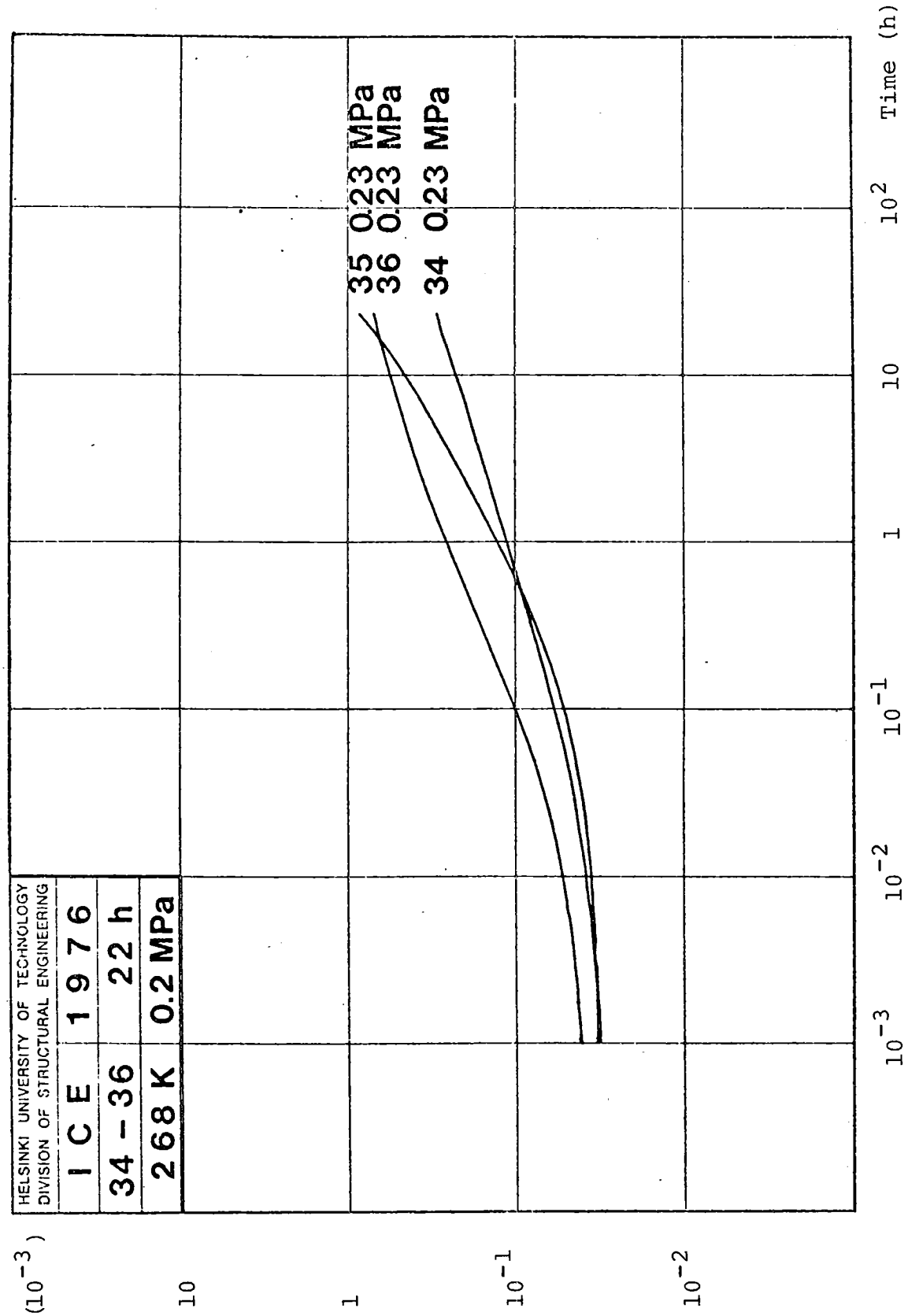
HELSINKI UNIVERSITY OF TECHNOLOGY
DIVISION OF STRUCTURAL ENGINEERING
ICE 1976
34 - 36 22 h
268 K 0.2 MPa
35 0.23 MPa
36 0.23 MPa
34 0.23 MPa
ε (10⁻³)
10
1
10⁻¹
10⁻²
10⁻³
10⁻²
10⁻¹
1
10
10²
Time (h)

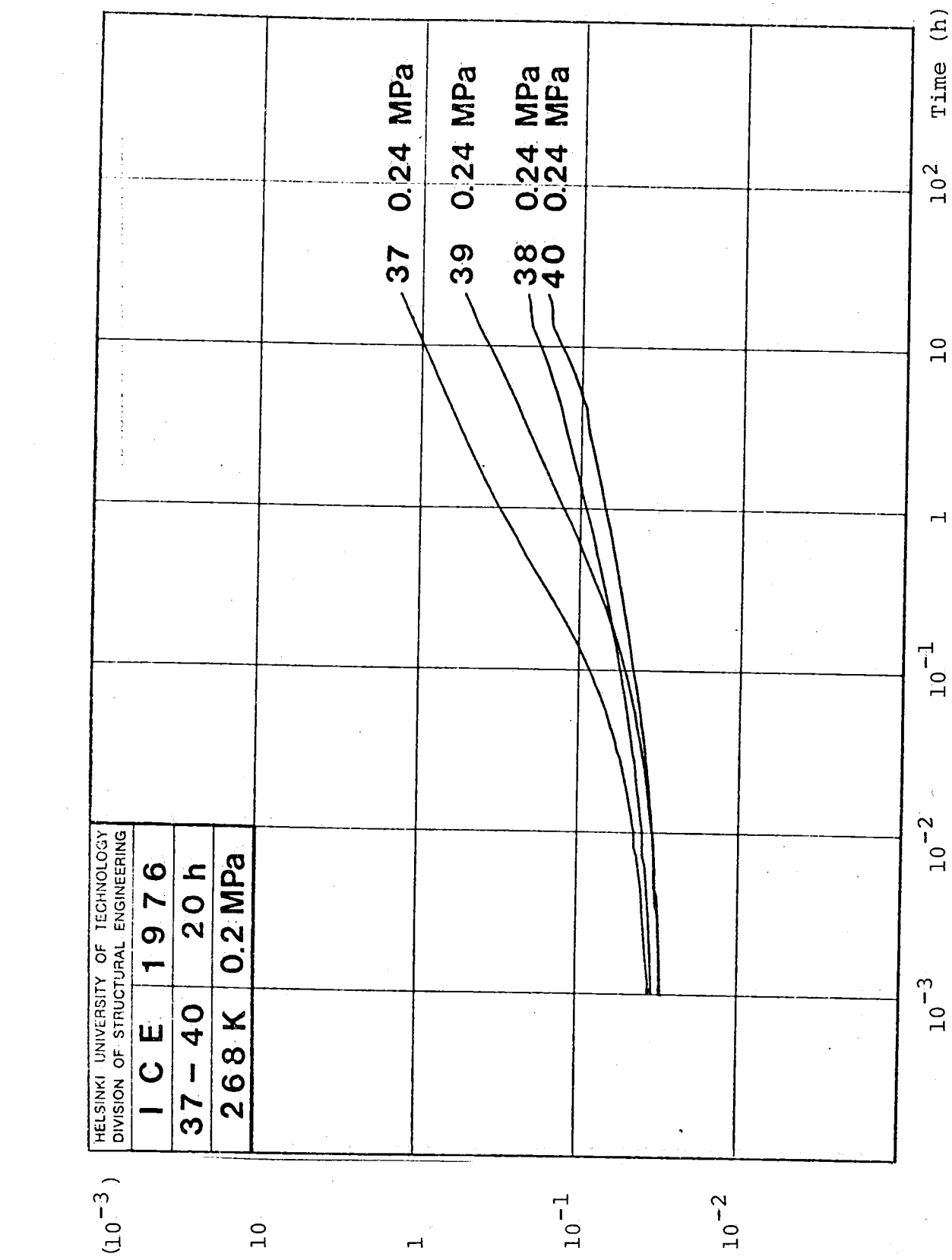
HELSINKI UNIVERSITY OF TECHNOLOGY
DIVISION OF STRUCTURAL ENGINEERING
ICE 1976
37 – 40 20 h
268 K 0.2 MPa
37 0.24 MPa
39 0.24 MPa
38 0.24 MPa
40 0.24 MPa
ε (10⁻³)
10
1
10⁻¹
10⁻²
10⁻³
10⁻²
10⁻¹
1
10
10²
Time (h)

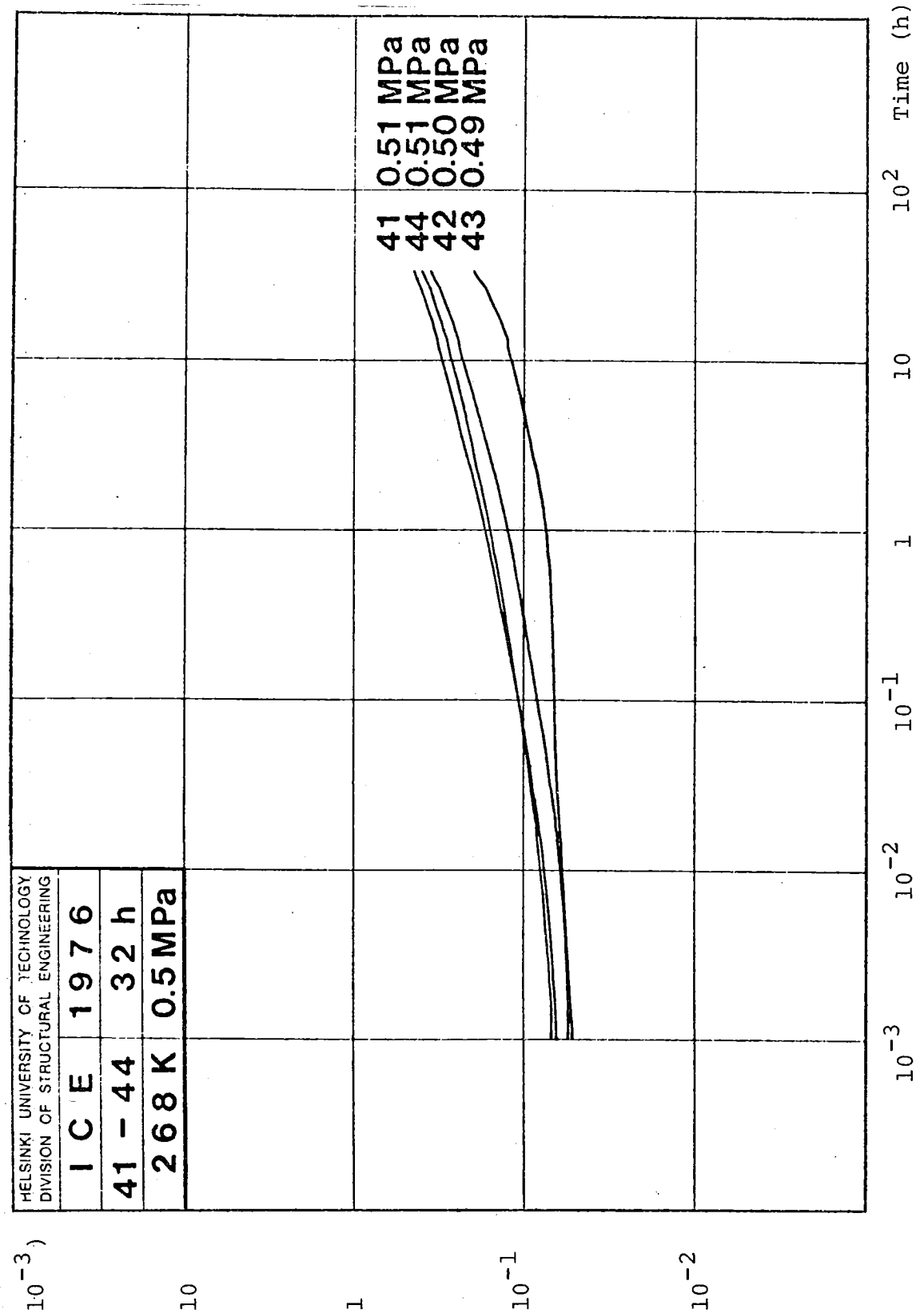
HELSINKI UNIVERSITY OF TECHNOLOGY
DIVISION OF STRUCTURAL ENGINEERING
ICE 1976
41 - 44 32 h
268 K 0.5 MPa
41 0.51 MPa
44 0.51 MPa
42 0.50 MPa
43 0.49 MPa
ε (10⁻³)
10
1
10⁻¹
10⁻²
10⁻³
10⁻²
10⁻¹
1
10
10²
Time (h)

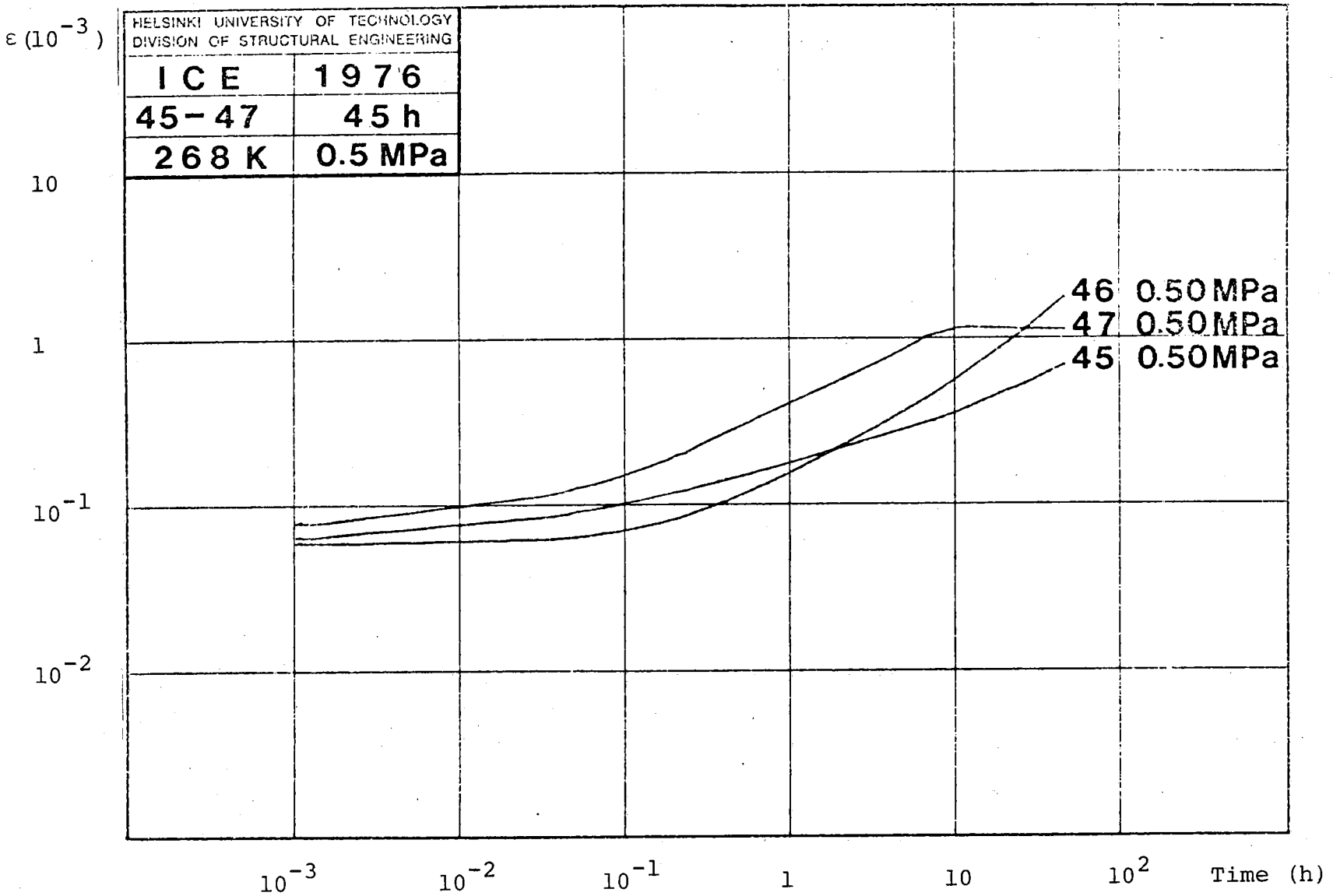
HELSINKI UNIVERSITY OF TECHNOLOGY
DIVISION OF STRUCTURAL ENGINEERING
ICE 1976
45-47 45 h
268 K 0.5 MPa
ε (10^-3)
10
1
10^-1
10^-2
46 0.50MPa
47 0.50MPa
45 0.50MPa
10^-3
10^-2
10^-1
1
10
10^2
Time (h)

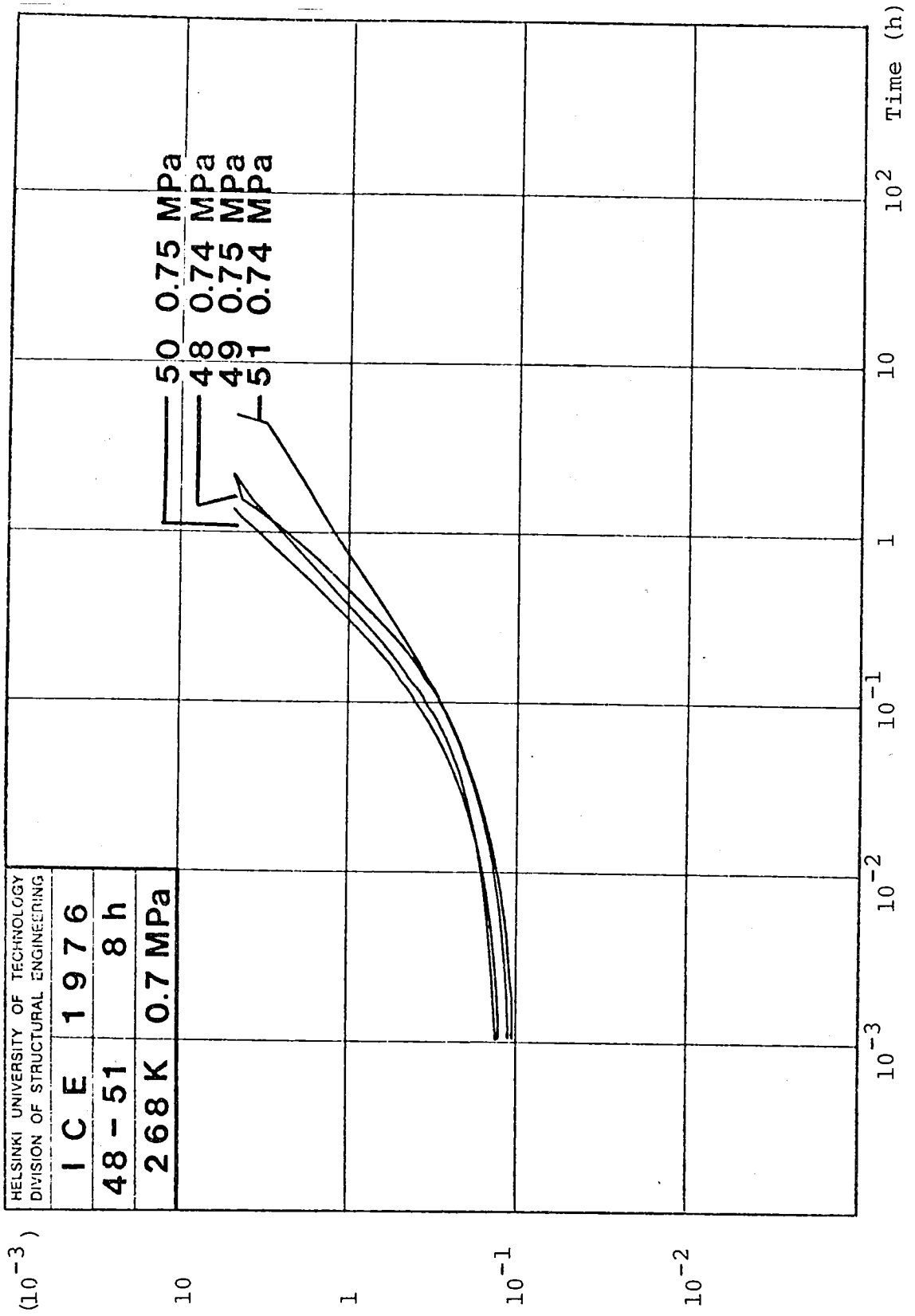
HELSINKI UNIVERSITY OF TECHNOLOGY
DIVISION OF STRUCTURAL ENGINEERING
ICE 1976
48 - 51 8 h
268 K 0.7 MPa
50 0.75 MPa
48 0.74 MPa
49 0.75 MPa
51 0.74 MPa
ε (10⁻³)
10
1
10⁻¹
10⁻²
10⁻³
10⁻²
10⁻¹
1
10
10²
Time (h)

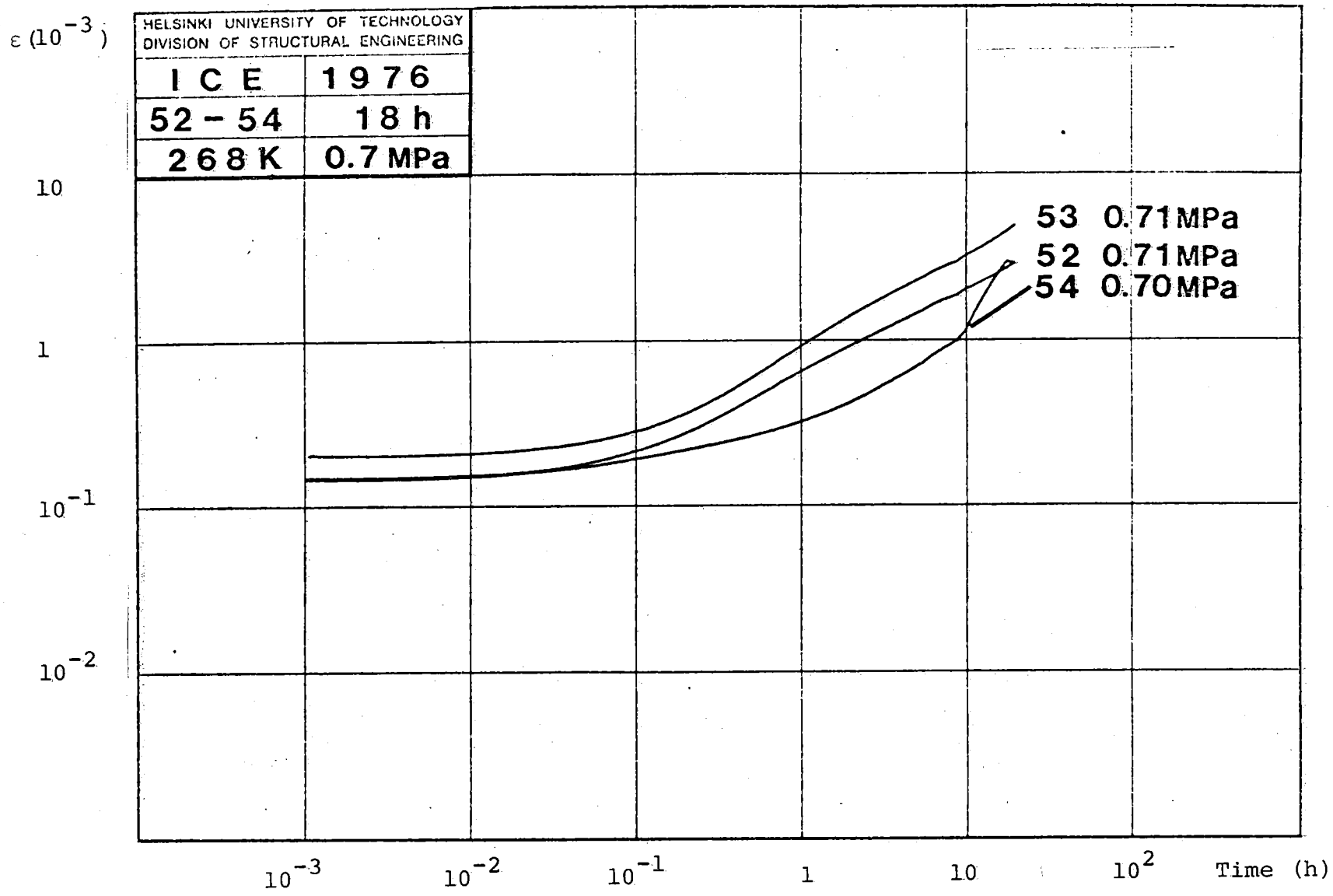
HELSINKI UNIVERSITY OF TECHNOLOGY
DIVISION OF STRUCTURAL ENGINEERING
I C E
1976
52 - 54
18 h
268 K
0.7 MPa
ε (10^-3)
10
1
10^-1
10^-2
53 0.71MPa
52 0.71MPa
54 0.70MPa
10^-3
10^-2
10^-1
1
10
10^2
Time (h)

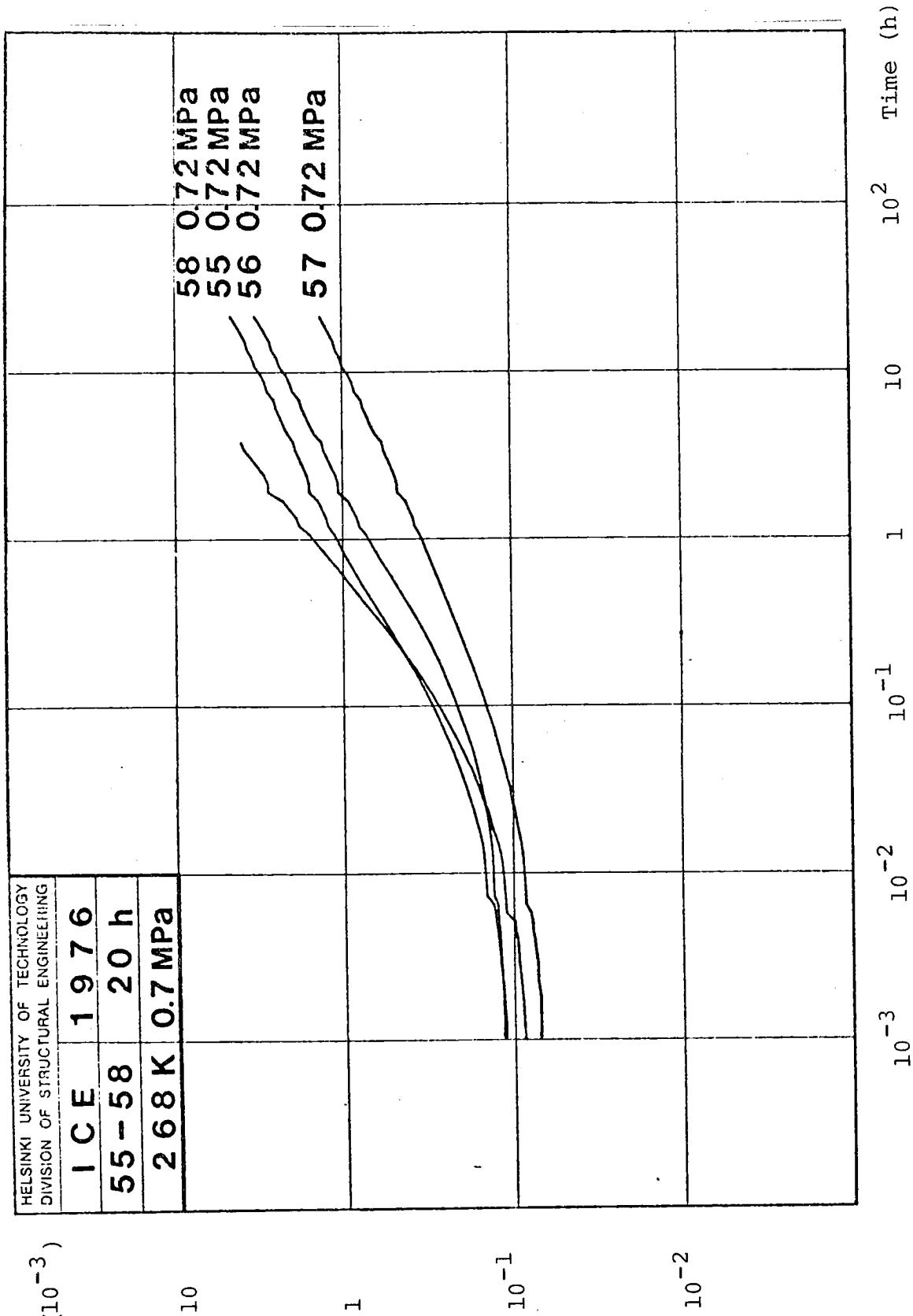
HELSINKI UNIVERSITY OF TECHNOLOGY
DIVISION OF STRUCTURAL ENGINEERING
ICE 1976
55-58 20 h
268 K 0.7 MPa
58 0.72 MPa
55 0.72 MPa
56 0.72 MPa
57 0.72 MPa
ε (10⁻³)
10
1
10⁻¹
10⁻²
10⁻³
10⁻²
10⁻¹
1
10
10²
Time (h)

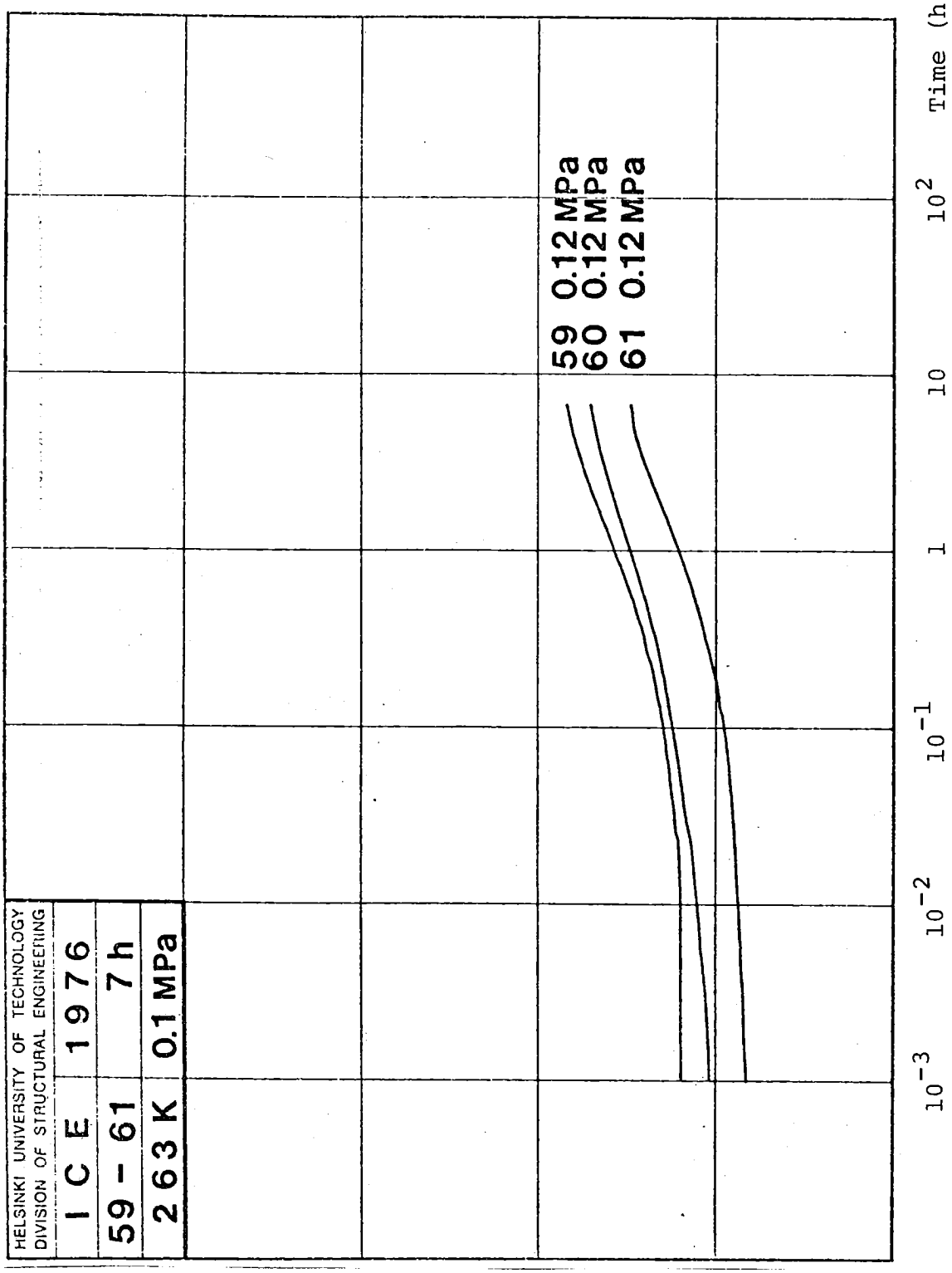
HELSINKI UNIVERSITY OF TECHNOLOGY
DIVISION OF STRUCTURAL ENGINEERING
ICE 1976
59 - 61 7 h
263 K 0.1 MPa
59 0.12 MPa
60 0.12 MPa
61 0.12 MPa
ε (10⁻³)
10
1
10⁻¹
10⁻²
10⁻³
10⁻²
10⁻¹
1
10
10²
Time (h)

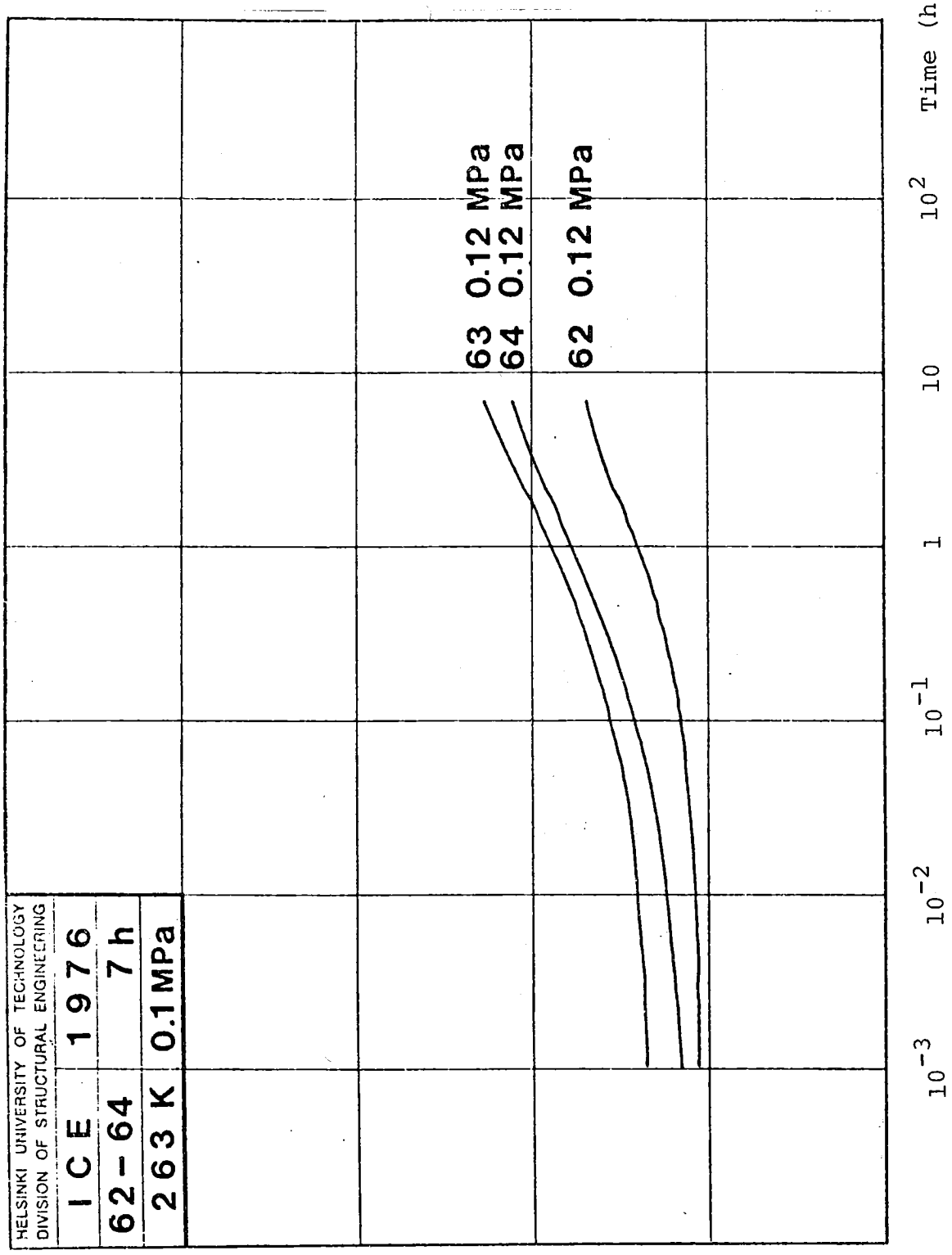
HELSINKI UNIVERSITY OF TECHNOLOGY
DIVISION OF STRUCTURAL ENGINEERING
ICE 1976
62-64 7h
263 K 0.1MPa
63 0.12 MPa
64 0.12 MPa
62 0.12 MPa
ε (10⁻³)
10
1
10⁻¹
10⁻²
10⁻³
10⁻²
10⁻¹
1
10
10²
Time (h)

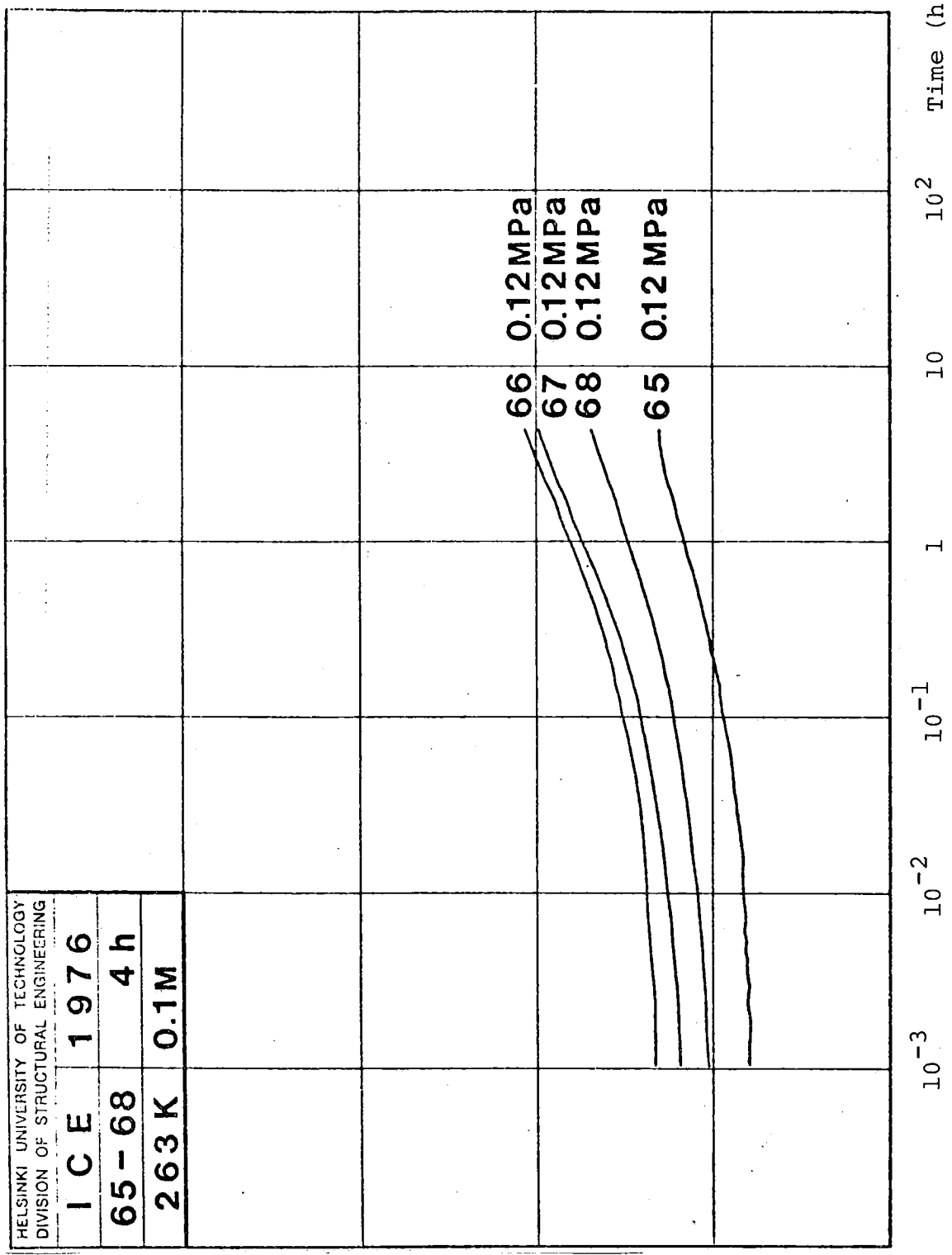
HELSINKI UNIVERSITY OF TECHNOLOGY
DIVISION OF STRUCTURAL ENGINEERING
ICE 1976
65-68 4h
263K 0.1M
66 0.12MPa
67 0.12MPa
68 0.12MPa
65 0.12MPa
ε (10⁻³)
10
1
10⁻¹
10⁻²
10⁻³
10⁻²
10⁻¹
1
10
10²
Time (h)

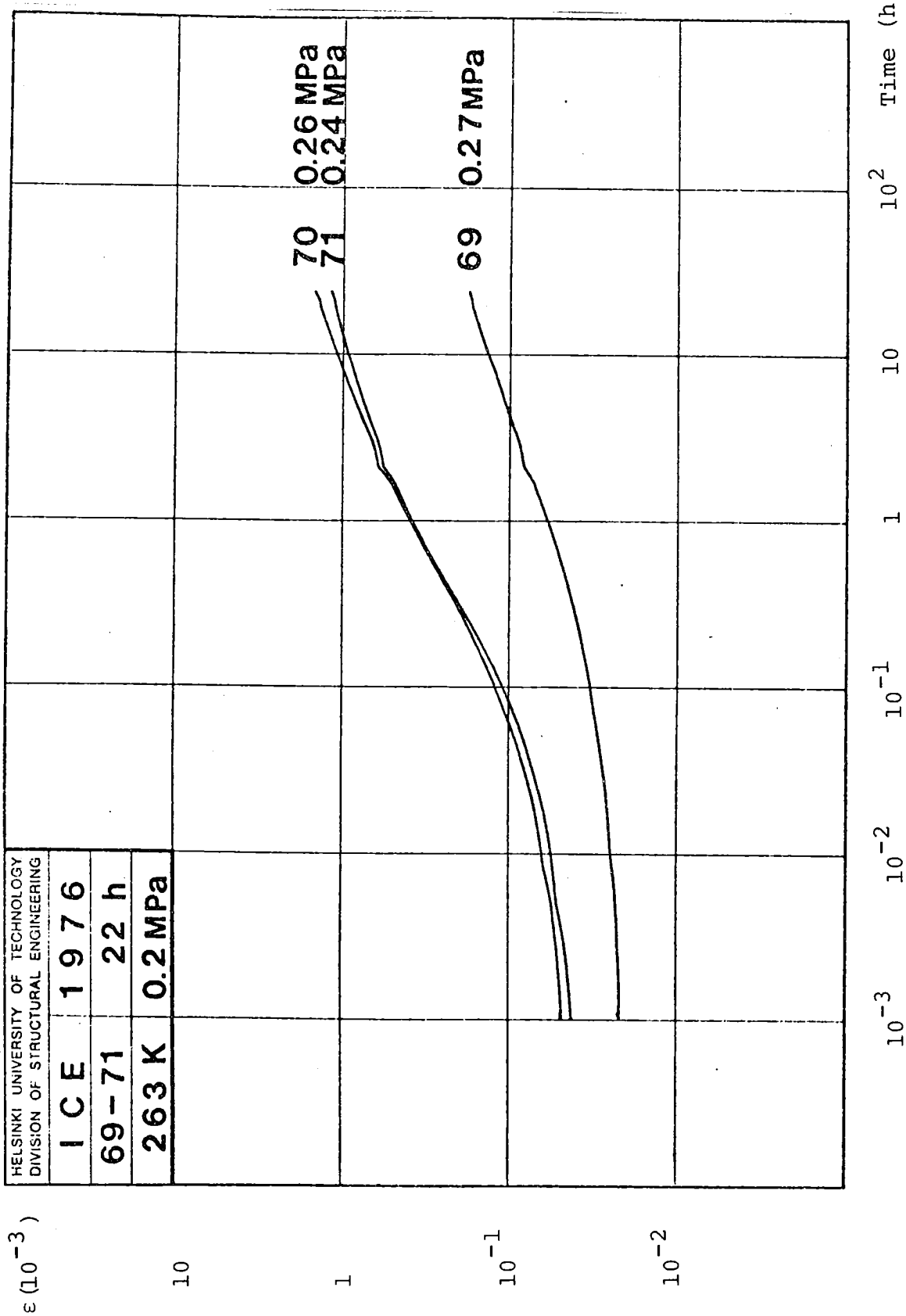
HELSINKI UNIVERSITY OF TECHNOLOGY
DIVISION OF STRUCTURAL ENGINEERING
ICE 1976
69-71 22 h
263 K 0.2 MPa
70 0.26 MPa
71 0.24 MPa
69 0.27 MPa
ε (10⁻³)
10
1
10⁻¹
10⁻²
10⁻³
10⁻²
10⁻¹
1
10
10²
Time (h)

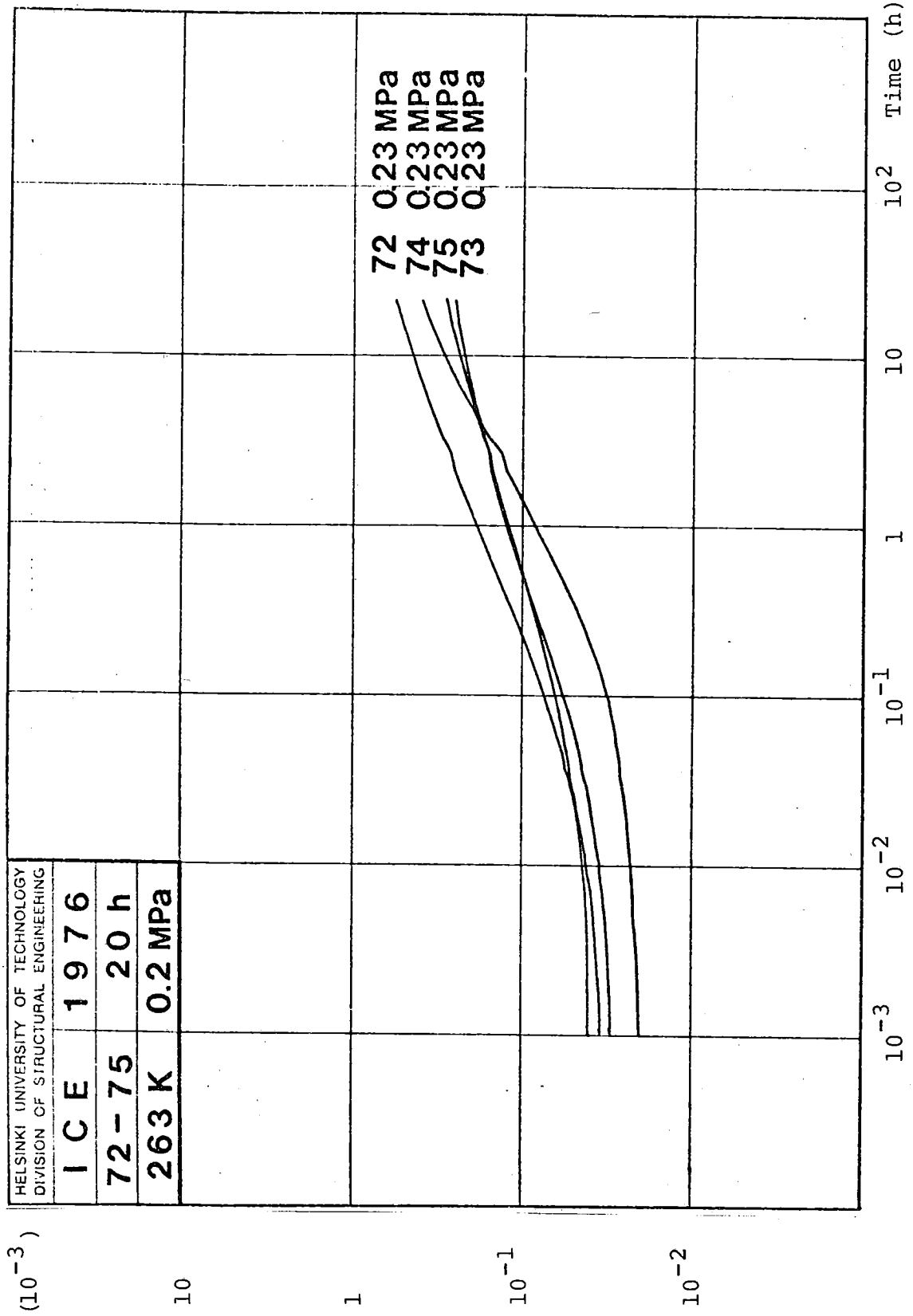
HELSINKI UNIVERSITY OF TECHNOLOGY
DIVISION OF STRUCTURAL ENGINEERING
ICE 1976
72-75 20 h
263 K 0.2 MPa
72 0.23 MPa
74 0.23 MPa
75 0.23 MPa
73 0.23 MPa
ε (10⁻³)
10
1
10⁻¹
10⁻²
10⁻³
10⁻²
10⁻¹
1
10
10²
Time (h)

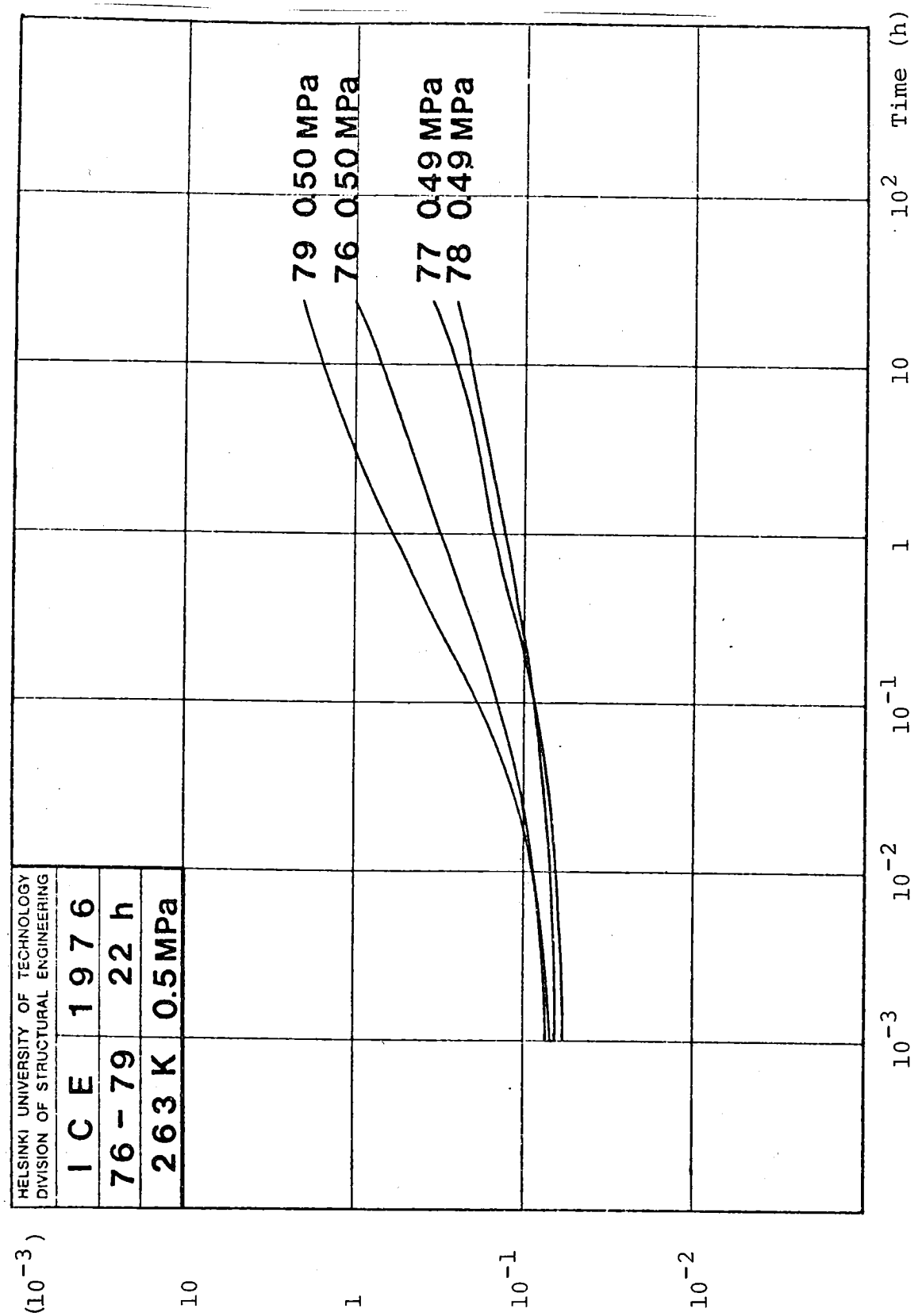
HELSINKI UNIVERSITY OF TECHNOLOGY
DIVISION OF STRUCTURAL ENGINEERING
ICE 1976
76-79 22 h
263 K 0.5MPa
79 0.50 MPa
76 0.50 MPa
77 0.49 MPa
78 0.49 MPa
ε (10⁻³)
10
1
10⁻¹
10⁻²
10⁻³
10⁻²
10⁻¹
1
10
10²
Time (h)

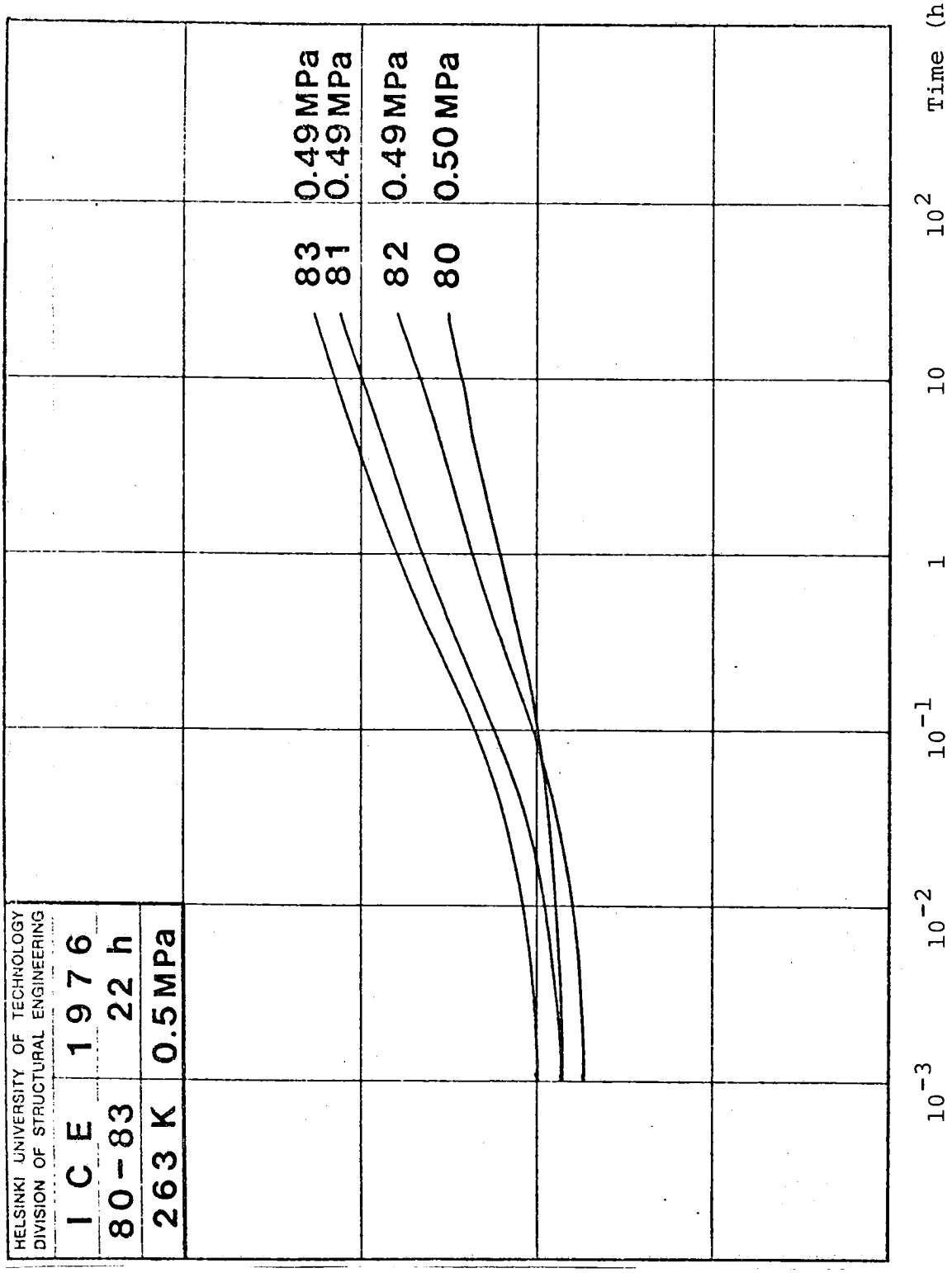
HELSINKI UNIVERSITY OF TECHNOLOGY
DIVISION OF STRUCTURAL ENGINEERING
ICE 1976
80-83 22 h
263 K 0.5MPa
83 0.49MPa
81 0.49MPa
82 0.49MPa
80 0.50MPa
ε (10⁻³)
10
1
10⁻¹
10⁻²
10⁻³
10⁻²
10⁻¹
1
10
10²
Time (h)

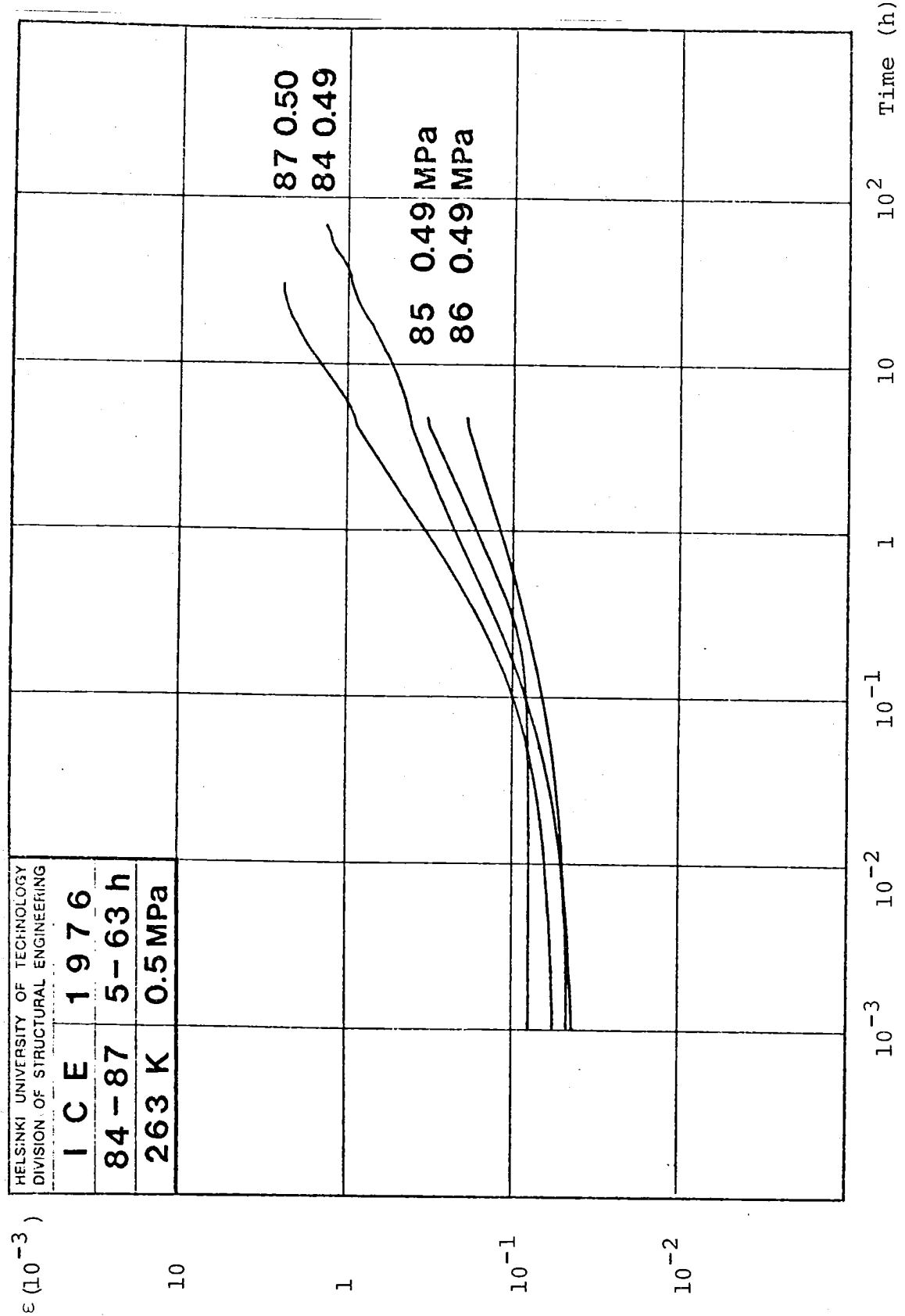
HELSINKI UNIVERSITY OF TECHNOLOGY
DIVISION OF STRUCTURAL ENGINEERING
ICE 1976
84-87 5-63 h
263 K 0.5 MPa
87 0.50
84 0.49
85 0.49 MPa
86 0.49 MPa
ε (10⁻³)
10
1
10⁻¹
10⁻²
10⁻³
10⁻²
10⁻¹
1
10
10²
Time (h)

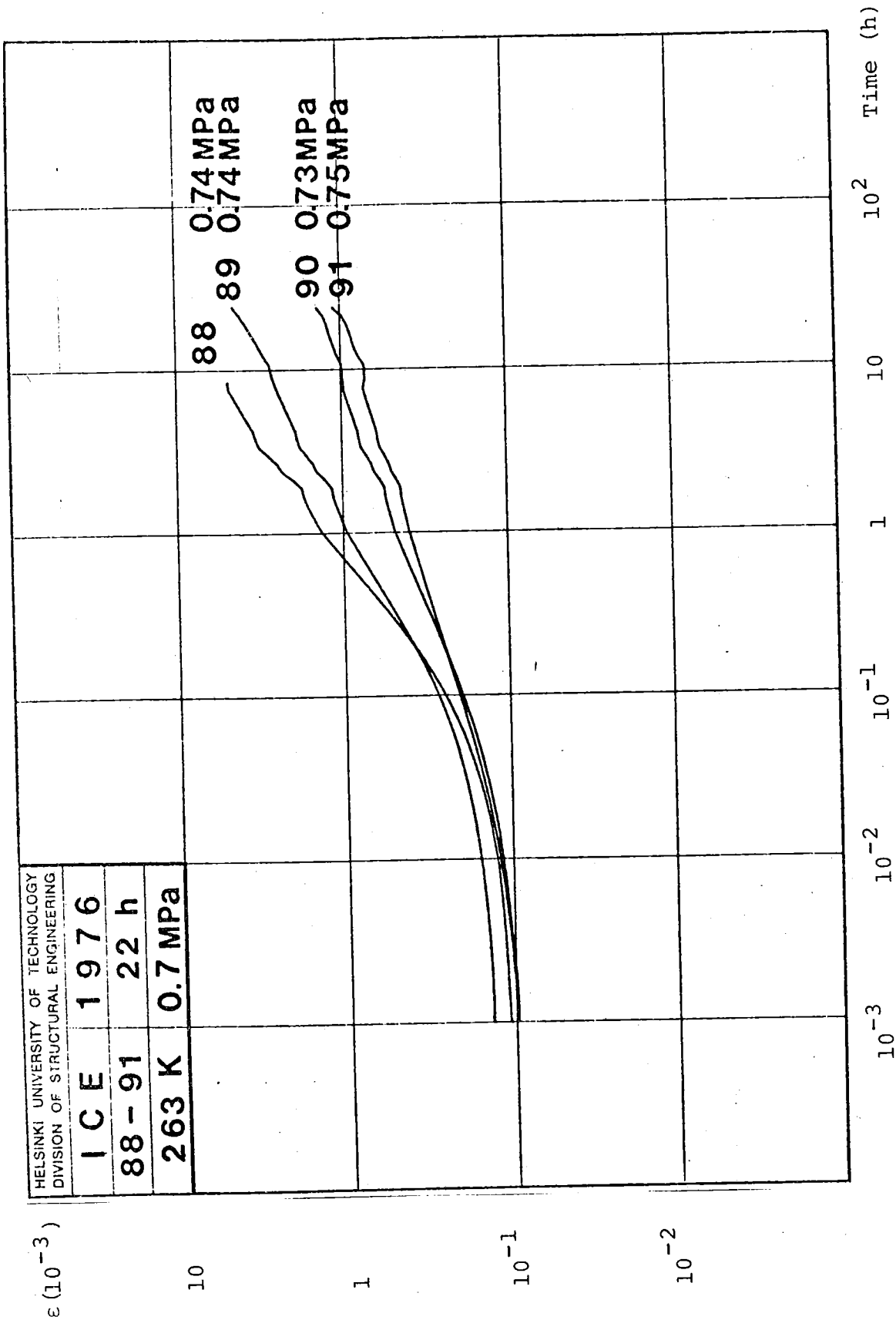
HELSINKI UNIVERSITY OF TECHNOLOGY
DIVISION OF STRUCTURAL ENGINEERING
ICE 1976
88-91 22 h
263 K 0.7 MPa
88 0.74 MPa
89 0.74 MPa
90 0.73 MPa
91 0.75 MPa
ε (10⁻³)
10
1
10⁻¹
10⁻²
10⁻³
10⁻²
10⁻¹
1
10
10²
Time (h)

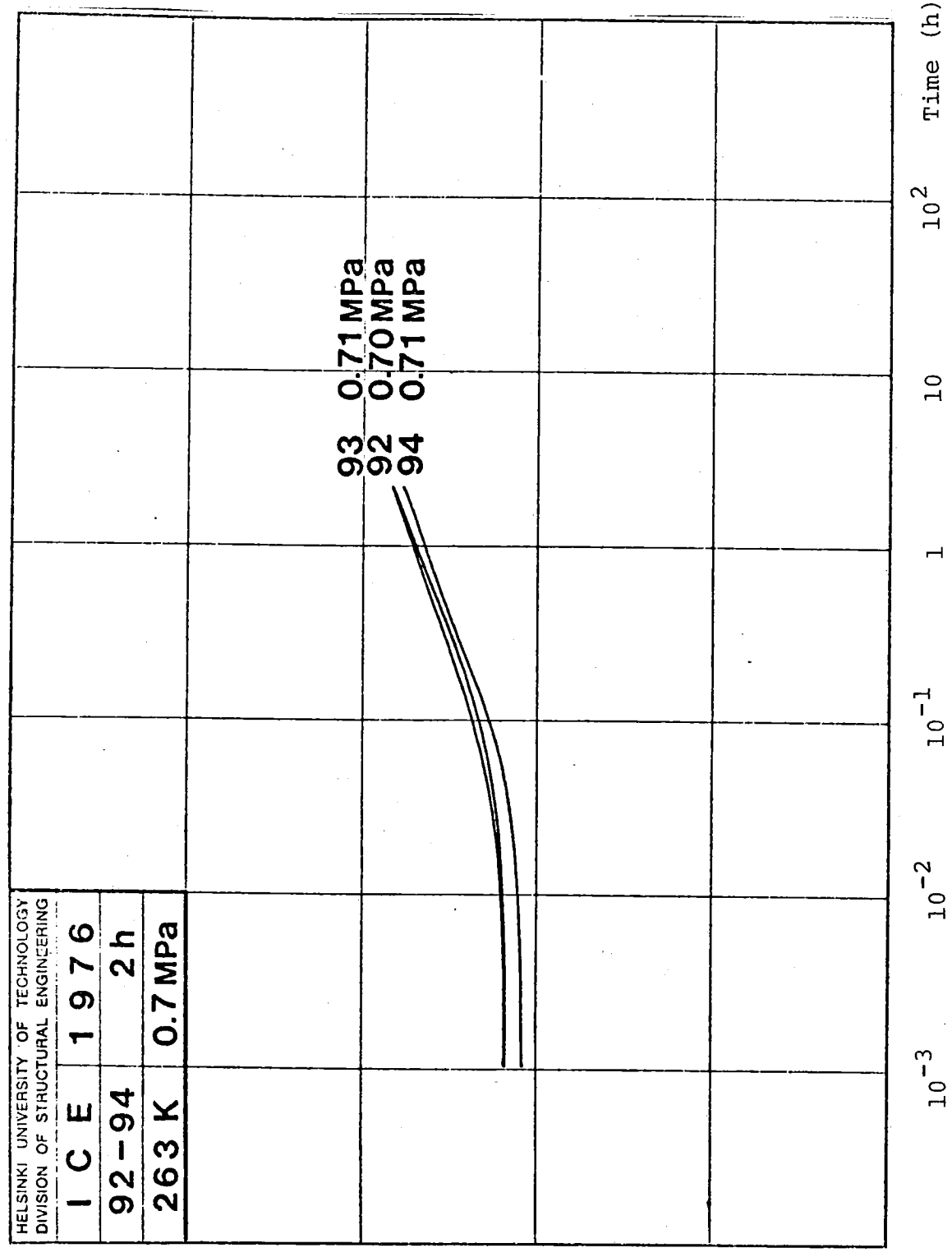
HELSINKI UNIVERSITY OF TECHNOLOGY
DIVISION OF STRUCTURAL ENGINEERING
ICE 1976
92-94 2h
263 K 0.7 MPa
93 0.71 MPa
92 0.70 MPa
94 0.71 MPa
ε (10⁻³)
10
1
10⁻¹
10⁻²
10⁻³
10⁻²
10⁻¹
1
10
10²
Time (h)

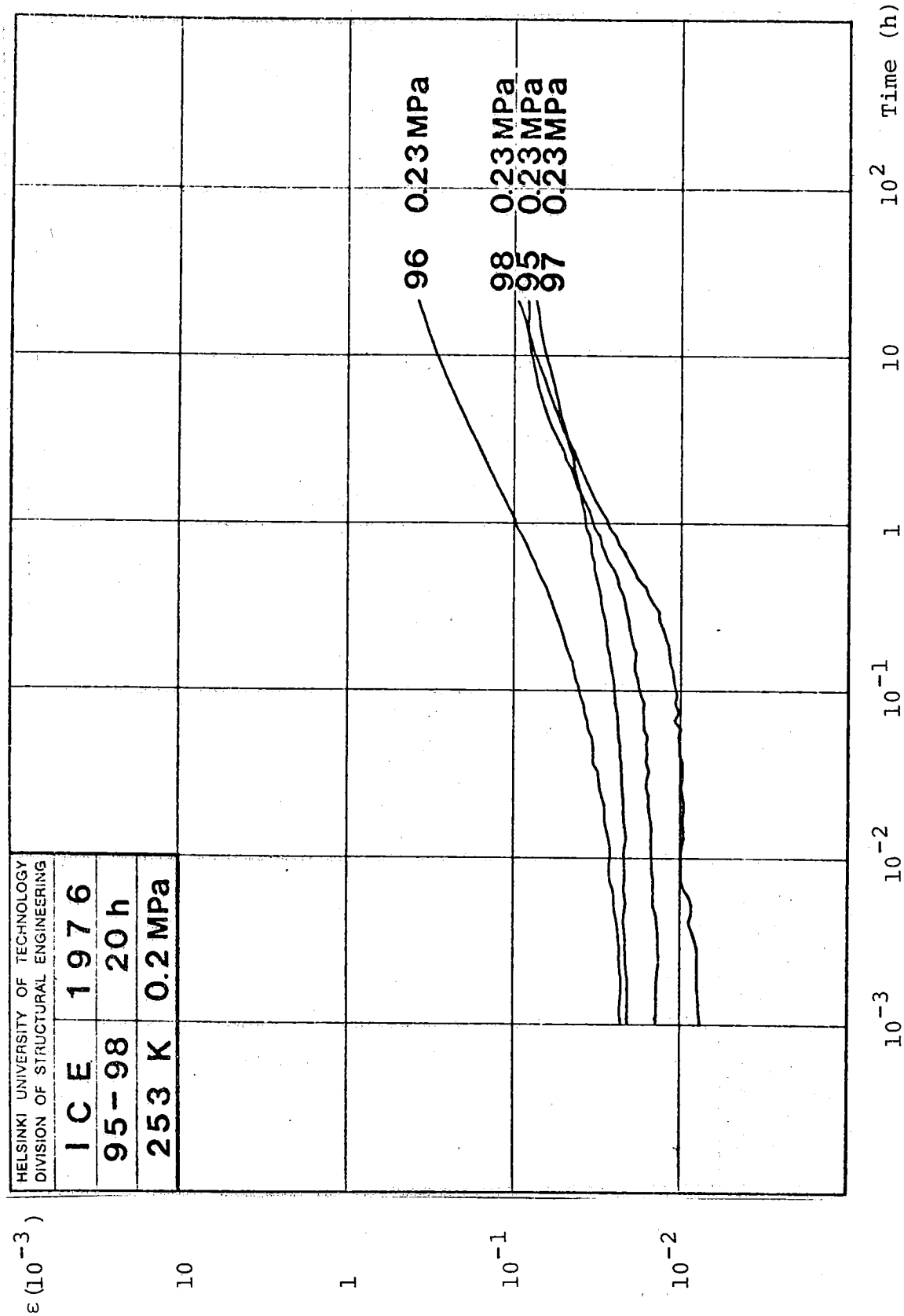
HELSINKI UNIVERSITY OF TECHNOLOGY
DIVISION OF STRUCTURAL ENGINEERING
ICE 1976
95-98 20h
253 K 0.2 MPa
96 0.23 MPa
98 0.23 MPa
95 0.23 MPa
97 0.23 MPa
ε (10⁻³)
10
1
10⁻¹
10⁻²
10⁻³
10⁻²
10⁻¹
1
10
10²
Time (h)

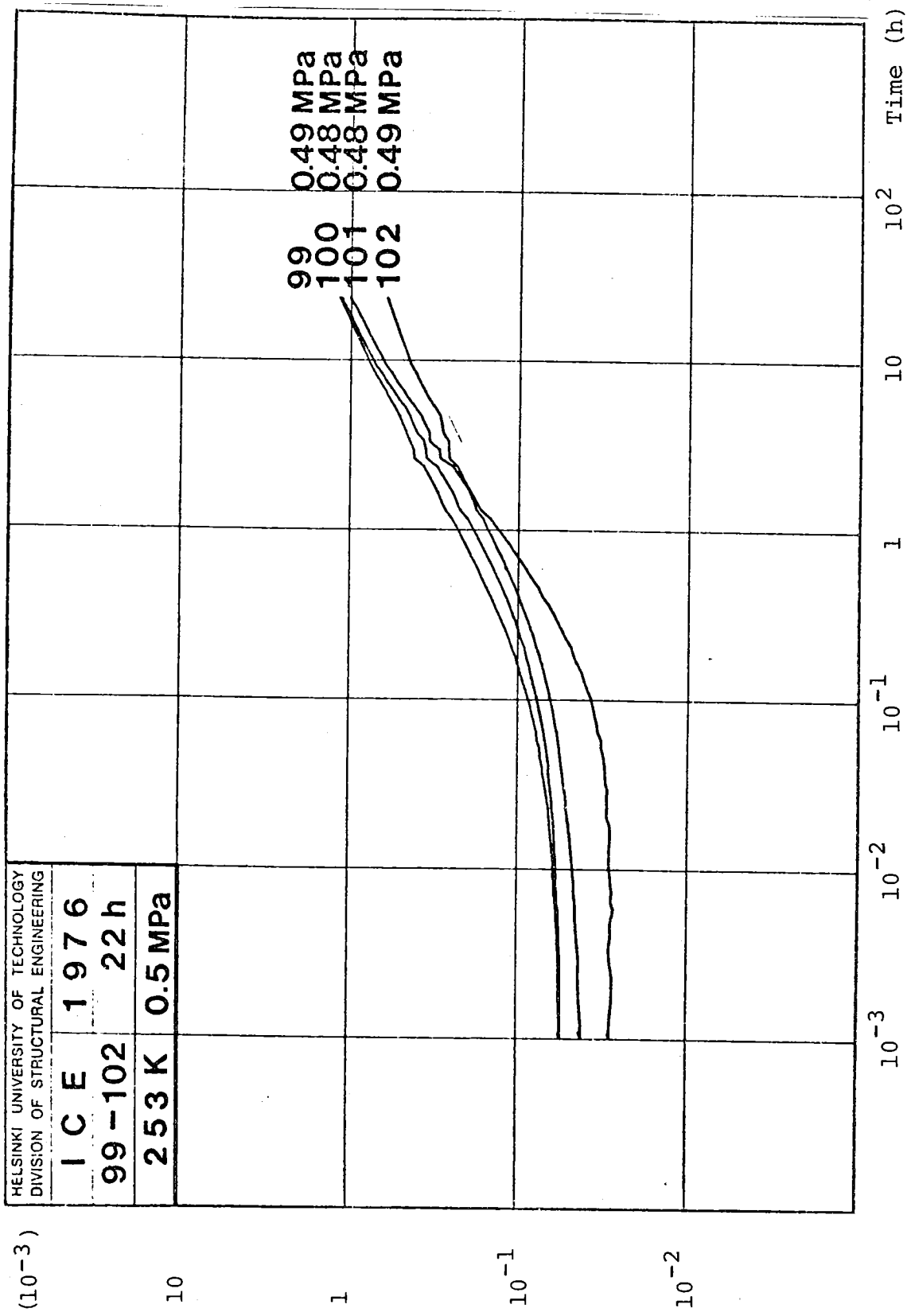
HELSINKI UNIVERSITY OF TECHNOLOGY
DIVISION OF STRUCTURAL ENGINEERING
ICE 1976
99-102 22 h
253 K 0.5 MPa
99 0.49 MPa
100 0.48 MPa
101 0.48 MPa
102 0.49 MPa
ε (10⁻³)
10
1
10⁻¹
10⁻²
10⁻³
10⁻²
10⁻¹
1
10
10²
Time (h)

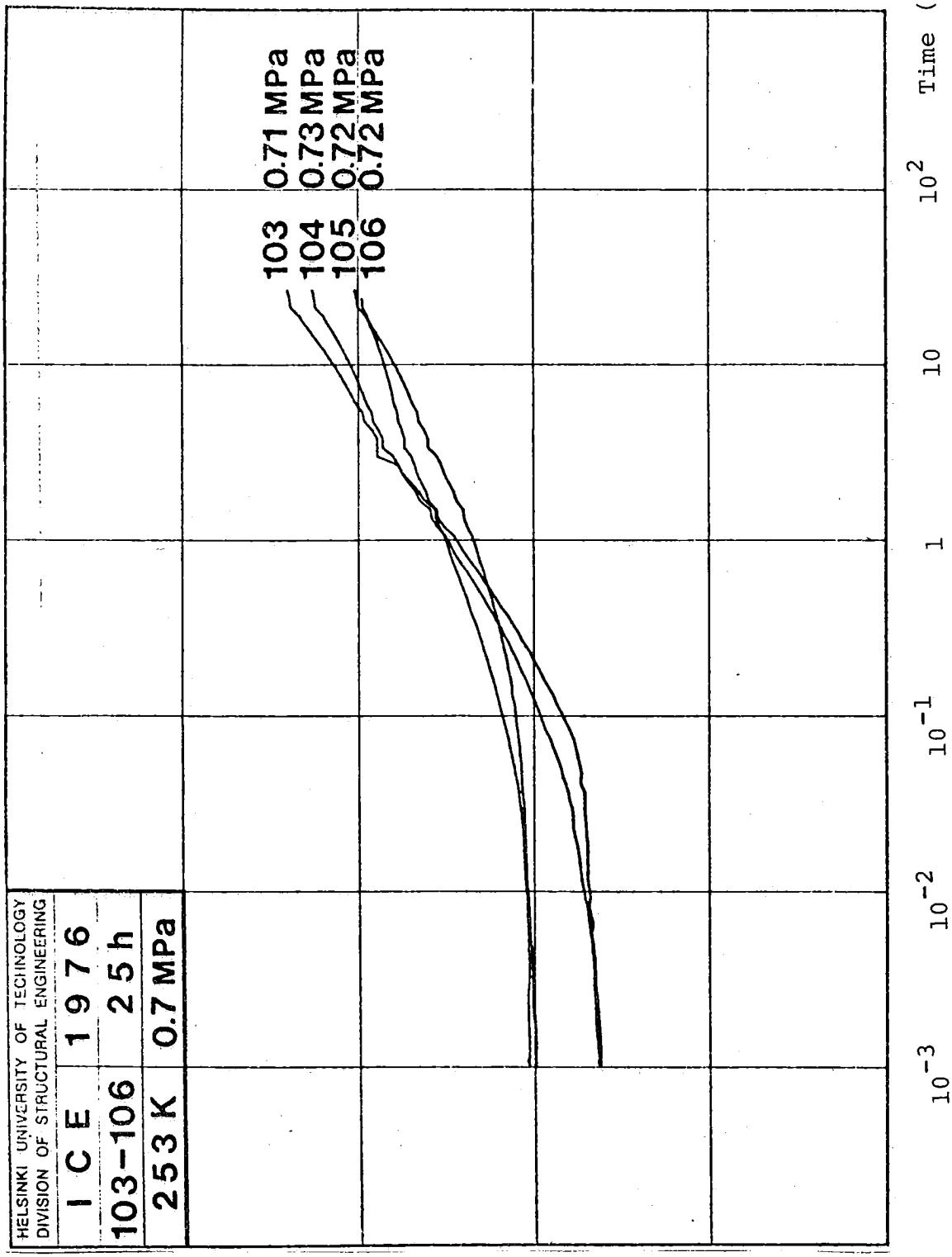
HELSINKI UNIVERSITY OF TECHNOLOGY
DIVISION OF STRUCTURAL ENGINEERING
ICE 1976
103–106 25 h
253 K 0.7 MPa
103 0.71 MPa
104 0.73 MPa
105 0.72 MPa
106 0.72 MPa
ε (10⁻³)
10
1
10⁻¹
10⁻²
10⁻³
10⁻²
10⁻¹
1
10
10²
Time (h)

APPENDIX 8

SOME TYPICAL CREEP CURVES AND COMPARISION THE EFFECT OF THE STRESS LEVEL AND TEMPERATURE

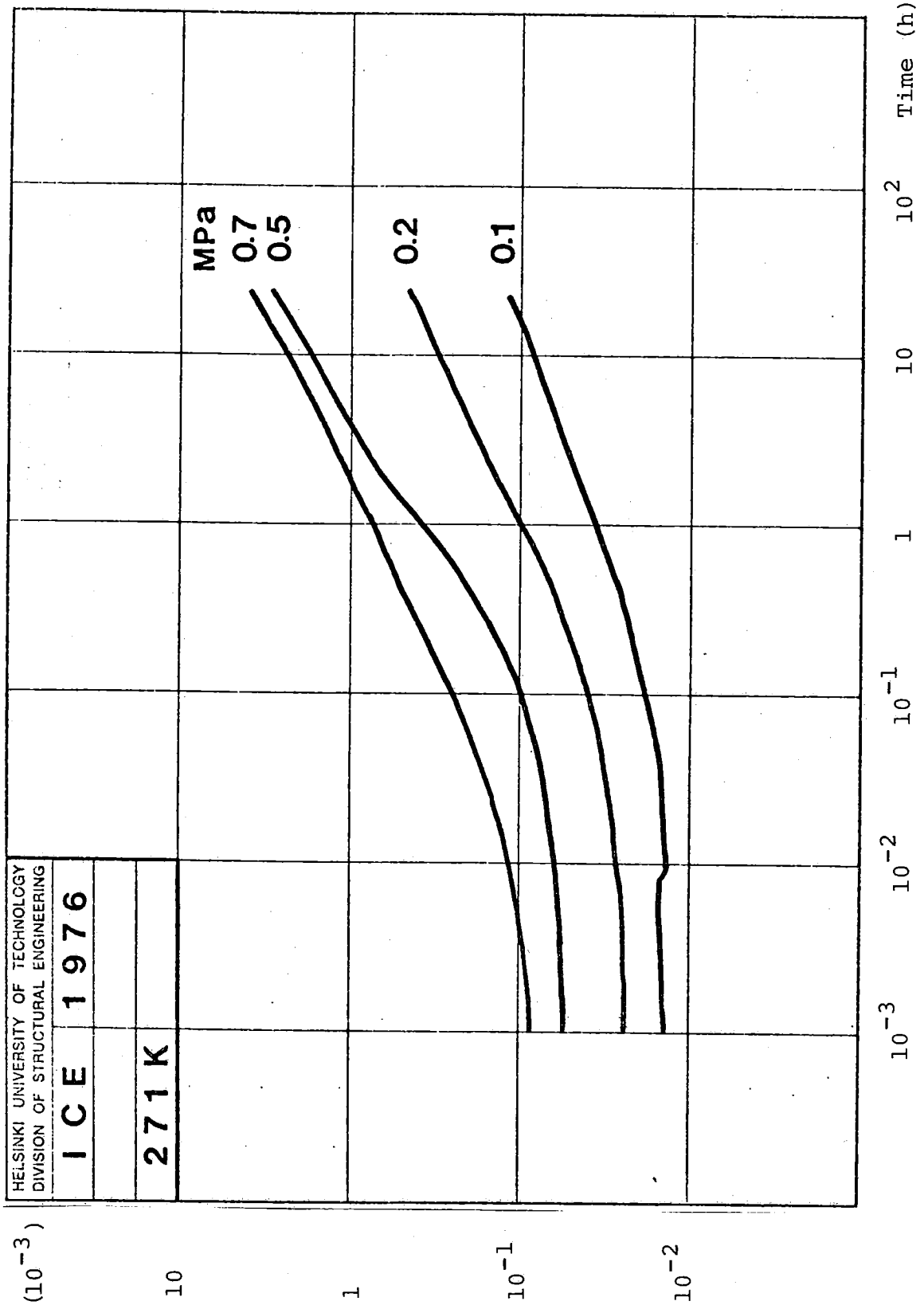
HELSINKI UNIVERSITY OF TECHNOLOGY
DIVISION OF STRUCTURAL ENGINEERING
ICE 1976
271 K
MPa
0.7
0.5
0.2
0.1
ε (10⁻³)
10
1
10⁻¹
10⁻²
10⁻³
10⁻²
10⁻¹
1
10
10²
Time (h)

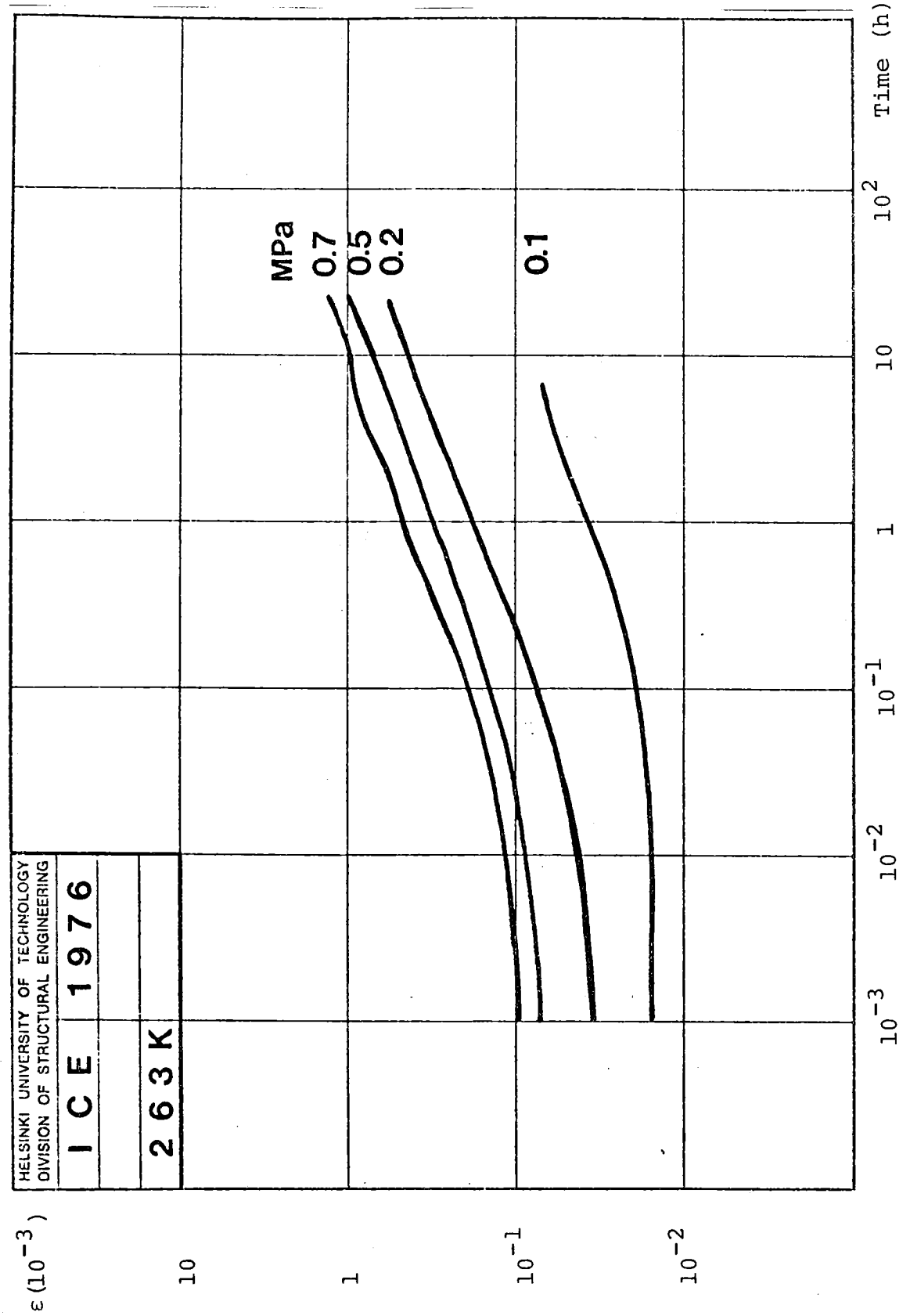
HELSINKI UNIVERSITY OF TECHNOLOGY
DIVISION OF STRUCTURAL ENGINEERING
ICE 1976
263K
MPa
0.7
0.5
0.2
0.1
ε (10⁻³)
10
1
10⁻¹
10⁻²
10⁻³
10⁻²
10⁻¹
1
10
10²
Time (h)

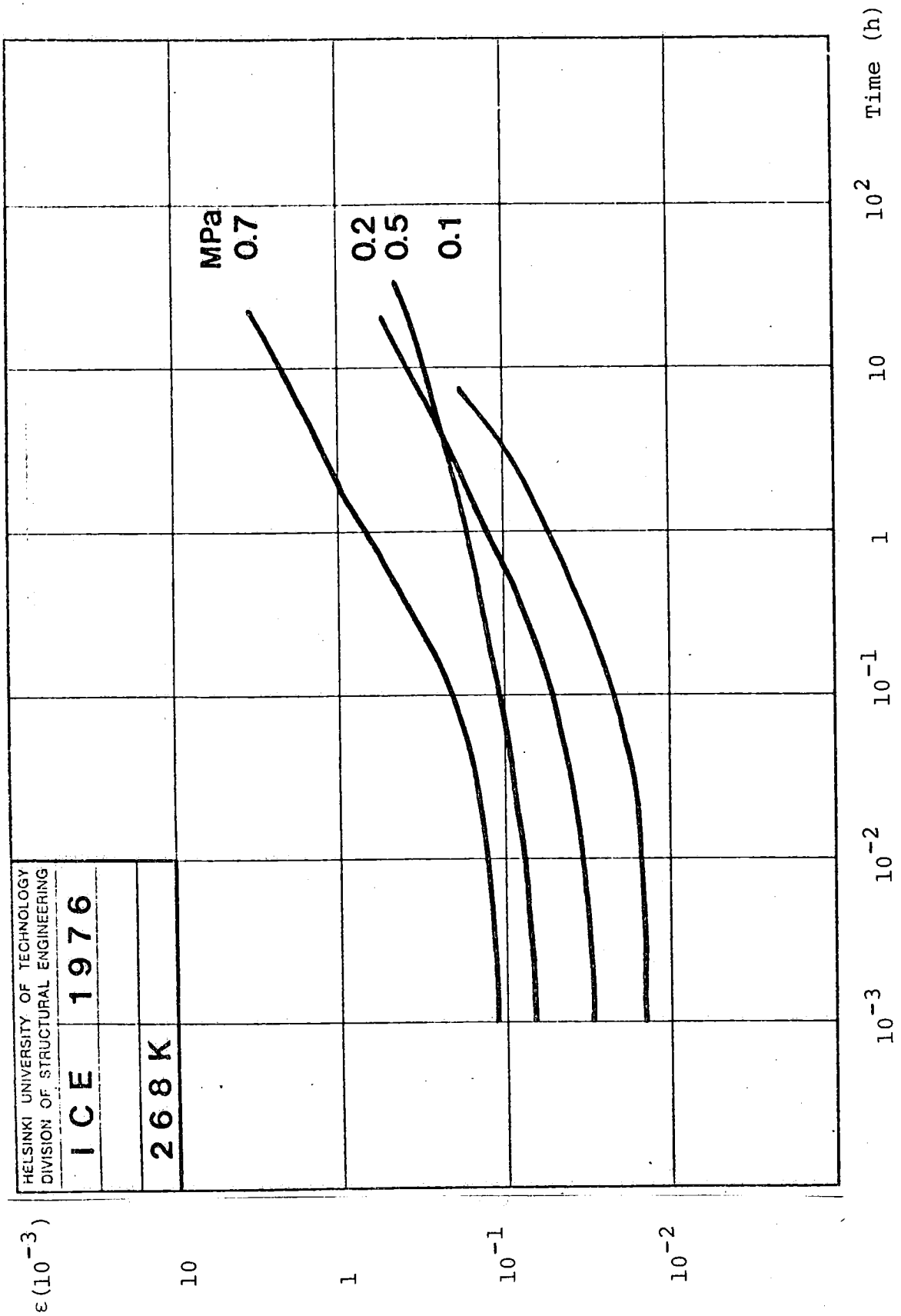
HELSINKI UNIVERSITY OF TECHNOLOGY
DIVISION OF STRUCTURAL ENGINEERING
ICE 1976
268 K
MPa
0.7
0.2
0.5
0.1
ε(10⁻³)
10
1
10⁻¹
10⁻²
10⁻³
10⁻²
10⁻¹
1
10
10²
Time (h)

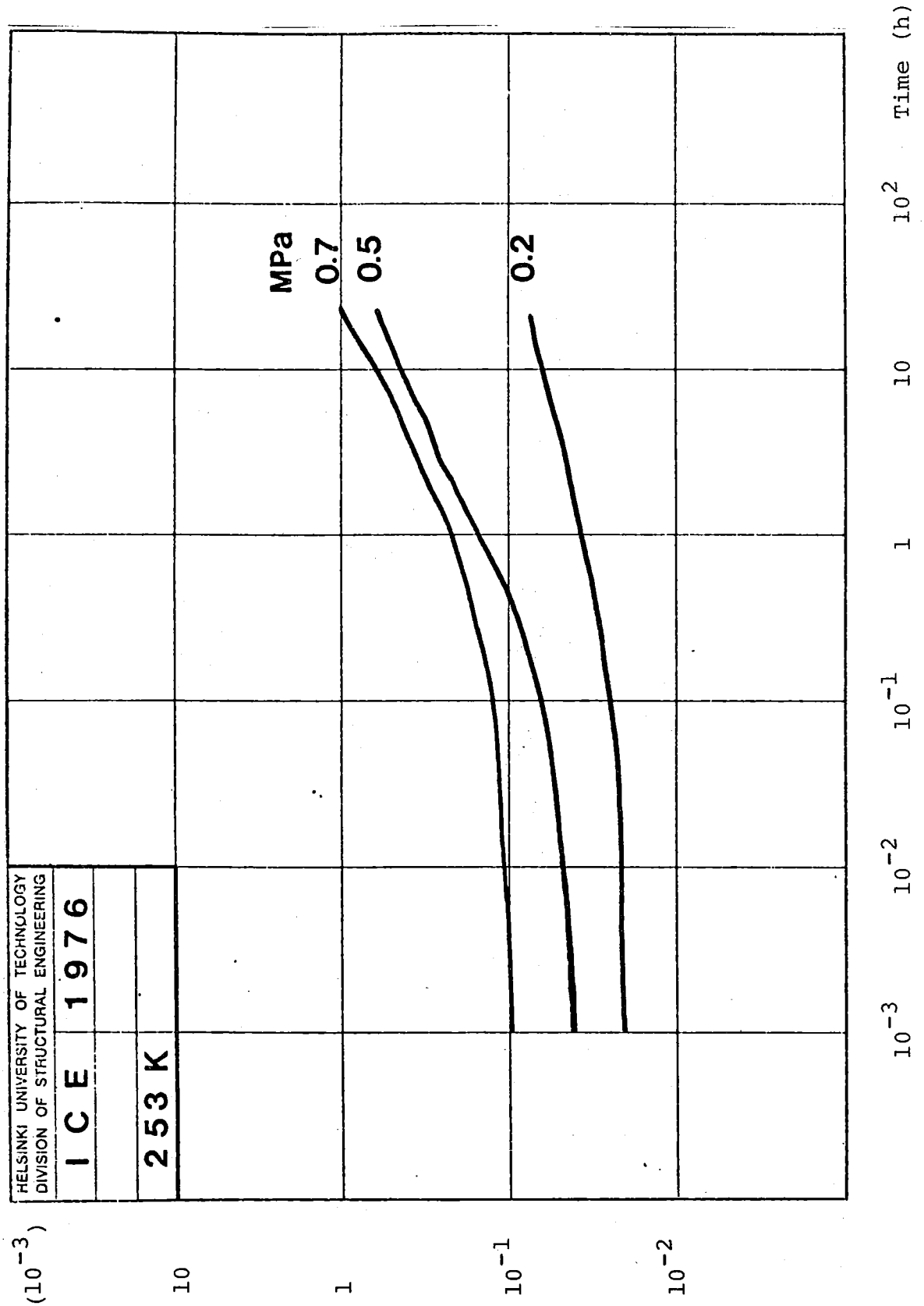
HELSINKI UNIVERSITY OF TECHNOLOGY
DIVISION OF STRUCTURAL ENGINEERING
ICE 1976
253 K
MPa
0.7
0.5
0.2
ε (10^-3)
10
1
10^-1
10^-2
10^-3
10^-2
10^-1
1
10
10^2
Time (h)

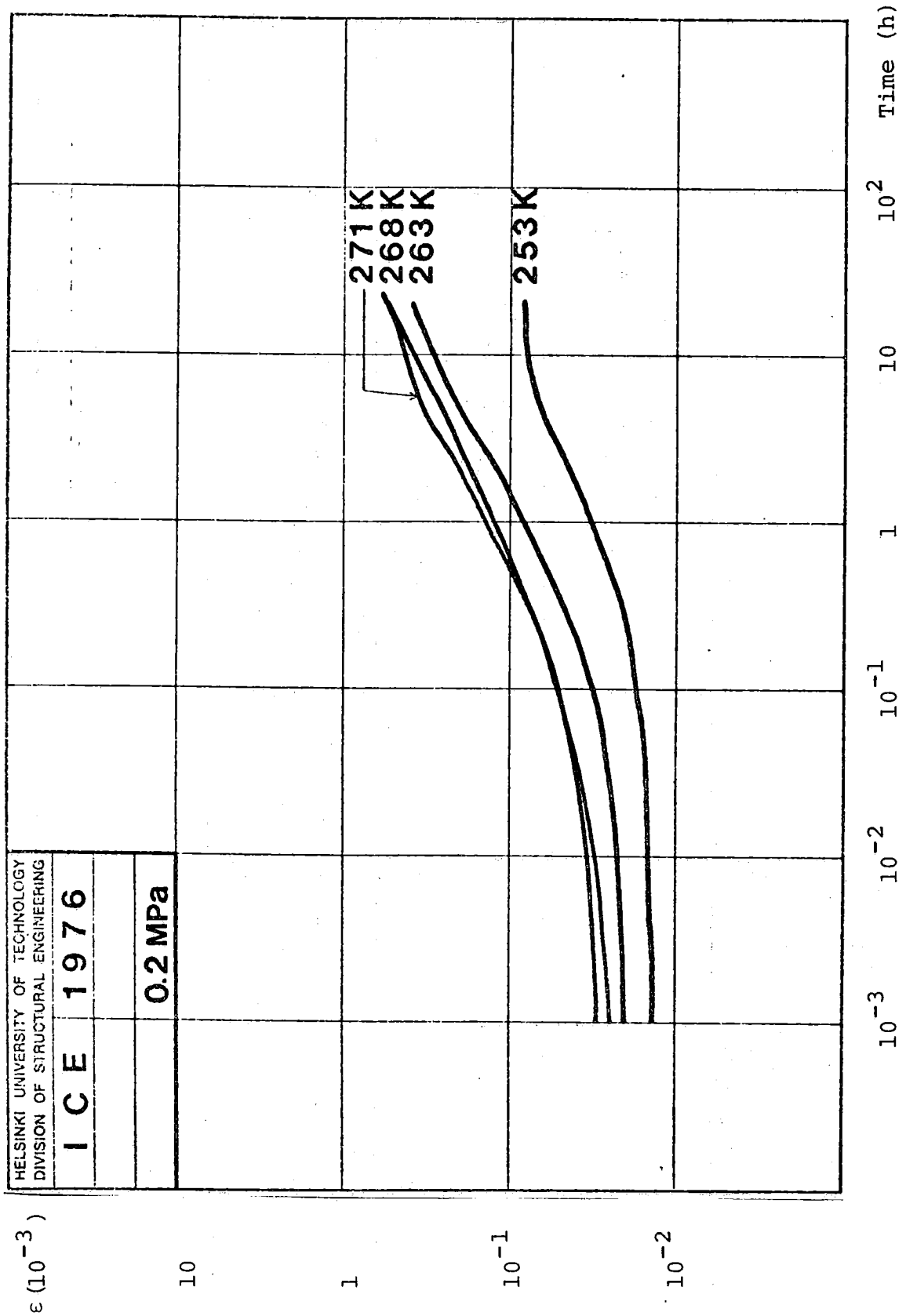
HELSINKI UNIVERSITY OF TECHNOLOGY
DIVISION OF STRUCTURAL ENGINEERING
ICE 1976
0.2 MPa
271K
268K
263K
253K
ε (10⁻³)
10
1
10⁻¹
10⁻²
10⁻³
10⁻²
10⁻¹
1
10
10²
Time (h)

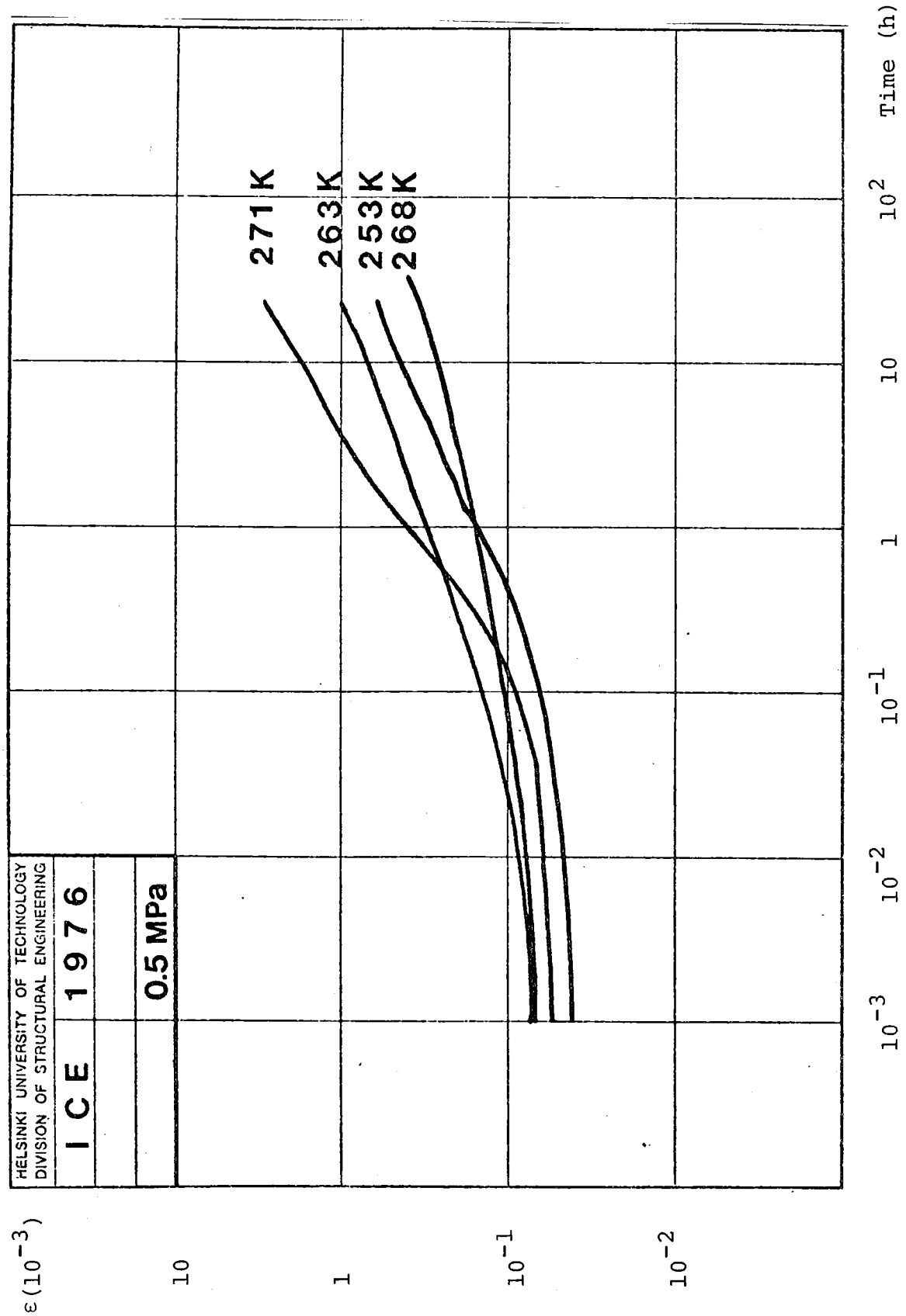
HELSINKI UNIVERSITY OF TECHNOLOGY
DIVISION OF STRUCTURAL ENGINEERING
ICE 1976
0.5 MPa
271 K
263 K
253 K
268 K
ε (10⁻³)
10
1
10⁻¹
10⁻²
10⁻³
10⁻²
10⁻¹
1
10
10²
Time (h)

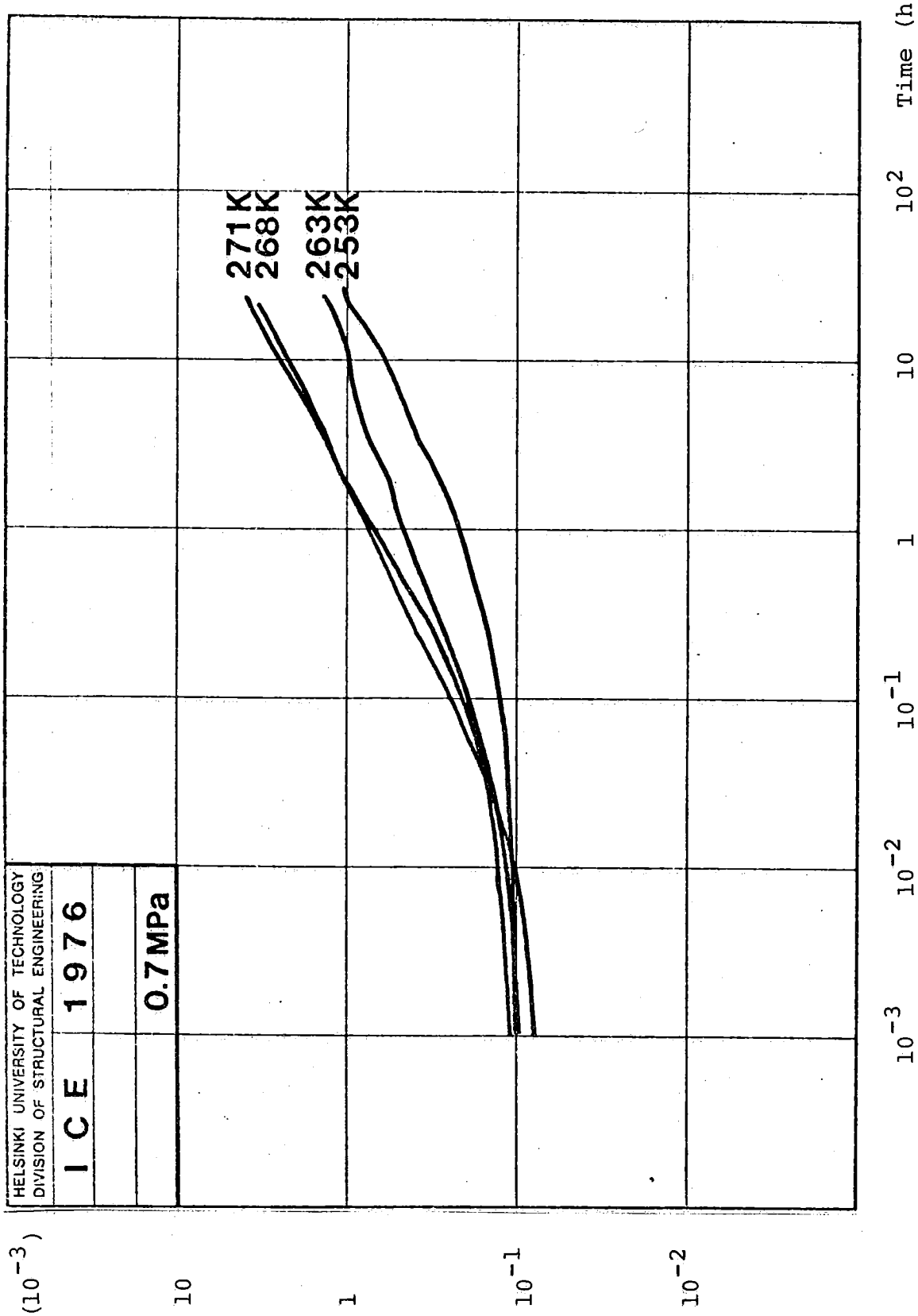
HELSINKI UNIVERSITY OF TECHNOLOGY
DIVISION OF STRUCTURAL ENGINEERING
ICE 1976
0.7MPa
271K
268K
263K
253K
ε(10⁻³)
10
1
10⁻¹
10⁻²
10⁻³
10⁻²
10⁻¹
1
10
10²
Time (h)

APPENDIX 9

PARAMETERS OF CREEP MODELS FOR TEST CURVES

(t) = h ; (D) = 1/MPa

Models:

$$D(t, T_o, \sigma_o) = a_1(T_o) + b_1(T_o)t^{n_1(T_o)} \quad (33)$$

$$D(t, T_o, \sigma_o) = a_2(T_o) - b_2(T_o)e^{n_2(T_o)t} \quad (34)$$

$$\log(D, T_o, \sigma_o) = a_3(T_o, \sigma_o) - b_3(T_o, \sigma_o) \times \operatorname{arsinh}\{\log n_3(T_o, \sigma_o)t\} \quad (35)$$

(by Mäkeläinen /79/)

- The model (33) has also been tested with constant power $n_1 = 1/3$
- The size of the point group used in the calculations is indicated with k in the table. Experiments 4, 14, 98, 102 and 106 have been calculated exceptionally with a smaller point group than the other experiments.
- S_{ri} (i = 1, 2, 3) and S_r (for model $n_1 = 1/3$) are given as per cent.

Test	k	$a_1 \times 10^3$ (1/MPa)	$b_1 \times 10^3$	n_1	S_{r1} (%)	$a_2 \times 10^3$ (1/MPa)	$b_2 \times 10^3$	n_2	S_{r2} (%)	a_3 (log 1/MPa)	b_3	n_3	S_{r3} (%)
1	87	0.09900	0.3477	0.4590	8.678	0.9599	0.8110	-0.2070	11.95	-3.1672	0.4009	0.1469	11.38
2	87	0.1016	0.2110	0.4590	6.905	0.8449	0.6994	-0.1980	12.47	-3.1734	0.3939	0.1081	10.16
3	87	0.05954	0.1953	0.4360	9.773	0.6939	0.5912	-0.2160	18.13	-3.3815	0.3975	0.2495	11.19
4	23	0.04767	0.3385	0.4950	15.91	1.508	1.395	-0.1500	27.59	-3.1995	0.5119	0.3148	16.38
5	79	0.1115	0.09355	0.4430	0.7143	0.3297	0.2018	-0.4430	6.212	-3.4945	0.2314	0.1268	3.648
6	80	0.1075	0.3879	0.4460	3.286	1.037	0.8634	-0.4360	13.56	-3.1718	0.3874	0.4285	4.478
7	79	0.1550	0.3105	0.3720	1.588	0.7430	0.5225	-0.6450	9.439	-3.2282	0.2751	0.4055	2.423
8	79	0.07739	0.1070	0.3190	1.338	0.2579	0.1533	-0.7870	7.342	-3.6654	0.2037	0.4581	1.413
9	88	0.02903	0.3705	0.4600	22.90	1.344	1.248	-02140	8.139	-3.2507	0.4954	0.3990	13.60
10	88	0.03039	0.6840	0.4410	19.15	2.334	2.167	-0.2170	20.22	-3.07862	0.4996	0.6237	6.853
11	88	0.07018	0.5697	0.5150	18.60	2.590	2.425	-0.1610	10.76	-2.9350	0.5333	0.2541	13.78
12	88	-0.006678	0.5148	0.4600	33.47	1.825	1.737	-0.2100	17.43	-3.2667	0.5616	0.7194	11.83
13	88	0.07336	0.4191	0.5210	9.274	2.051	1.901	-0.1390	21.16	-3.02815	0.5224	0.2388	9.061
14	24	0.1104	0.9297	0.6460	14.77	8.222	7.989	-0.07700	20.56	-2.495	0.6859	0.1422	13.93
15	91	0.1673	0.1879	0.4810	5.993	1.072	0.8620	-0.1140	12.54	-3.05963	0.3530	0.05521	6.906
16	91	0.1413	0.2415	0.4920	2.966	1.377	1.179	-0.1030	17.89	-2.9567	0.4337	0.05689	4.241
17	91	0.1108	0.3409	0.3880	2.152	1.248	1.040	-0.1610	22.93	-3.1582	0.3606	0.2594	2.268
18	91	0.1908	0.1861	0.5560	5.484	1.458	1.228	-0.0800	13.62	-2.9167	0.4033	0.03631	7.548
19	88	0.06480	1.069	0.6020	20.88	7.227	6.995	-0.09900	30.86	-2.6749	0.6635	0.3083	14.77
20	88	0.01891	1.759	0.5340	20.58	9.028	8.670	-0.1220	73.21	-2.7691	0.6448	0.9863	8.779
21	88	0.005720	1.188	0.5540	31.01	6.420	6.211	-0.1220	43.03	-2.8400	0.6598	0.6138	14.26
22	88	0.09718	0.3355	0.4780	4.155	1.448	1.281	-0.1600	19.00	-3.08337	0.4464	0.1945	5.816
23	88	0.03123	0.9350	0.6180	30.71	6.632	6.468	-0.0970	22.90	-2.7203	0.7006	0.2818	19.75
24	88	-0.01239	1.671	0.5210	26.43	8.129	7.807	-0.1270	83.68	-2.8603	0.6544	1.239	9.430
25	88	0.1016	0.9872	0.5600	4.220	5.901	5.613	-0.1040	59.30	-2.8083	0.5973	0.5140	7.268
26	88	0.04058	1.126	0.4370	10.53	4.006	3.694	-0.1750	57.72	-2.9771	0.5174	1.211	6.963
27	79	0.1019	0.4931	0.5190	12.96	1.461	1.298	-0.3850	19.75	-3.0485	0.4726	0.3855	14.43
28	79	0.1213	0.3034	0.4210	4.552	0.7582	0.5861	-0.5780	7.377	-3.2587	0.3217	0.4266	5.595
29	79	0.1134	0.2749	0.5720	5.464	0.9903	0.8497	-0.3280	4.583	-3.0928	0.4392	0.1585	12.20
30	79	0.09495	0.3944	0.4750	2.854	1.067	0.9134	-0.4380	14.64	-3.1836	0.4199	0.4477	3.370
31	79	0.1252	0.3622	0.7190	3.592	2.448	2.295	-0.1400	13.84	-2.7934	0.5924	0.1086	12.02
32	79	0.1430	0.2044	0.9740	2.508	18.47	18.32	-0.0110	2.814	-2.96534	0.4988	0.1107	22.63
33	79	0.1583	0.4646	0.7220	5.908	3.257	3.063	-0.1330	17.25	-2.6611	0.6105	0.1042	9.077
34	88	0.08813	0.4039	0.3560	3.383	1.140	0.9374	-0.2610	22.25	-3.2296	0.3474	0.5623	2.697
35	88	0.1462	0.4013	0.6960	3.783	4.818	4.613	-0.0570	24.01	-2.4668	0.6959	0.04487	12.04
36	88	-0.02327	1.168	0.3320	16.00	2.710	2.405	-0.3370	31.07	-3.0519	0.4292	1.828	3.607
37	87	0.02437	1.382	0.4920	21.51	5.5242	5.2376	-0.1740	40.38	-2.8384	0.5795	0.8433	8.502
38	87	0.1239	0.2805	0.3790	1.136	0.8971	0.6980	-0.2430	16.86	-3.2098	0.3215	0.2333	1.930
39	87	0.1063	0.4596	0.5410	4.604	2.3681	2.1805	-0.1360	21.66	-2.9032	0.5258	0.1795	7.695
40	87	0.1211	0.1724	0.4110	2.843	0.6720	0.5055	-0.1880	15.43	-3.1647	0.3514	0.05636	2.570

41	91	0.1151	0.2305	0.3470	0.7052	0.7724	0.5839	-0.1900	17.44	-3.2771	0.2948	0.1954	1.907
42	91	0.1008	0.1601	0.3850	2.556	0.6414	0.4916	-0.1460	18.35	-3.2751	0.3320	0.07980	1.862
43	91	0.1231	0.03262	0.6080	4.110	0.4493	0.3185	-0.0500	7.216	-3.5010	0.2148	0.03097	7.257
44	91	0.1114	0.2087	0.3320	2.390	0.6860	0.5030	-0.1840	19.23	-3.3067	0.2834	0.1722	3.485
45	94	0.1110	0.2387	0.4350	6.351	1.268	1.081	-0.0820	27.83	-3.1034	0.4039	0.09397	7.754
46	94	0.1194	0.1825	0.7710	4.267	5.761	5.609	-0.0200	19.78	-2.5586	0.6969	0.02410	19.32
47	82	0.1035	0.7337	0.4970	7.577	2.364	2.149	-0.2950	18.51	-2.9522	0.4885	0.5105	6.056
48	67	0.1343	3.481	1.094	9.187	329.3	329.7	-0.0110	26.07	-2.1342	0.9791	0.3750	22.05
49	67	0.1605	3.479	0.9650	6.799	38.18	38.02	-0.0970	6.900	-2.1468	0.9161	0.3890	20.49
50	63	0.1934	5.064	1.157	6.469	455.1	455.0	-0.0110	17.73	-2.1333	0.9519	0.5188	19.82
51	74	0.1764	1.494	0.8330	11.93	17.82	17.58	-0.0790	29.96	-2.0904	0.9028	0.1365	12.20
52	86	0.1368	0.8365	0.5520	11.74	4.109	3.839	-0.1520	18.70	-2.7037	0.5558	0.2249	13.25
53	86	0.1937	1.231	0.6010	13.90	7.321	6.956	-0.1260	16.40	-2.4302	0.6179	0.1596	16.85
54	86	0.2785	0.1013	1.302	18.93	218.4	218.1	-0.0010	12.03	-2.6051	0.5558	0.04753	19.70
55	87	0.03398	1.522	0.4930	17.62	6.231	5.895	-0.1640	51.82	-2.8175	0.5813	0.9630	7.392
56	87	0.09013	0.9401	0.5400	13.65	4.649	4.396	-0.1400	28.86	-2.7855	0.5738	0.3758	10.76
57	87	0.07969	0.4186	0.5000	2.392	1.858	1.695	-0.1530	30.44	-3.08632	0.4935	0.3243	4.304
58	87	-0.9548	3.409	0.2550	137.9	5.168	5.104	-0.6920	26.42	-3.1374	0.6235	6.442	23.83
59	78	0.1135	0.2056	0.4930	4.916	0.6019	0.4632	-0.5050	3.900	-3.2953	0.3335	0.2259	9.176
60	78	0.07563	0.1867	0.3770	2.198	0.4190	0.3063	-0.7090	10.60	-3.5123	0.2887	0.5754	2.080
61	78	0.05063	0.08350	0.4950	3.945	0.2517	0.1907	-0.4900	4.500	-3.6682	0.3235	0.2123	8.064
62	78	0.08684	0.1305	0.5240	3.407	0.4276	0.3260	-0.4360	4.098	-3.4343	0.3271	0.1803	8.814
63	78	0.1723	0.5118	0.5690	1.987	1.748	1.522	-0.3380	10.13	-2.8255	0.4812	0.1644	8.113
64	78	0.09866	0.4229	0.4880	4.113	1.115	0.9595	-0.4750	12.04	-3.1431	0.4289	0.4436	5.272
65	73	0.04554	0.08003	0.4050	2.470	0.1702	0.1124	-1.113	5.384	-3.8271	0.2576	0.5023	4.033
66	74	0.1708	0.4082	0.5490	1.512	1.098	0.8888	-0.5610	7.449	-3.001127	0.4010	0.2265	7.056
67	73	0.1200	0.3570	0.5320	1.755	0.8517	0.6972	-0.6680	8.931	-3.1101	0.4202	0.2812	5.466
68	73	0.08228	0.1767	0.4650	0.7851	0.3987	0.2936	-0.8190	8.583	-3.4050	0.3433	-0.5730	3.332
69	88	0.06666	0.1672	0.4270	3.916	0.6188	0.5138	-0.2030	14.07	-3.3955	0.3694	0.1936	4.834
70	88	-0.02031	1.616	0.4210	23.51	5.115	4.774	-0.2220	36.68	-2.8555	0.5272	1.175	5.501
71	88	-0.1235	1.732	0.3620	3260	4.302	4.994	-0.3120	32.20	-2.9595	0.5096	2.004	7.306
72	87	0.05378	0.7972	0.3960	10.62	2.300	2.057	-0.2620	28.31	-3.0642	0.4426	0.9204	3.896
73	87	0.01058	0.5289	0.2740	11.03	1.004	0.8226	-0.5280	18.48	-3.3585	0.3333	1.991	3.619
74	87	0.06572	0.3366	0.5640	10.01	1.822	1.705	-0.1360	14.76	-3.0224	0.5575	0.1667	11.47
75	87	0.1143	0.4312	0.3500	5.115	1.160	0.9292	-0.3180	16.02	-3.1819	0.3239	0.5309	3.749
76	88	0.09840	0.5518	0.4080	4.449	1.825	1.588	-0.2060	27,23	-3.0801	0.4100	0.5082	3.963
77	88	0.9305	0.2139	0.3420	3.448	0.6267	0.4690	-0.2660	16.61	-3.3693	0.2923	0.2838	4.315
78	88	0.1063	0.1656	0.3090	2.060	0.4692	0.3116	-0.3540	10.14	-3.4528	0.2279	0.293	2.059
79	88	-0.04576	1.322	0.3940	24.56	3.779	3.508	-0.2490	41.41	-3.0137	0.5191	1.622	5.580
80	88	0.1025	0.2325	0.2990	4.346	0.5895	0.4156	-0.4080	10.06	-3.4047	0.2437	0.5000	3.030
81	88	0.01584	0.9190	0.3580	13.02	2.391	2.124	-0.2760	35.51	-3.1006	0.4365	1.455	4.904
82	88	0.04854	0.4281	0.3460	7.526	1.116	0.9447	-0.2820	26.96	-3.3167	0.3732	0.9572	4.854
83	88	0.003177	1.303	0.3610	16.26	3.377	3.028	-0.2840	32.89	-2.9621	0.4480	1.462	5.356
84	74	0.0677	0.4018	0.5120	6.035	0.8785	0.7713	-0.6890	9.726	-3.2670	0.4596	-0.1570	6.959
85	74	0.1507	0.1907	0.7490	5.279	0.8856	0.7294	-0.3050	2.822	-3.2659	0.3158	0.2168	16.65

86	74	0.08388	0.1665	0.4610	2.167	0.3883	0.2829	-0.8000	6.226	-3.4467	0.3200	0.3020	5.353
87	89	0.06151	0.7129	0.6230	17.34	5.625	5.457	-0.0840	24.50	-2.7312	0.6729	0.2075	13.41
88	79	0.5720	1.779	0.6780	23.38	8.277	8.103	-0.2160	9.444	-2.5833	0.7371	0.5297	15.41
89	88	0.08426	1.208	0.5090	14.79	5.561	5.240	-0.1420	36.46	-2.7628	0.5608	0.5176	9.563
90	88	0.03082	0.6349	0.3470	12.45	1.583	1.382	-0.3200	23.91	-3.2076	0.4021	1.156	4.849
91	88	0.06536	0.4764	0.3290	4.736	1.178	0.9713	-0.3180	25.79	-3.2596	0.3481	0.9594	4.367
92	67	0.1982	0.5454	0.6000	2.985	1.058	0.8315	-1.079	2.666	-3.03311	0.3699	0.4539	9.414
93	67	0.1867	0.5769	0.5240	3.608	0.9823	0.7528	-1.420	3.784	-3.04193	0.3657	0.5521	7.546
94	67	0.1446	0.5118	0.5290	4.870	0.8489	0.6681	-1.432	3.334	-3.1157	0.3848	0.5957	8.660
95	87	0.04081	0.1197	0.3930	12.61	0.3657	0.3001	-0.3150	3.933	-3.6550	0.3316	0.3357	11.43
96	87	0.06589	0.4005	0.4880	9.105	1.623	1.483	-0.1830	18.97	-3.1254	0.4864	0.3221	6.676
97	87	0.07103	0.08477	0.3830	3.246	0.3094	0.2078	-0.2810	6.614	-3.5794	0.2452	0.1271	5.351
98	23	0.02193	0.1073	0.4570	17.07	0.4094	0.3676	-0.3676	11.52	-3.6709	0.4428	0.2606	14.80
99	88	0.08298	0.4328	0.5570	10.02	2.449	2.293	-0.1210	10.08	-2.9166	0.5574	0.1671	11.50
100	88	0.09492	0.3362	0.6340	8.281	2.665	2.523	-0.09000	11.70	-2.7490	0.6241	0.06855	15.61
101	88	0.02790	0.3027	0.6420	24.09	2.378	2.312	-0.09100	10.58	-2.9943	0.6979	0.1384	22.19
102	24	0.05950	0.2836	0.4810	10.96	1.291	1.176	-0.1450	16.19	-3.1918	0.4735	0.2118	9.841
103	89	0.02567	0.4584	0.6630	26.16	4.405	4.316	-0.0700	23.71	-2.8861	0.7389	0.1888	20.57
104	89	0.01655	0.4790	0.5340	22,23	2,540	2,434	-0.1190	36.83	-3.1604	0.6115	0.4753	9.476
105	89	0.1409	0.1945	0.6170	2.400	1.677	1.504	-0.0790	10.92	-2.9002	0.4816	0.04426	12.68
106	23	0.106	0.3748	0.4090	10.82	1.252	1.067	-0.2350	13.71	-3.1555	0.3779	0.3141	10.47

MODEL $a_4 + b_4 t^{1/3}$

Koe	$a_4 \times 10^3$ (1/MPa)	$b_4 \times 10^3$	S_r(%)
1	0.03541	0.3505	20.10
2	0.04742	0.2987	16.66
3	0.01858	0.2604	18.87
4	-0.06887	0.5381	51.20
5	0.09571	0.1164	3.520
6	0.03815	0.4907	14.19
7	0.1354	0.3374	3.450
8	0.07996	0.1037	1.230
9	-0.07031	0.5321	52.73
10	-0.1252	0.9336	50.11
11	-0.1526	0.9461	62.42
12	-0.1448	0.7395	84.29
13	-0.0749	0.7077	43.72
14	-0.6502	2.351	156.3
15	0.1004	0.2990	13.62
16	0.04805	0.3972	17.88
17	0.06741	0.4083	8.281
18	0.08486	0.3693	17.96
19	-0.5848	2.222	143.2
20	-0.7513	3.074	153.5
21	-0.5701	2.183	160.0
22	-0.006451	0.5062	26.09
23	-0.5760	2.023	176.1
24	-0.6924	2.822	165.0
25	-0.3941	1.846	99.14
26	-0.2069	1.522	47.13
27	-0.03197	0.6993	29.89
28	0.07978	0.3625	10.14
29	0.01987	0.4246	25.21
30	0.01108	0.5193	18.57
31	-0.07056	0.7070	44.45
32	-0.0547	0.5903	52.04
33	-0.09543	0.9121	44.83
34	0.06850	0.4332	5.928
35	-0.2114	1.062	76.11
36	-0.02079	1.164	15.80
37	-0.4260	2.127	89.55
38	0.09752	0.3204	4.474
39	-0.09303	0.8004	45.48
40	0.09364	0.2151	4.711
41	0.1076	0.2416	1.325
42	0.08155	0.1899	3.363
43	0.09885	0.07547	7.629
44	0.1119	0.2080	2.445
45	0.04710	0.3414	13.36
46	-0.2026	0.7725	99.58
47	-0.09739	1.053	37.64
48	-1.048	4.589	218.0
49	-0.9372	4.465	157.8
50	-0.9736	4.839	162.7

51	-0.5524	2.687	115.7
52	-0.4608	2.926	60.32
53	-0.9532	4.830	79.50
54	-0.1822	1.056	71.72
55	-0.4662	2.351	90.05
56	-0.3150	1.633	77.76
57	-0.06433	0.6583	37.91
58	-0.3793	2.635	78.51
59	0.06685	0.2745	13.55
60	0.06263	0.2041	4.472
61	0.03145	0.1119	12.21
62	0.05213	0.1830	13.03
63	0.07645	0.7692	24.45
64	0.05156	0.5605	20.94
65	0.03802	0.08902	4.848
66	0.06958	0.5462	14.83
67	0.04063	0.4596	14.99
68	0.05411	0.2117	7.025
69	0.03354	0.2197	13.67
70	-0.3195	2.088	57.60
71	-0.2294	1.892	43.57
72	-0.04859	0.9546	24.36
73	0.07703	0.4377	7.717
74	-0.9751	0.6198	60.18
75	0.09923	0.4534	6.523
76	0.01124	0.6879	16.59
77	0.08897	0.2199	3.674
78	0.1148	0.1534	1.799
79	-0.2154	1.584	48.39
80	0.1195	0.2084	3.470
81	-0.03267	0.9916	18.49
82	0.03676	0.4456	9.025
83	-0.07379	1.418	22.92
84	-0.01961	0.5153	26.24
85	0.07252	0.3121	22.18
86	0.05710	0.2009	8.174
87	-0.4386	1.610	144.2
88	-0.7945	3.244	169.9
89	-0.3734	1.978	75.41
90	0.01202	0.6628	14.82
91	0.06941	0.4705	4.474
92	0.08563	0.6405	14.99
93	0.09046	0.6586	12.43
94	0.05774	0.5854	14.73
95	0.02619	0.1421	17.74
96	-0.06122	0.6104	40.90
97	0.07238	0.09793	5.125
98	-0.005958	0.1539	37.57
99	-0.1301	0.8018	61.21
100	-0.1387	0.7577	70.48
101	-0.1888	0.6956	136.9
102	-0.03684	0.4485	41.29
103	-0.3533	1.151	203.6
104	-0.2023	0.8538	116.7
105	0.007344	0.4331	32.17
106	0.04223	0.4701	19.43

APPENDIX 10

PARAMETERS OF DIFFERENT CREEP MODELS
BY TEMPERATURES AND STRESS LEVELS

(The parameters of practically all the tests are marked in the figures.)

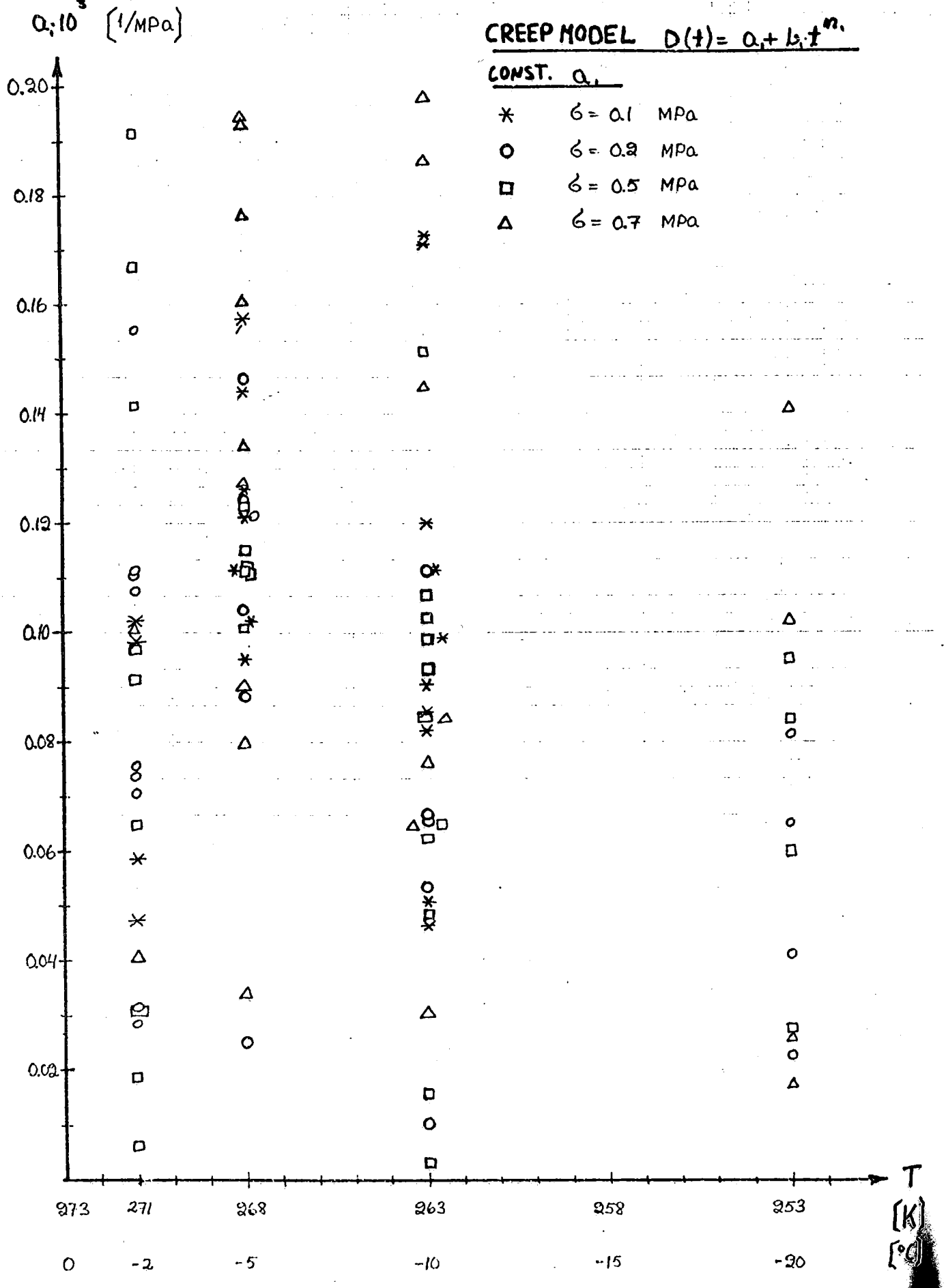
a₁·10³ [1/MPa]
CREEP MODEL D(t) = a₁ + b₁·t^n₁
CONST. a₁
σ = 0.1 MPa
σ = 0.2 MPa
σ = 0.5 MPa
σ = 0.7 MPa
0.20
0.18
0.16
0.14
0.12
0.10
0.08
0.06
0.04
0.02
T
273
271
268
263
258
253
[K]
0
-2
-5
-10
-15
-20
[°C]

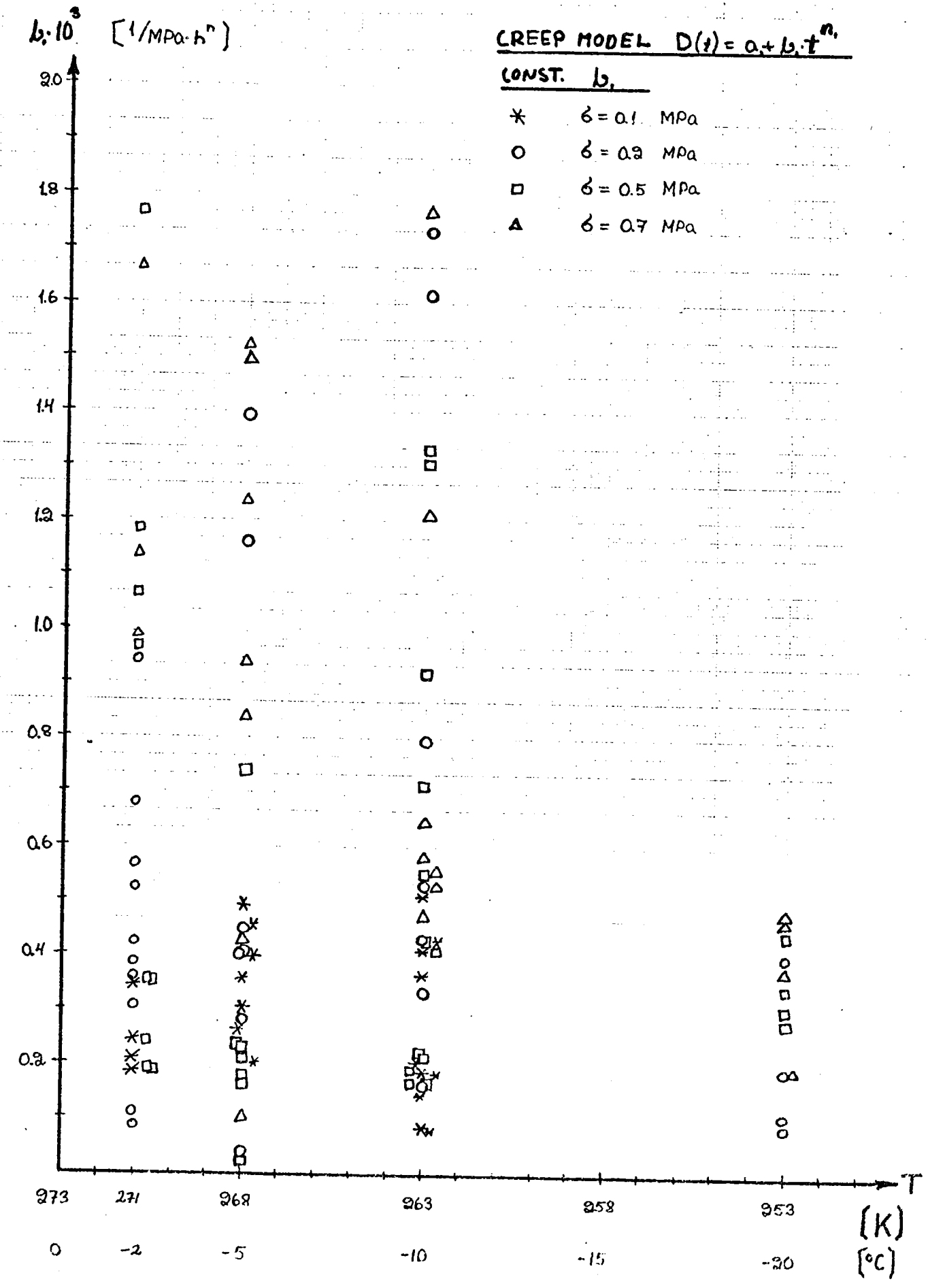
$b_1 \cdot 10^3$ [1/MPa·h^n]
CREEP MODEL $D(t) = a_1 + b_1 \cdot t^{n_1}$
CONST. b_1
σ = 0.1 MPa
σ = 0.3 MPa
σ = 0.5 MPa
σ = 0.7 MPa
2.0
1.8
1.6
1.4
1.2
1.0
0.8
0.6
0.4
0.2
T
273
271
268
263
258
253
(K)
0
-2
-5
-10
-15
-20
[°C]

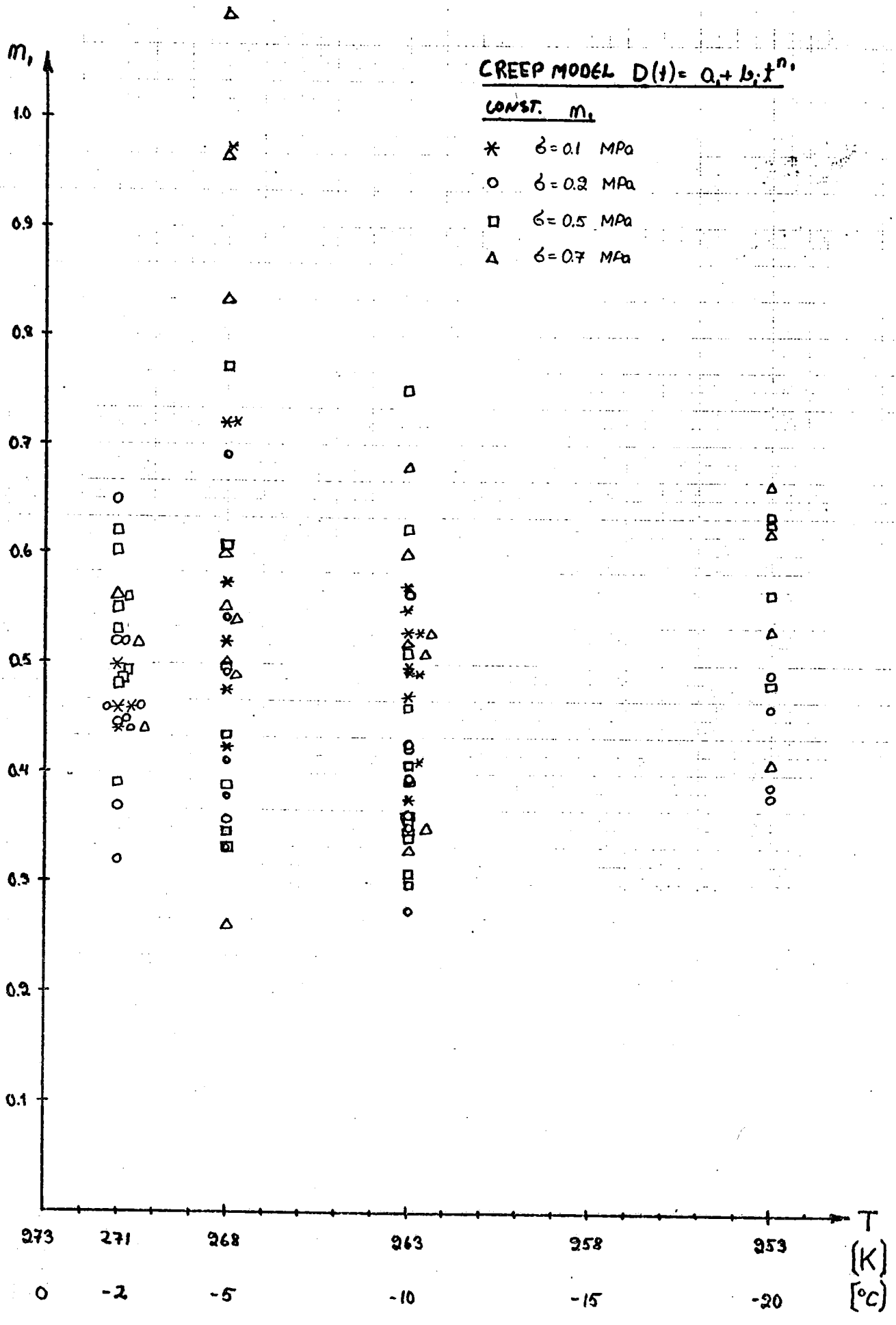
CREEP MODEL $D(t) = a_1 + b_1 t^{n_1}$
CONST. m_1
$\sigma = 0.1$ MPa
$\sigma = 0.2$ MPa
$\sigma = 0.5$ MPa
$\sigma = 0.7$ MPa
m_1
1.0
0.9
0.8
0.7
0.6
0.5
0.4
0.3
0.2
0.1
T
273 271 268 263 258 253 (K)
0 -2 -5 -10 -15 -20 [°C]

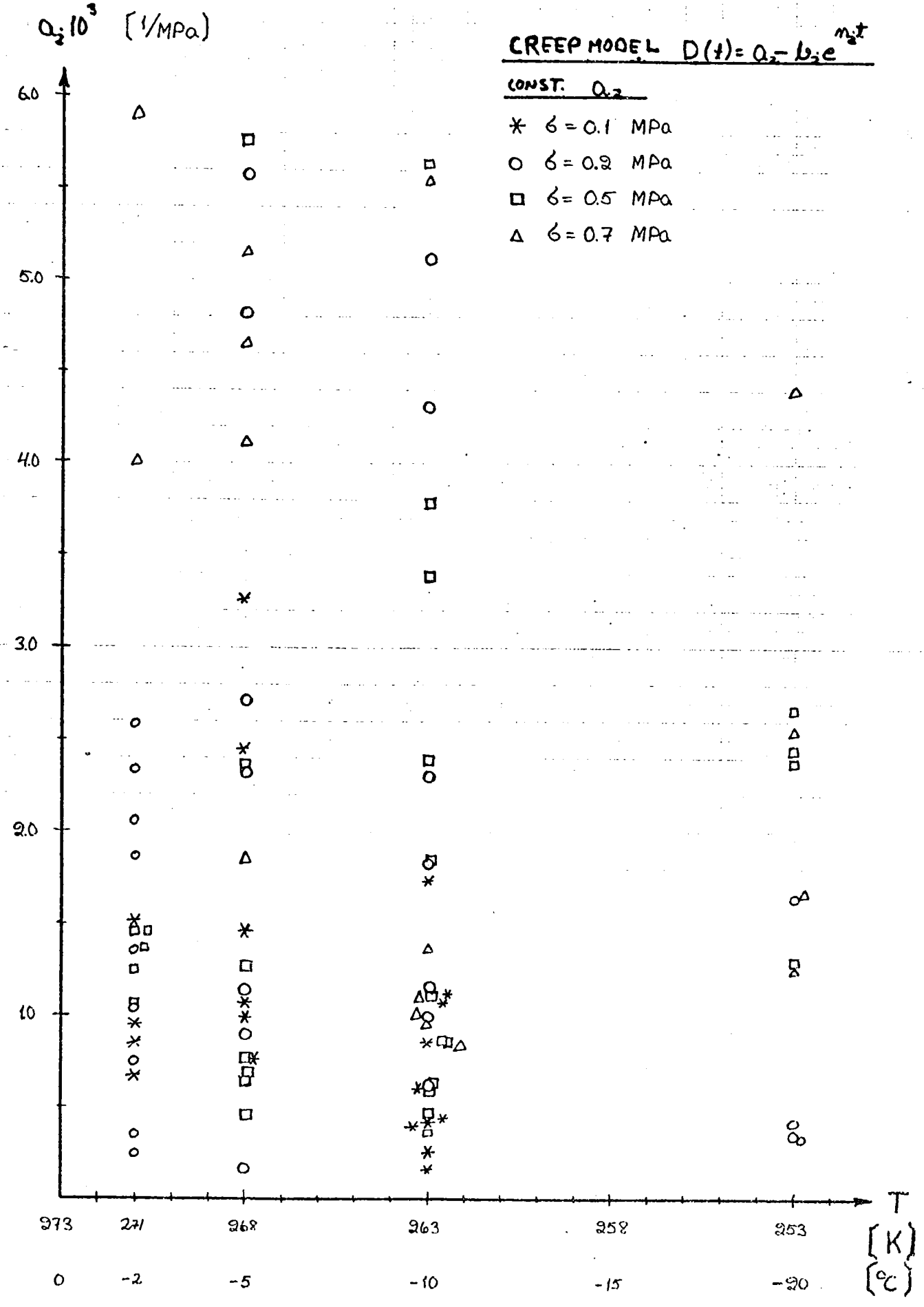
$a_2 10^3$ [1/MPa]
CREEP MODEL $D(t) = a_2 - b_2 e^{n_2 t}$
CONST. a_2
* $\sigma = 0.1$ MPa
o $\sigma = 0.2$ MPa
□ $\sigma = 0.5$ MPa
△ $\sigma = 0.7$ MPa
6.0
5.0
4.0
3.0
2.0
1.0
T
273
271
268
263
258
253
[K]
0
-2
-5
-10
-15
-20
[°C]

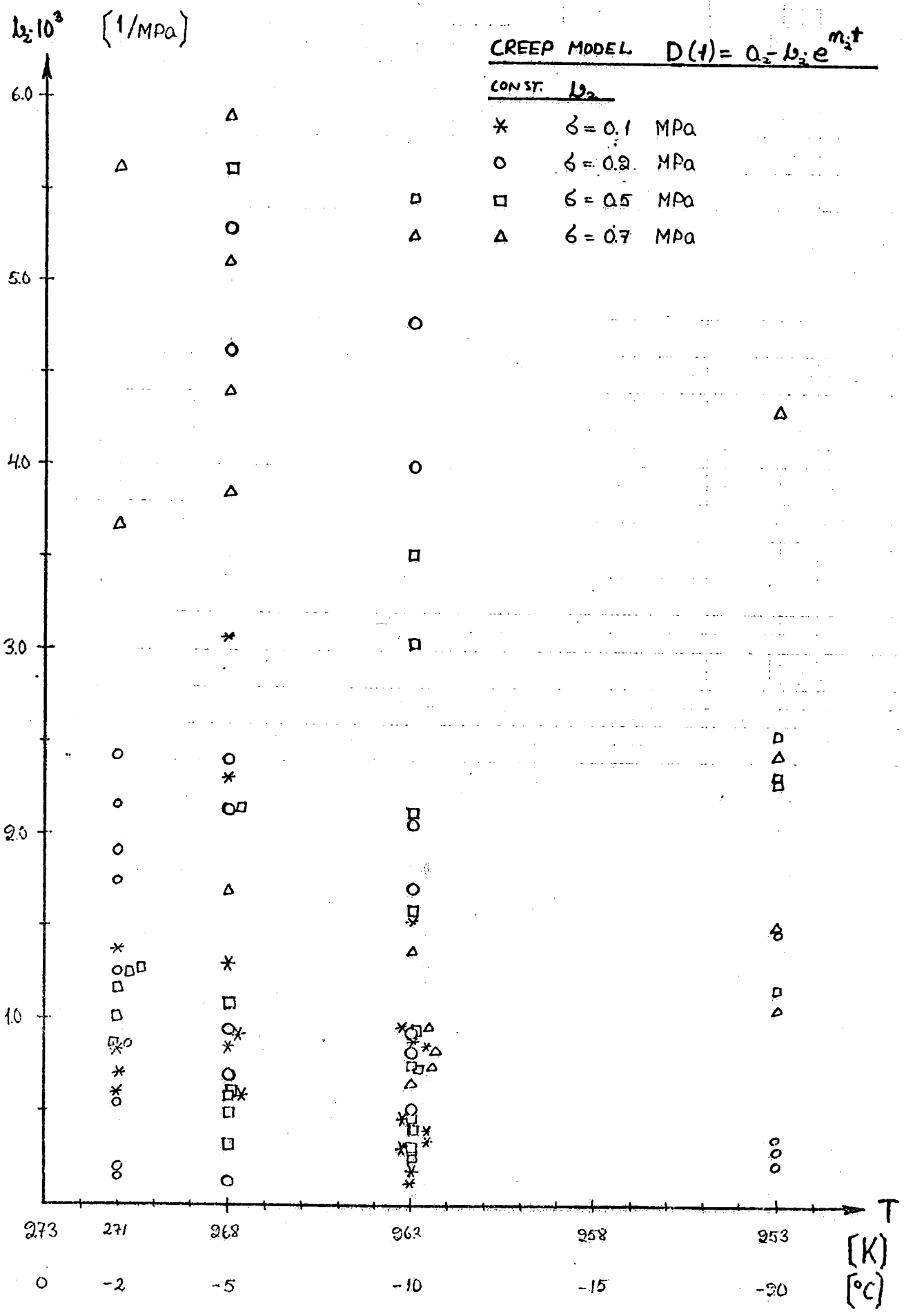
$b_2 \cdot 10^3$ [1/MPa]
CREEP MODEL $D(t) = a_2 - b_2 e^{m_2 t}$
CONST. b_2
* $\sigma = 0.1$ MPa
o $\sigma = 0.2$ MPa
□ $\sigma = 0.5$ MPa
Δ $\sigma = 0.7$ MPa
6.0
5.0
4.0
3.0
2.0
1.0
T
273 271 268 263 258 253 [K]
0 -2 -5 -10 -15 -20 [°C]

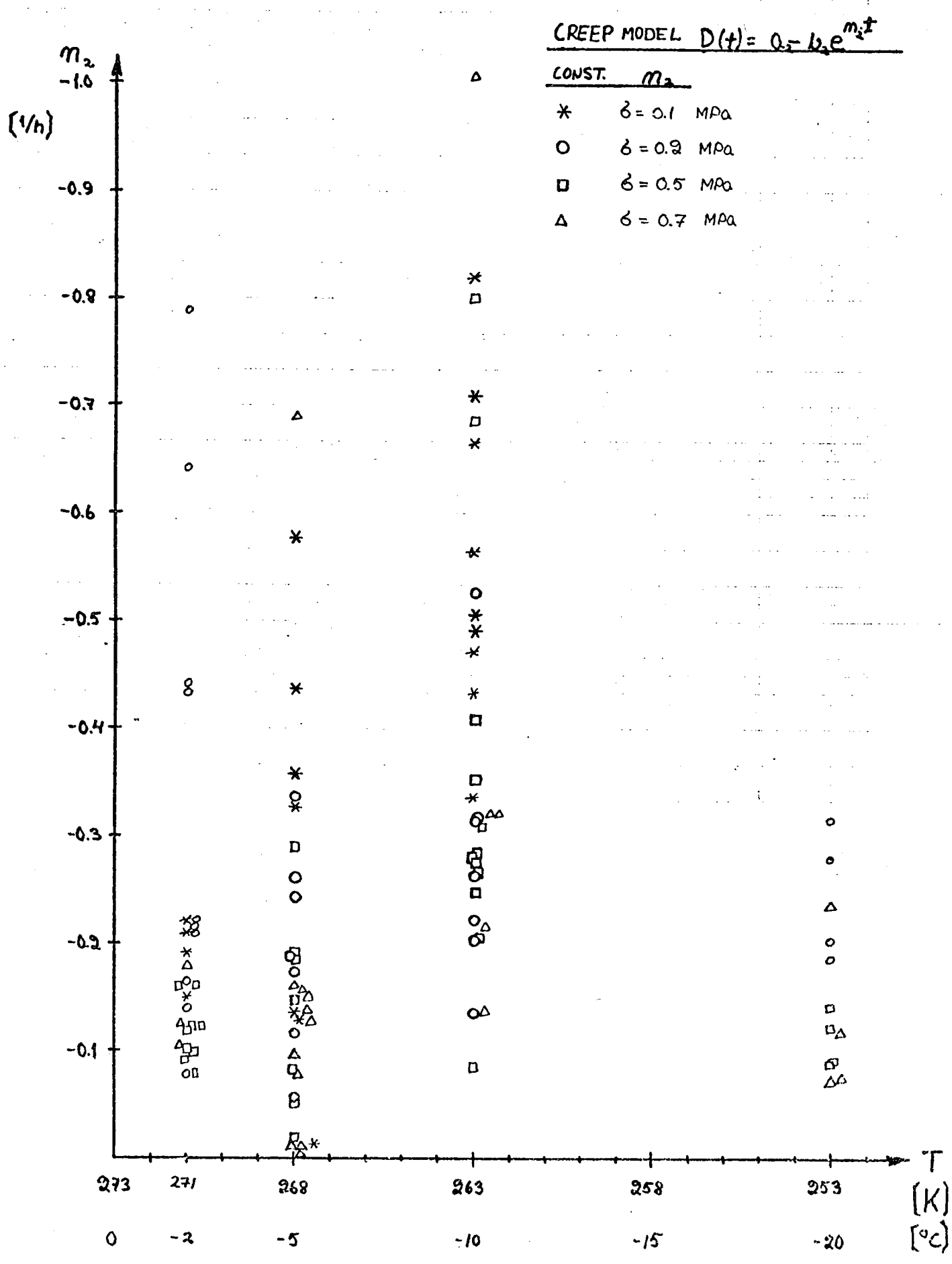
CREEP MODEL $D(t) = a_2 - b_2 e^{m_2 t}$
CONST. m_2
* $\sigma = 0.1$ MPa
O $\sigma = 0.2$ MPa
□ $\sigma = 0.5$ MPa
Δ $\sigma = 0.7$ MPa
m_2
[1/h]
-1.0
-0.9
-0.8
-0.7
-0.6
-0.5
-0.4
-0.3
-0.2
-0.1
T
273
271
268
263
258
253
[K]
0
-2
-5
-10
-15
-20
[°C]

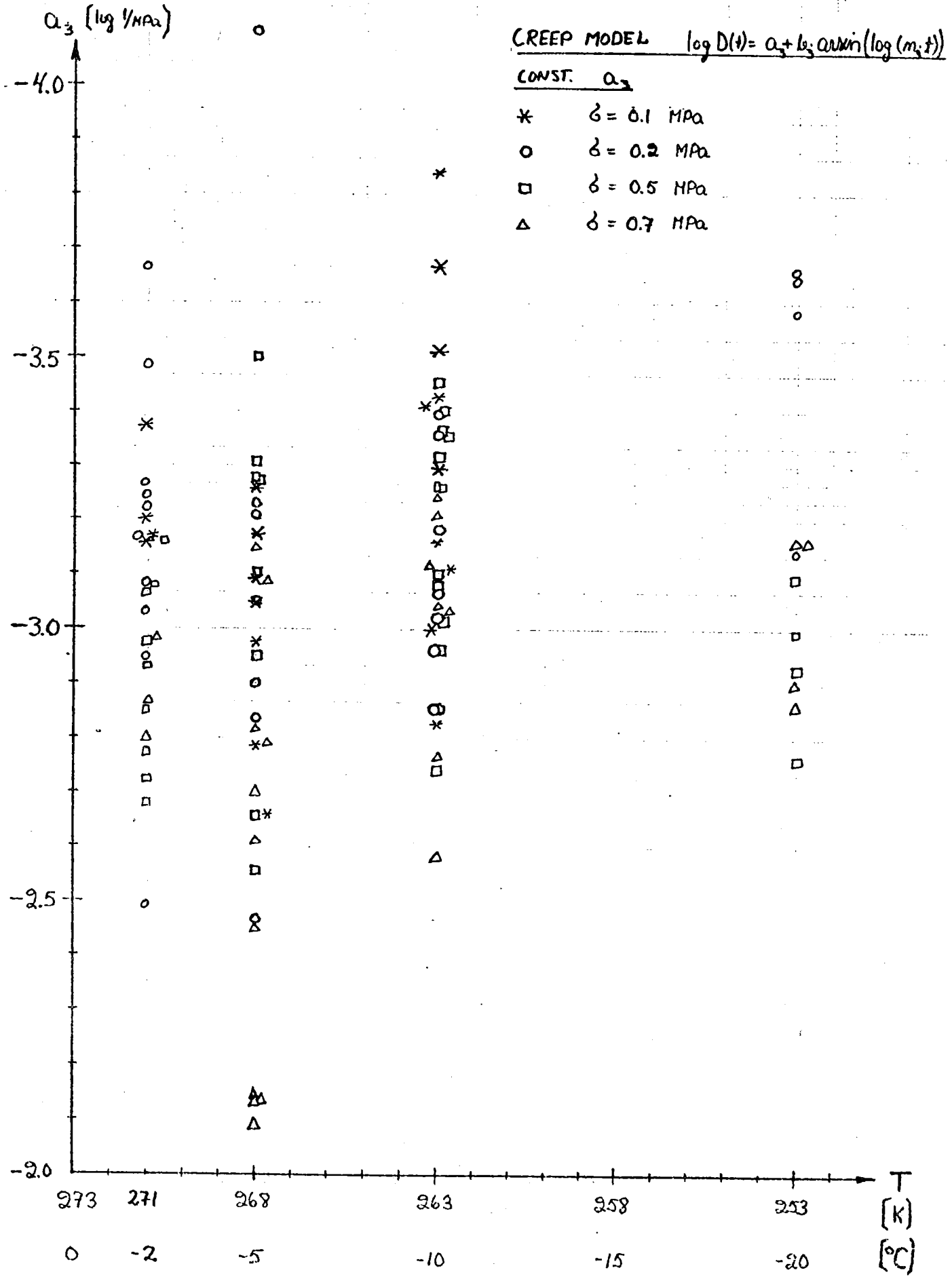
a_3 [log 1/MPa)
CREEP MODEL $\log D(t) = a_3 + b_3 \arcsin(\log(m_3 t))$
CONST. a_3
σ = 0.1 MPa
σ = 0.2 MPa
σ = 0.5 MPa
σ = 0.7 MPa
-4.0
-3.5
-3.0
-2.5
-2.0
T
273
271
268
263
258
253
[K]
0
-2
-5
-10
-15
-20
[°C]

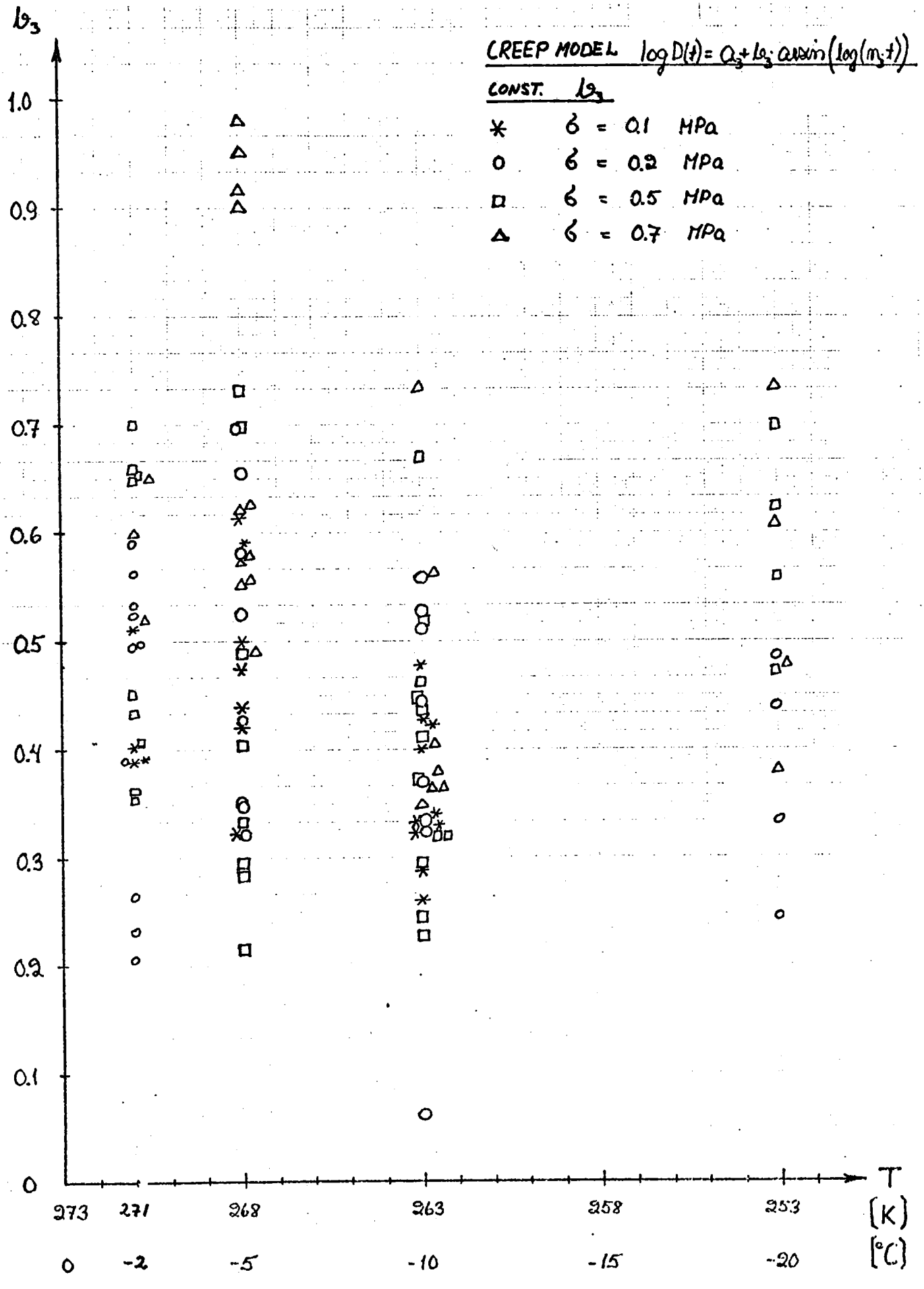
b_3
CREEP MODEL $\log D(t) = a_3 + b_3 \operatorname{asin}(\log(m_3 t))$
CONST. b_3
* σ = 0.1 MPa
o σ = 0.2 MPa
□ σ = 0.5 MPa
△ σ = 0.7 MPa
1.0
0.9
0.8
0.7
0.6
0.5
0.4
0.3
0.2
0.1
0
T
273 271 268 263 258 253 [K]
0 -2 -5 -10 -15 -20 [°C]

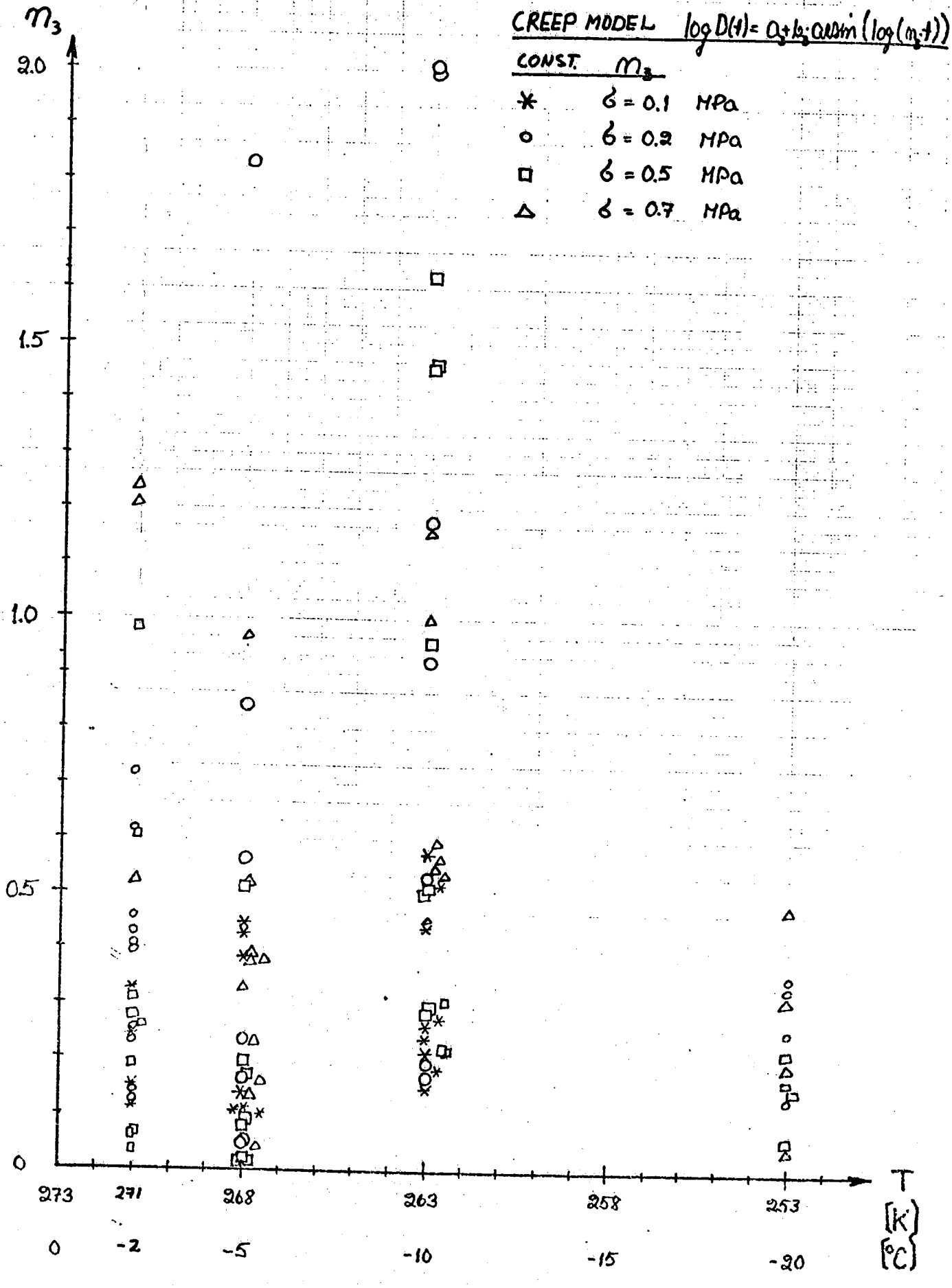
m_3
CREEP MODEL $\log D(t) = a_3 + b_3 \cdot \operatorname{arsinh}(\log(m_3 t))$
CONST. m_3
$\sigma = 0.1$ MPa
$\sigma = 0.2$ MPa
$\sigma = 0.5$ MPa
$\sigma = 0.7$ MPa
2.0
1.5
1.0
0.5
0
273
271
268
263
258
253
T [K]
0
-2
-5
-10
-15
-20
[°C]

ISBN 951-46-2521-8